SITES FOR WIND POWER INSTALLATIONS

TECHNICAL REPORT

BOUNDARY LAYER TURBULENCE
OVER TWO-DIMENSIONAL HILLS

by

Michael A. Rider

and

V. A. Sandborn

Civil Engineering
Colorado State University
Fort Collins, Colorado 80523

September 1977

CER77-78MAR-VAS4

SUMMARY

Measurements of the mean and turbulent velocities for turbulent
boundary layers over two-dimensional hills have been made.
Triangular hills, with aspect ratios (height to vertical distance to
crest) of 1:2, 1:4, and 1:6, were subjected to two different approach
turbulent boundary layer flows. Mean velocities, longitudinal and
vertical turbulent velocities, Reynolds stress and the wall static
pressure distributions are reported for a number of positions upstream,
along, and at the crest of the hills.

As the flow advances up the hills, systematic changes in the
mean and turbulent velocities occurred in the region near the hill
surface. The flow in the outer region of the boundary layers above
the hills were found to remain similar to the flow upstream of the
hill. As the flow passed from the base of the hill to the crest there
was an increase in mean velocity, shear stress, and vertical turbulent
velocity near the surface. The longitudinal turbulent velocity was
found to decrease in magnitude as the flow progressed from the base to
the crest of the hill.

ACKNOWLEDGMENTS

TABLE OF CONTENTS

LIST OF FIGURES

LIST OF SYMBOLS

Symbol	Definition	Dimensions
A	constant King's Law	
B	constant King's Law	
C_f	friction coefficient	
C_p	pressure coefficient	
E_1, E_2	mean voltage of a hot wire, 1 normal, 2 yawed	V
e, e_1, e_2	voltage fluctuation	V
$\overline{e^2}$	mean square of voltage fluctuation	V^2
$\sqrt{\overline{e^2}}$	root mean square of voltage fluctuation	V
$\overline{e_1 e_2}$	mean of product of e_1 and e_2	V^2
H	form factor	
h	height of hill	L
m	exponent	F/L^2
p	pressure	VT
S_u	sensitivity dE/dU of a hot wire	$\dfrac{VT}{L}$
S_1	sensitivity dE/dU of a normal hot wire	$\dfrac{VT}{L}$
S_2	sensitivity dE/dU of a yawed hot wire	$\dfrac{VT}{L}$
S_v	sensitivity, $1/U\ dE/U\phi$, to angle	$\dfrac{VT}{L}$
U	local mean velocity	L/T
U_e	characteristic velocity	L/T
U_{TOT}	total velocity	L/T
$U_{F.S.}$, U_∞	free stream velocity	L/T
U_τ	friction velocity	L/T
u, v	velocity fluctuation in x-, y-direction	L/T
$\sqrt{\overline{u^2}}$, $\sqrt{\overline{v^2}}$	root mean square velocity fluctuations	L/T
$\overline{uv}$	time mean product of u and v	L^2/T^2

Symbol	Definition	Dimensions
x	longitudinal direction	L
y	vertical direction	L
z	horizontal direction	L
ΔP	pressure difference	F/L^2
ΔS	mean velocity speedup	
δ	boundary layer thickness	L
δ^*	displacement thickness	L
η	nondimensional distance from wall, y/δ	
θ	momentum thickness	L
ν	kinematic viscosity	L^2/T
ρ	mass density	m/L^3
ρ_e	characteristic mass density	m/L^3
τ	shear stress	F/L^2
τ_e	characteristic shear stress	F/L^2
τ_{ref}	reference wall shear stress	F/L^2
τ_w	wall shear stress	F/L^2
$\tau_{w\ local}$	local wall shear stress	F/L^2
ϕ	angle of probe with x axis	

Chapter I

INTRODUCTION

Annual mean and peak wind velocities are available for general areas throughout the United States and the world. This information is critical for the development of wind power. However, rarely will the data be recorded at a proposed wind power site. It would be very beneficial to the wind power engineer to be able to predict from general wind data the flow characteristics at a specific location.

Needed, for a wind power site, are reliable estimates of the local flow properties. If the available wind data for the general area is at a station some distance from the site a means to correlate the desired information would be required.

In general, the approach terrain will affect the mean and turbulent flow properties. Moreover, to utilize the speedup affect of a hill, the predicted change in the airstream properties would be required. There are literally endless combinations of approach flow conditions and hill configurations. This study was limited to investigating two approach flow conditions and three two-dimensional triangular shaped model hills.

The investigation started with a turbulent boundary layer developed over a flat plate with a zero pressure gradient. The turbulent boundary layer was then subjected to one of three triangular shaped hills. Aspect ratios of the hills were (rise over run) 1:2, 1:4, and 1:6. Surveys were made of the mean velocity, the longitudinal and vertical turbulent velocities and the shear stress distributions. The measurement gave a reference to how these different flow properties change in magnitude over a two-dimensional ridge. Next by adding upstream roughness a different turbulent boundary layer was formed. The measurements during

this flow case consisted of the mean velocity and the longitudinal turbulence.

The flat plate case represented a calibration point from which to build. In an effort to model atmospheric boundary layers in the wind tunnel, Zoric and Sandborn (1,2) have shown that similarity of turbulent boundary layers does exist for large Reynolds numbers. With their measurements in the Meteorological Wind Tunnel at Colorado State University, Sandborn and Zoric have documented that for a flat plate turbulent boundary layer with a zero pressure gradient similarity of the mean and turbulent velocities were present. When the turbulent quantities $\sqrt{\overline{u^2}}$, $\sqrt{\overline{v^2}}$ and $\overline{uv}$ are normalized by dividing by the local wall shear and multiplying by the density each of the turbulent flow properties follow a similarity curve.

Chapter II

THEORETICAL BACKGROUND

To utilize wind power to the fullest in a particular area the local terrain effects must be known. Different hills or ridges will produce different degrees of speedup of the airstream as it approaches the summit. Thus, to take advantage of the speedup it is important to find the most advantageous location and to choose a proper wind system for the local conditions. The mean velocity distribution is of primary interest, but turbulent quantities must be known to insure structural stamina. The present study was directed toward evaluating the effect of a hill on a flow. The fundamental concerns were the mean velocity and the longitudinal turbulent velocity component distributions. Also sought were the vertical turbulent velocity component and shear stress distributions.

Of specific interest was how far up into the boundary layer would the impression of the hill be evident. Due to inertia of the flow, the outer reaches of the boundary layer were expected to remain similar to that upstream. The only portion of the flow expected to change was the region closest to the wall.

It was known prior to the test that there would be a speedup of the mean velocity in the region nearest the wall. Furthermore, the increase in velocity gradient would produce an increase in surface shear stress. Not as obvious was the change in the turbulent components. A report by Ribner and Tucker (3), which discussed turbulence in a contracting stream gave some insight. Although the report dealt with isotropic turbulent flows which were undergoing simple contraction, it was felt the results could give an insight to the present problem.

Ribner and Tucker showed that when a flow was subjected to a contraction the longitudinal turbulent velocity component decreased and the lateral component increased. Regarding the hill as a local contraction, it was anticipated that similar results would be found.

Surface Shear Stress Evaluation

Two methods were used to determine the skin friction. The empirical Ludwieg-Tillmann equation and the "law of the wall."

The Ludwieg-Tillmann skin friction relation reads

$$C_f \equiv \frac{\tau_w}{1/2\ U_\infty^2} = .246 \times 10^{-.678H}(\frac{U_\infty \theta}{\nu})^{-.268} \tag{1}$$

where: the momentum thickness is

$$\theta \equiv \int_0^\delta \frac{U}{U_\infty}(1 - \frac{U}{U_\infty})\ dy$$

the form factor is

$$H \equiv \frac{\delta^*}{\theta}$$

the displacement thickness is

$$\delta \equiv \int_0^\delta (1 - \frac{U}{U_\infty})\ dy$$

and δ is the boundary layer thickness.

Justification for using this relation is based on earlier work reported by Tieleman (4). During his experiments Tieleman required skin friction measurements at several points in the wind tunnel. To check the reliability of the Ludwieg-Tillmann equation, Tieleman compared direct measurements from a floating element shear plate and values determined from the Ludwieg-Tillmann equation (1), Figure 1.

The agreement shown on Figure 1 demonstrated that the Ludwieg-Tillmann equation was adequate for the flat plate--zero pressure gradient boundary layers.

The "law of the wall", credited to Prandtl (5), applies to the region nearest the wall where viscous effects are important. Nondimensionally the "law of the wall" reads

$$\frac{U}{U_\tau} = f(\frac{U_\tau y}{\nu}) \tag{2}$$

where $\quad U_\tau^2 \equiv \frac{\tau_w}{\rho}$

Patel (6) gives the following definitions of f for the given flow conditions

(a) a linear sublayer

$$U/U_\tau = U_\tau y/\nu \tag{3a}$$

(b) a fully turbulent region

$$U/U_\tau = A \, \log_{10}(\frac{U_\tau y}{\nu}) + B \tag{3b}$$

(c) a transition zone

$$U/U_\tau = A \, \log_{10}\left[(\frac{U_\tau y}{\nu}) + C\right] + B \tag{3c}$$

Where the constants A, B and C are believed universal. From his work and other investigators, Patel assigns the following values for the fully turbulent region.

$$A = 5.5 \quad \text{and} \quad B = 5.45 \, .$$

The "law of the wall" is limited to zero and moderate pressure gradients. Patel suggests the "law of the wall" may be used to

determine the surface shear stress for pressure gradients in the range

$$0 > \frac{\nu}{(\rho U_\tau^3)} \frac{dP}{dX} > -.007 \tag{4}$$

within approximately 6%. For the zero and moderate pressure gradients, both the Ludwieg-Tillmann and the "law of the wall" give approximately the same value for the shear stress. Figure 2 gives values of C_f evaluated for the flat plate flow of the present study.

Shear Stress Distribution Evaluation

The following similarity method reported by Sandborn and Horstman (7) to evaluate turbulent boundary layer shear stress distributions of the approach flow was used for the present study. This theoretical model accurately predicted the shear stress distributions over a flat plate--zero pressure gradient flow. Figure 3 is a comparison of the shear stress measured by Zoric and Sandborn and another by Klebanoff with the similarity predictions. The solid line is the shear stress distribution evaluated directly from the mean velocity profile.

For a turbulent boundary layer the equation of motion in the x-direction is

$$\rho U \frac{\partial U}{\partial x} + \rho V \frac{\partial U}{\partial y} = \frac{\partial p}{\partial x} + \frac{\partial \tau}{\partial y} \tag{5}$$

where the shear stress τ is made up of two parts. The two parts are the mean and the turbulent stress

$$\tau \equiv \mu \frac{\partial U}{\partial y} + \rho \overline{uv} \tag{6}$$

The boundary conditions require that at the wall

$$\tau = \tau_w \quad \text{and} \quad \frac{d\tau}{dy} = \frac{dp}{dx}$$

where p is the surface static pressure. Also at the outer limit of the turbulent boundary layer the shear stress approaches zero.

Sandborn assumed for a compressible flow (although for the present study an incompressible flow is assumed) the following similarity

$$\rho U = \rho_e U_e f_{\rho U}(\eta)$$

$$U = U_e f_U(\eta)$$

$$\tau = \tau_e \psi(\eta) \tag{7}$$

where $\rho_e U_e$ is a characteristic mass flow, U_e the characteristic velocity and τ_e as the characteristic shear stress. η is a non-dimensional variable resulting from dividing the vertical distance y by the characteristic length δ_e. Evaluating the differentials in terms of the similarity variables gives

$$\frac{\partial U}{\partial x} = f_U \frac{\partial U_e}{\partial x} + U_e \frac{\partial f_U}{\partial x} = f_U \frac{\partial U_e}{\partial x} - \frac{U_e}{\delta} \frac{d\delta}{dx} \eta f_U' U \tag{8}$$

$$\frac{\partial U}{\partial y} = \frac{U_e}{\delta} f_U' \tag{9}$$

and from continuity

$$\rho V = - \int_0^\eta \delta \frac{\partial \rho_e U_e}{\partial x} f_{\rho U} d\eta + \rho_e U_e \frac{d\delta}{dx} \int_0^\eta f_{\rho U}' \eta d\eta \tag{10}$$

Substituting in the similarity values into the equation of motion yields

$$\rho_e U_e f_{\rho U}[f_U \frac{\partial U_e}{\partial x} - \frac{U_e}{\delta} \frac{d\delta}{dx} \eta f_U'] + \frac{U_e}{\delta} f_U'[- \delta \frac{\partial \rho_e U_e}{\partial x} \int_0^\eta f_{\rho U} d\eta$$

$$+ \rho_e U_e \frac{d\delta}{dx} \int_0^\eta f_{\rho U}' \eta d\eta] = - \frac{\partial p}{\partial x} + \frac{\tau_w}{\delta} \psi' \quad . \tag{11}$$

Solving for ψ' and integrating gives

$$\psi \equiv \frac{\tau}{\tau_e} = \frac{\rho_e \delta_e U_e}{\tau_e} \frac{dU_e}{dx} (\int_0^\eta f_{\rho U} f_U d\eta - \eta)(\frac{\delta_e U_e}{\tau_e} \frac{d\rho_e U_e}{dx}$$

$$+ \frac{\rho_e U_e^2}{\tau_e} \frac{d\delta_e}{dx}) \int_0^\eta \{f_U' \int_0^{\eta'} f_{\rho U} d\eta'\} d\eta + C \tag{12}$$

For similarity it is required that the equation (11) be independent of x. Requiring that for compressible flow

$$\frac{\delta_e \rho_e U_e}{\tau_e} \frac{dU_e}{dx} = A \text{ (a constant independent of x)} \tag{13}$$

and

$$\frac{\delta_e U_e}{\tau_e} \frac{d\rho_e U_e}{dx} + \frac{\rho_e U_e^2}{\tau_e} \frac{d\delta_e}{dx} = B \text{ (a constant independent of x)} \tag{14}$$

For incompressible flow, $\frac{\delta\rho_e}{\delta x} = 0$, thus the similarity requirements are

$$\rho \frac{\delta U_e}{\tau_e} \frac{dU_e}{dx} = A \tag{13a}$$

$$\rho \frac{U_e^2}{\tau_e} \frac{d\delta}{dx} = B \tag{14a}$$

To evaluate equation (12) the following similarity characteristics were used: $U_e = U_\infty$, $\rho_e = \rho_\infty$, $\tau_e = \tau_w$, and δ_e, the characteristic length, was equal to δ where $\delta = y$ at $\tau = 0$. The final form of equation (12) for an incompressible flat plate flow, with a zero pressure gradient is

$$\psi \equiv \frac{\tau}{\tau_w} = 1 - \frac{U_\infty^2}{U_\tau^2} \frac{d\delta}{dx} \int_0^\eta \{\frac{d(U/U_\infty)}{d\eta} \int_0^{\eta_1} (\frac{U}{U_\infty}) d\eta_1\} d\eta \tag{15}$$

where $U_\tau^2 \equiv \frac{\tau_w}{\rho}$ and the boundary condition at $\eta = 0\,(\frac{\tau}{\tau_w} = 1)$ was used to evaluate the constant of integration.

TURBULENT VELOCITY COMPONENT SIMILARITY

Work by different experimenters show that similarity does exist in the total shear stress and the turbulent velocity terms. Measurements by Zoric (2) at high Reynolds numbers and Klebanoff (8) at low Reynolds numbers demonstrate this within experimental limits, (10). Figures 3 and 4 show the agreement of the total shear stress distribution when referenced to the wall shear stress and the boundary layer thickness. When referenced similarly, the longitudinal component, $\sqrt{\frac{\rho \overline{u^2}}{\tau_w}}$, compares well for $y/\delta \geq .05$, Figure 5. The vertical turbulent component, $\sqrt{\frac{\rho \overline{v^2}}{\tau_w}}$, distributions do not agree as well as the total shear stress or the longitudinal turbulent component, Figure 6. The measurements of Zoric do not show the drop in the $\sqrt{\overline{v^2}}$ as did that of Klebanoff. An additional set of data recorded by Tieleman (4) very close to the wall reveal a very distinct maximum followed by a sharp decline in the vertical turbulent component.

It is important to point out that the turbulent quantities $\sqrt{\overline{u^2}}$, $\sqrt{\overline{v^2}}$ and $\overline{uv}$ will be presented, unless indicated, nondimensionalized by multiplying by the density and the furthest upstream estimations of the wall shear stress. The study of Sandborn and Horstman (7) suggest the characteristic wall shear stress may be the upstream value when rapid pressure changes occur. Also, as the flow continues over the hills direct quantitative changes in the turbulence terms can easily be compared. In the derivation of the similarity relation between the shear stress and the mean flow the characteristic values are not defined.

Thus, the characteristic shear stress and characteristic length need not be the local wall shear stress and the local boundary layer thickness. For rapid distortion the turbulent properties apparently cannot change quickly, so they will be convected along by the mean flow without undergoing major changes. As noted, the work of Sandborn and Horstman suggested that an upstream value of the surface shear stress may be a possible choice for the present flow cases. For the present evaluation a value of wall shear stress at a specific upstream location (x = 55.8 cm from the crest for smooth surface case, and x = 50.8 cm from the crest for the rough surface case) was used for the characteristic shear stress. The particular locations are somewhat arbitrary, but were selected to be upstream of where the flow is disturbed by the presence of the hill.

The characteristic length must reflect the distortion of the boundary layer coordinate system as the layer develops. If it is assumed that the hill models influence only the part of the boundary layer near the surface and not that of the outer part of the layer; then a characteristic length equivalent to the layer development without the hill might be employed. This assumption of neglecting the perturbation of the hill on the boundary layer thickness length obviously would only be valid when the approach layer is thick compared to the hill height. For the present study it was found that the boundary layer thickness develops nearly linear with x-distance, Zoric and Sandborn (1). The present undisturbed boundary layers for both the smooth and rough surfaces appeared to grow at a rate of 1 cm for every 10 cm in the x-direction. Thus, the characteristic length, δ_e, was taken as the extrapolated boundary layer thickness (in the ratio of 1 to 10) from

the measured approach profile thickness. Again this selection of a characteristic length is somewhat arbitrary. It is mainly justified in that it appears to produce a good correlation of the turbulence data over the hills in the outer part of the boundary layer. Other coordinate changes, such as following streamline paths, have been suggested, however for rapid distortions the boundary layer thickness appears to produce the most consistent correlation.

BOUNDARY CONDITIONS

In the atmosphere a wide spectrum of possible approach conditions might exist. In general the effect of a small hill in a deep boundary layer will depend on the energy distribution within the approach flow. The thicker the boundary layer the less the energy will be distributed in the region near the surface; thus the less will be the speedup effect of the hill. Local roughness of the approach surface will also act to remove more energy near the surface (which will also be seen in a thickening of the boundary layer). It is apparent that the higher the hill compared to the boundary layer thickness the larger will be the speedup. Likewise for boundary layers of the same thickness, but different surface roughness, the one over a smoother surface will produce the greater speedup. Two different approach turbulent boundary layers are considered in the present study. The first case is that of a smooth surface, while the second is produced by a long fetch of roughness.

Classical boundary layer theory generally employs a coordinate system which is perpendicular to the surface at all points along and near the surface (curvilinear coordinates). Over the hills this requirement of a curvilinear coordinate can also be expected to be valid.

However, for engineering applications of velocity distributions for wind power use, surveys and data in the vertical direction are desired. For the present study a simple rectangular coordinate system was employed, both for measurements and analysis. The x-distance coordinate originated at the crest of the hill and was measured positive in the upstream direction along the tunnel floor. The y-direction coordinate was measured positive from the local surface of the model at each x-location.

Evaluation of the local surface shear stress from equations (1) or (2) requires the curvilinear-boundary layer coordinate system be employed. As a demonstration of the deviation from boundary layer theory in the use of a vertical coordinate, an estimate of the surface shear from the law-of-the-wall concept was made for both a vertical and a curvilinear-coordinate evaluation, Figure 7. The deviation shown in Figure 7 is mainly important in the lower portion of the hill.

Chapter III

EXPERIMENTAL SETUP

The measurements were taken in the Meteorological Wind Tunnel located in the Fluid Dynamics and Diffusion Laboratory at Colorado State University. The purpose of the experiment was to make surveys of flow characteristics over models of hills emersed in deep turbulent layers. The following sections will discuss the experimental facility equipment and technique.

Wind Tunnel Facility

As mentioned above the measurements were performed in the recirculating Meteorological Wind Tunnel, Figure 8. The flow rate in the tunnel is controlled by a variable-pitch, variable-speed propeller and can be set between 0.3 and 37 m/s with no more than one-half percent deviation from the desired velocity. The test section is approximately 1.8 m square, 27 m in length, and is proceeded by a 9:1 contraction. A zero pressure gradient along the length of the test section was maintained with the adjustable ceiling. The ambient temperature was kept at a constant within ±1/2°C by the tunnel air conditioning system.

The experimentation was scheduled in two parts. Each of the two parts had different upstream conditions, however, there were features which were similar to both. At the entrance to the test section during both tests a 1.22 m long section of 1.27 cm gravel fastened to the floor followed by a 3.80 cm high sawtooth fence spanning the width of the tunnel was used to prompt the formation and growth of a large turbulent boundary layer.

In the initial test, a false floor was installed to which the models were secured, Figure 9. The false floor was comprised of

three sections--the approach ramp, horizontal test section, and the
trailing down ramp. The floor originated 5.60 m from the sawtooth
fence. The approach ramp, constructed from .32 cm masonite, was at an
angle of 0.84° with the horizontal and had a length of 1.30 m. Fol-
lowing the upstream ramp was a 8.55 m long test section. This section
was built from 1.91 cm plywood. The models tested were mounted directly
on the plywood. Masonite, .32 cm thick, was then used in assembling
the trailing ramp. This ramp was .90 m in length and formed on angle
of -1.21° with the horizontal.

During the second test there was no false floor. However, a
roughness beginning at 1.83 m from the sawtooth fence and ending at
11.43 m gave a different approach velocity profile, Figure 10. The
roughness was made up of aluminum sheets with ribs .16 cm in height.
The ribs were randomly spaced normal and parallel to the flow. In this
phase of the experimentation the models were mounted directly on the
aluminum floor of the wind tunnel.

As mentioned above, a sawtooth boundary-layer trip was used to
prompt the growth of turbulent boundary layer. A similarity velocity
profile was attained within 6.1 m of the test section entrance. During
the initial test the models were set 14.0 m from the entrance and during
the second 18.6 m. For both flows the ceiling of the wind tunnel was
adjusted to produce a near zero pressure gradient in the free streams
of the test section. A slight acceleration occurred along the approach
ramp.

Model Description

A series of triangular-shaped hills were designed and used for the
tests, Figure 11. The models were constructed using 9 cross-section

ribs made of 1.27 cm Plexiglas. The hill surface was placed over the ribs, and was made of .32 cm thick Plexiglas. The crest height of each was 5.08 cm and with aspect ratios of 1/2, 1/4 and 1/6. All models were 183 cm in length. Each of the models were equipped with static pressure taps.

Instrumentation

Actuator and Carriage

The measurements for this experiment required vertical surveys (y-direction) of the flow at particular longitudinal points (x-direction) along the center of the tunnel. To accomplish this the existing carriage of the wind tunnel was employed. The carriage had been constructed on a rail and wheel system. The rails 101.6 cm from the floor run the full length of the test section. This allows the carriage to be positioned at any desired point in the x-direction. A control unit outside the tunnel monitors the vertical movement of the probes and probe support through the boundary layer. This actuator system, with a total traverse of 65 cm, provided a constant voltage change for a particular change in height.

In both tests a stop rod attached tightly to the probe support would make contact with the floor prior to the other instruments. The purpose of the stop rod was to protect the probes from being driven into the floor and possibly damaged. In addition, because the vertical distance between the bottom of the stop rod and the probes were known, y_o was known, Figure 11. An electric indicator was triggered when the stop rod contacted the floor. During the second set of tests a .00254 cm dial indicator was employed to determine more accurately the y-locations of the probes within .5 cm of the wall.

Static Pressure Measurements

Four different probes were used to measure the static pressure. The particular probe used depended on the location of the desired measurements. While making measurements of the mean velocity in the boundary layer above the surface of the hill, two probes were used as static pressure references. Commercial cylindrical pitot-static tube was used along with a commercial disk probe. In general, cylindrical probes are acceptable for free stream and boundary-layer measurements. However, as this type probe nears the wall of the tunnel and in particular the surface of the hill errors occur due to the rapidly varying flow direction. Specifically, the flow becomes something other than parallel to the axis of the cylindrical probe. To compensate for the error due to "pitch" angle between the airflow and pitot-static tube, measurements were made with the disk probe in the vicinity of the surface.

The disk probe samples the local static pressure through a small static tap drilled in the center of the .62 cm thin disk. The disk probe gave systematically lower static pressure readings, but was found to be insensitive to "pitch" angles of ±30°. The geometry of the disk probe restricted measurements near the surface. The cylindrical probe had a diameter of .18 cm with an elliptical nose. The static taps were located 2.22 cm from the support stem. This probe had a .040 cm hole for total pressure measurements.

Static pressure measurements were also taken on the surface of the models and the floor of the tunnel. Each of the models contained a set of static pressure taps distributed over the centerline of the hill, Figure 12. The static taps, sharp edged and .064 cm in diameter, were

drilled perpendicular to the model surface. On the floor of the tunnel, static probes constructed from .079 cm i.d. and .139 cm o.d. brass tubing were used. The end of the tubes were soldered closed and a series of taps were drilled in a circle around the circumference of the tubing. The probes were secured to the wall of the tunnel.

When making static pressure measurements, the reference was the static pressure in the free stream. A commercial pitot-static tube .318 cm diameter was used. It was a cylindrical probe with an elliptical nose. The total pressure tap in the tip of the nose was .079 cm in diameter. The static taps were 5.08 cm from the support stem. The only static pressures reported are wall static pressures upstream and on the hills. The purposes of the other static pressure probes were to correct the measurements of the disk probe and their use as reference pressures.

Velocity Measurements

Three different probes were used to measure the total pressure. Two of the probes were commercial pitot-static tubes described earlier and the third was a commerical Kiehl probe.

The two pitot-static probes were used mainly for control and calibration. The pitot-static tube used to survey the static pressure above the hill was also incorporated as a standard used to calibrate the hot-wire probes. The second, which was maintained as a static-pressure reference, monitored the tunnel flow. This second probe was fixed in the free stream approximately 1 m ahead of the models.

The mean velocity measurements made during the surveys were sampled with the Kiehl probe. This probe has the capability of measuring total pressure even when the flow angles are ±40°. The disk probe pressure was used as a reference.

For the range of velocities measured in the present study all three probes agreed with the laboratory standard pitot probe. No correction to the readings were made because of the total pressure probes.

Turbulence and Shear Stress Measurements

Two types of hot-wire data were recorded. In the initial test a cross-wire system was used, while in the second a single horizontal wire fulfilled the requirement. The cross wire employed was not of the usual x wire type, but had one wire normal and one wire yawed to the flow. Both probes were constructed in the Fluid Dynamics and Diffusion Laboratory at Colorado State University. The wire in both cases was 80% platinum and 20% iridium and 1.02×10^{-3} cm in diameter. The length of the wires varied but all were approximately .16 cm. The wires were soldered at each end to a support which was protruding from a ceramic probe shielded by brass tubing. The sensor was then secured to the actuator system. A detailed discussion of the evaluation of the hot-wire output is given in Appendix A.

The hot wires were operated with commercial constant temperature anemometers. The output of the anemometers was amplified and read with mean d.c., and true r.m.s. voltmeters. The voltmeters were equipped with R-C time constants to allow long time averages of the signals. An analog multiplier was employed to obtain the product of the fluctuating output of the cross wires. The multiplier circuit was checked using a sine-wave generator.

Two capacitance pressure transducers were used for pressure measurements. The transducers were calibrated using a standard water micromanometer. These transducers are equipped with self-environmental

control to maintain a constant operating temperature. Figure 13 is a schematic of the equipment setup.

Chapter IV

RESULTS AND DISCUSSION

The major effect of a hill is to increase the local velocity near the surface. This effect is of great importance in wind power application. The alteration of the mean wind profile will also be expected to alter the turbulence near the surface. Thus, the present study was directed at evaluating the effect of the hill on the mean and turbulent properties. Such data is needed in order to design wind power units.

Mean Velocity

Primary consideration for wind power is the change in the mean velocity distribution. It was found as the flow proceeded down the tunnel that similarity was maintained, Figure 14. At the windward foot of the model hills a slowdown of the airstream near the surface was evident. Once the flow passed over the base of the hill there was a continuous increase of the velocity near the surface. The greatest speedup for all models tested was recorded at the crest. The similarity was maintained in the outer region of the flow, Figure 15. It is important to note that the outer flow pressure was fixed approximately constant which would help the flow to remain similar in the outer region. The largest increase in velocity for the first flow case was recorded with the 1:4 hill followed by the 1:6 and finally the 1:2, Figure 16.

Flow case II with increased upstream roughness produced the same results for the two models tested, 1:2 and 1:6, Figure 17.

The 1:2 and 1:6 model hills caused a greater mean velocity speedup for flow case I than for flow case II. Flow case I, with a .17 power law profile, produced a maximum speedup, ΔS, of .62 for the 1:6 model hill and .33 for the 1:2 model hill where

$$\Delta S = \frac{U_{crest}(\eta) - U_{upstream}(\eta)}{U_{F.S.}} \tag{16}$$

and $\eta_{crest} = \eta_{upstream} \approx 0.5$. The 1:4 model hill gave the maximum speedup of .68 for the same flow case. Flow case II, representing a .26 power law profile, was subjected to maximum speedups of .43 and .26 for the 1:6 and 1:2 model hills respectively.

Note that the turbulence terms are non-dimensionalized by dividing by τ_w or τ_{ref}. As described earlier τ_w are values calculated for upstream profiles. The values used were $\tau_w = .1074 \ n/m^2$ for flow case I at $x = 5.88$ cm and $.0952 \ n/m^2$ at $x = 50.80$ cm for flow case II.

Longitudinal Turbulent Velocities

The longitudinal turbulent velocities in both flow cases varied in the same manner. At the foot of the hill the greatest magnitudes were recorded. This was succeeded by a continuous decrease in $\sqrt{\overline{u^2}}$ near the surface with the decrease being greatest at the crest. A greater decrease in the longitudinal turbulent velocity component was noted for the second flow case with the larger values of approach turbulence. The alteration of the turbulence was restricted to that region near the wall, Figures 18, 19, 20, 21.

The longitudinal turbulent velocity component, $\sqrt{\overline{u^2}}$, compared closely with that found by Zoric (2) for the first test, Figure 22. As expected for the second flow case the $\sqrt{\overline{u^2}}$ component did not agree with Zoric but was higher. In both cases the measurements of the longitudinal turbulent velocity component were reproducible, Figure 23.

22

Vertical Turbulent Component

The vertical turbulent component, $\sqrt{\overline{v^2}}$, which was measured only in flow case I also varied as it passed over the hill. This turbulent component decreased up to the base of the hill, following them was a continuous increase in $\sqrt{\overline{v^2}}$ to the crest. The change only involved the flow near the surface, Figures 24 and 25. As discussed in Chapter II the increase in $\sqrt{\overline{v^2}}$ was expected from results for a contracting flow. When compared to Zoric's data in the outer region, the values obtained for $\sqrt{\overline{v^2}}$ were close. However, when compared to Tieleman's data (4) near the wall the measurements appear to be somewhat lower, Figure 26. (The data reported by Tieleman (4) were taken at a station almost 30 meters downstream in the tunnel compared to the present data taken at a distance of 14 meters.) The disagreement may in part be attributed to the strong velocity and turbulent gradients acting on the yawed wire in this region. A problem which Tieleman compensated for when he presented his results. A discussion of this is given by Sandborn (12). In addition, the first flow case may not be a true flat plate flow. There could have been some change in the flow because of the false floor.

Shear Stress Distribution and Surface Static Pressure

As the flow passed from the furthest upstream station toward the base of the hills there was a decrease in surface shear stress and an increase in the surface static pressure. After passing the foot of the hill, the trend reversed and an increase in wall shear was present. The surface static pressure decreased along the reach of the hill. Figure 27 shows the change in surface shear stress and surface static pressure as friction and pressure coefficients where

$$C_f = \frac{\tau_{wall\ local}}{1/2\ \rho U^2_{local}} \qquad (17)$$

and

$$C_p = \frac{P_{static\ local} - P_{static\ F.S.}}{1/2\ \rho U^2_{local}} \qquad (18)$$

The surface shear stress at each station was estimated using the Ludwieg-Tillmann equation and the "law of the wall." The values found using the "law of the wall" may be somewhat questionable for the pressure gradients obtained. Based on work done by Patel (5) which was described earlier, the "law of the wall" applies within approximately 6% in the range of

$$0 > \frac{\nu}{(\rho U^3_\tau)}\frac{dP}{dx} > -.007 \qquad (4)$$

For the present study the range was exceeded. For the 1:6 hill an average of about $\Delta \simeq .032$ was computed. As a result, the values obtained for the wall shear stress on the surface of the hill would be expected to be consistently high. However, the numbers obtained do give approximate values. For the 1:6 and 1:2 hills the Ludwieg-Tillmann equation gives lower values than the "law of the wall."

The affect of the hill on the shear stress distribution was a local one. The shear stress distribution remained unaffected in the outer region. Near the wall the distribution changed accordingly with the wall shear stress, Figure 28. For Figures 28 ai, aii, bi, ci, cii, 29, and 30 all the points shown were calculated from the similarity equation (15). For the other cases shown on Figure 28 the data points were evaluated from the cross-wire data. The curves through the cross-wire

data were faired using the upstream similarity distribution and an approximate extrapolation to the known surface shear stress value. The local slope of most of the shear stress curves at the wall $(\partial \tau / \partial y |_{y=0} = \partial P / \partial x)$ are very steep, and as such were not shown on the fairings.

In Chapter II an explanation was given for the method used to evaluate the upstream shear stress distributions. Because the analysis depends on the mean velocity measurements and not the direct measure of the Reynolds stresses it was possible to evaluate for both flow cases the upstream shear stress distribution. When compared to Zoric's data, it was found that the shear stress distribution of the first test was repeatedly lower, Figure 29. Again this is attributed to the false floor. The second flow case yielded a similar result. However, these results were higher than that found in flow case I but still less than what Zoric found, Figure 30.

The Reynolds stresses, $\overline{uv}$, were employed to evaluate the vertical turbulent velocity component $\sqrt{\overline{v^2}}$. The cross correlation $\overline{uv}$ was the most uncertain term to evaluate. It was believed that a multiplying circuit used in the measurements did not function as well as desired. The result was a greater scatter in the data for the $\overline{uv}$ terms. Determination of the $\sqrt{\overline{v^2}}$ terms was also affected but since it is presented as a square root the scatter does not appear so pronounced.

Chapter V

CONCLUSIONS

The present investigation studied two different flow cases subjected to three different triangular hills. These two-dimensional model hills with aspect ratios of 1:2, 1:4 and 1:6 changed the mean and turbulent properties of the flow near the surface. From the experimental evidence the following conclusions can be drawn.

1. As the flow progressed from the upstream station to the crest there was no effect from the hill on the flow properties in the outer region. The flow properties included are mean velocity and the longitudinal and vertical turbulent velocities along with the shear stress.

2. For the region near the wall there was a velocity speedup as the flow passed over the hill with the maximum above the crest. The greatest speedup was for the 1:4 hill.

3. The longitudinal turbulent velocity, $\sqrt{\overline{u^2}}$, increased to the foot of the hill then decreased as the flow passed over the hill. The decrease is greater for a turbulent boundary layer with larger turbulent velocities. The decrease is on the order of 12%.

4. The vertical turbulent velocity $\sqrt{\overline{v^2}}$ decreased as the flow approached the base of the hill then increased to the summit. Both the increase in the vertical turbulent velocity and the decrease in the longitudinal turbulent velocity were consistent with theoretical results for a contracting flow.

5. The shear stress term $\overline{uv}$ and the wall shear stress decreased from the upstream station to the base of the hill. Over the hill an increase of the shear stress was found.

6.   A decrease in surface pressure and increase in wall shear coincided with the increase in mean velocity. The opposite was true when the mean velocity decreased.

REFERENCES

1. Zoric, D. and Sandborn, V. A.: Similarity of Large Reynolds Number
    Boundary Layers. Boundary Layer Meteorology, Vol. 2, No. 3,
    pp. 326-333, 1972.

2. Zoric, D. L.: Approach of Turbulent Boundary Layer to Similarity.
    Ph.D. Dissertation, Colorado State University, Report CER68-69DLZ9,
    1968.

3. Ribner, H. S. and Tucker, M.: Spectrum of Turbulence in a
    Contracting Stream. National Advisory Committee for Aeronautics
    Rep. 1113, 1953.

4. Tieleman, H. W.: Viscous Region of Turbulent Boundary Layer. Ph.D.
    Dissertation, Colorado State University, Report No. CER67-68HWT21,
    1967.

5. Prandtl, L.: Recent Results of Turbulence Research. NACA Tech.
    Memo. 720, 1933.

6. Patel, V. C.: Calibration of the Preston Tube and Limitations on
    Its Use in Pressure Gradients. J. Fluid Mech., Vol. 23, Part 1,
    pp. 185-208, 1965.

7. Sandborn, V. A. and Horstman, C. C.: Boundary Layer Shear Stress
    in Subsonic and Supersonic Flow. Symposium on Turbulent Shear
    Flow, Pennsylvania State University, 1977.

8. Klebanoff, P. S.: Characteristics of Turbulence in a Boundary
    Layer with Zero Pressure Gradient. NACA TN 3178, 1954.

9. Sandborn, V. A.: Class Notes for Experimental Methods in Fluid
    Mechanics. Civil Engineering Department, Colorado State University,
    CER71-72VAS40, 1972.

10. Sandborn, V.A.: A Review of Turbulence Measurements in Compressible
    Flow. NACA Tech. Memo., X62, 337, March, 1974.

11. Schlichting, H.: Boundary Layer Theory. McGraw-Hill Book Company,
    Inc., New York, 1960.

12. Sandborn, V. A.: Effect of Velocity Gradients on Measurements of
    Turbulent Shear Stress. Colorado State University, AIAA J.,
    Vol. 14, No. 3, pp. 400-402, March, 1976.

FIGURES
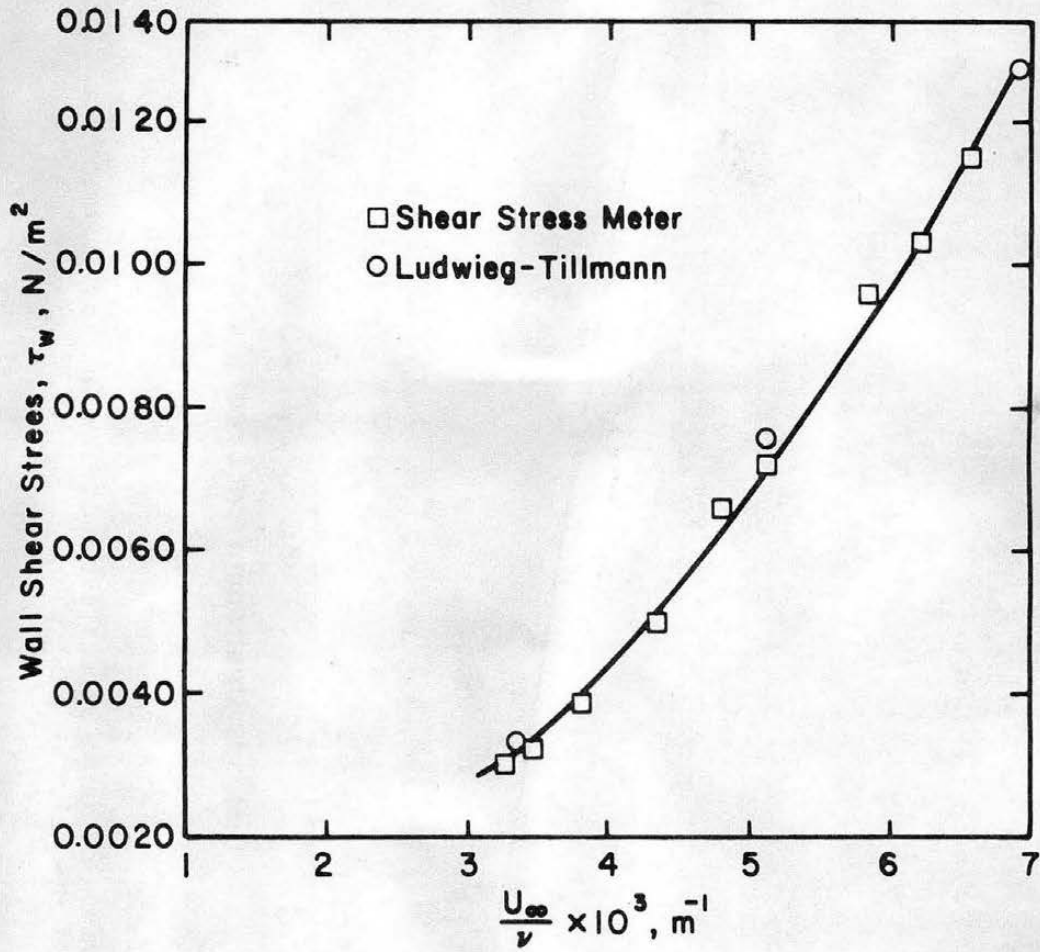
Figure 1. Comparison of Ludwieg-Tillmann equation and shear-stress meter (4).
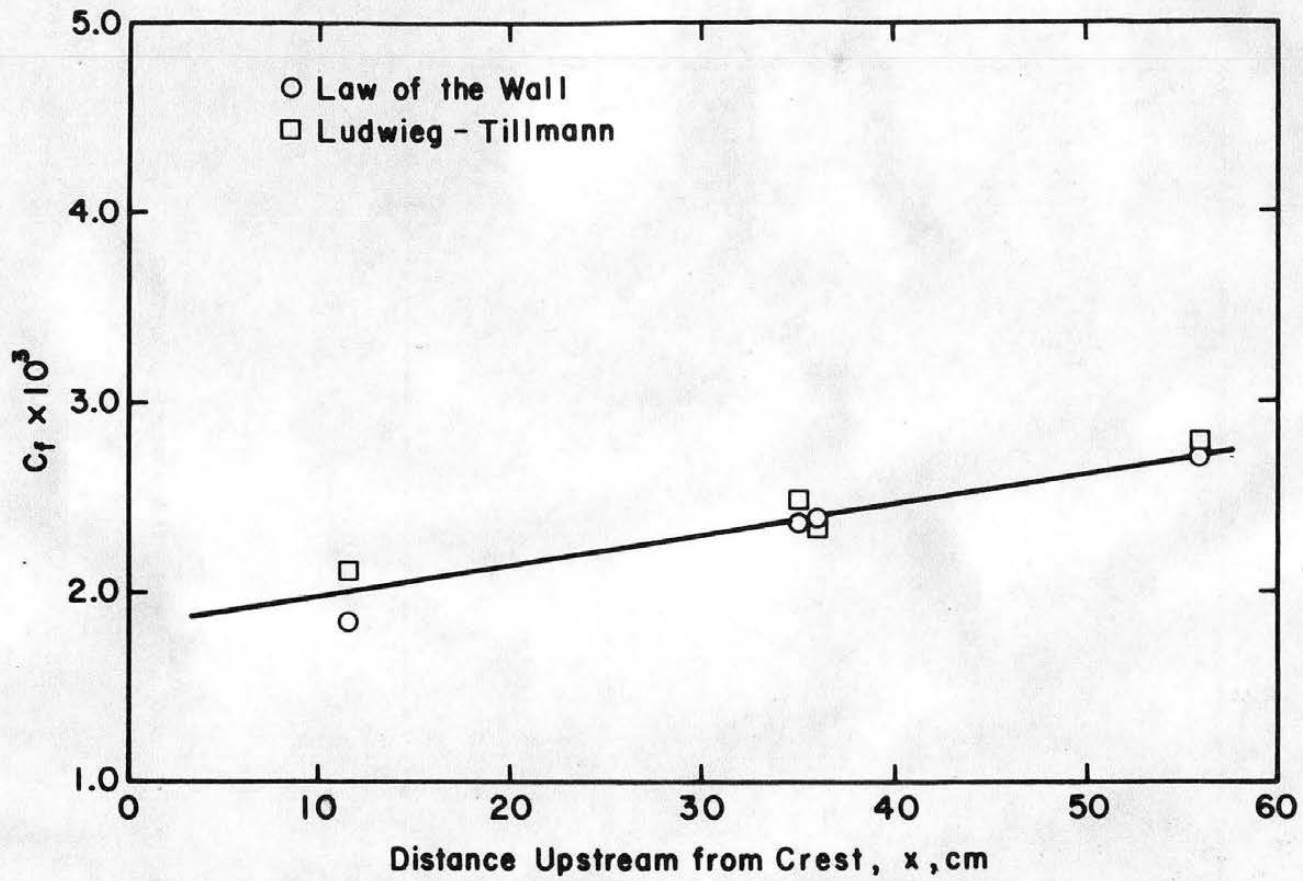
Figure 2. Comparison of shear stress evaluated by Ludwieg-Tillmann equation and "law of the wall" on flat plate.
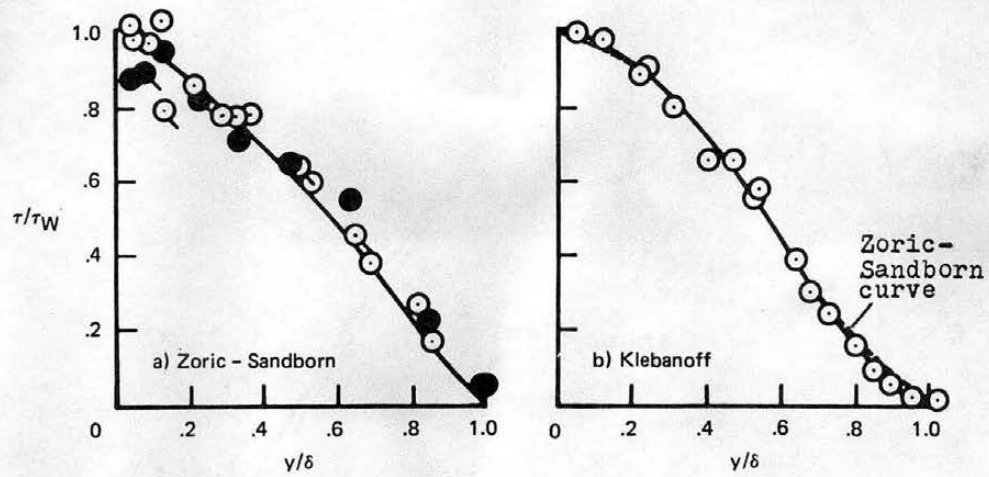
Figure 3. Comparison of shear stress distribution
zero pressure gradient and values
determined from equation 15, (7).
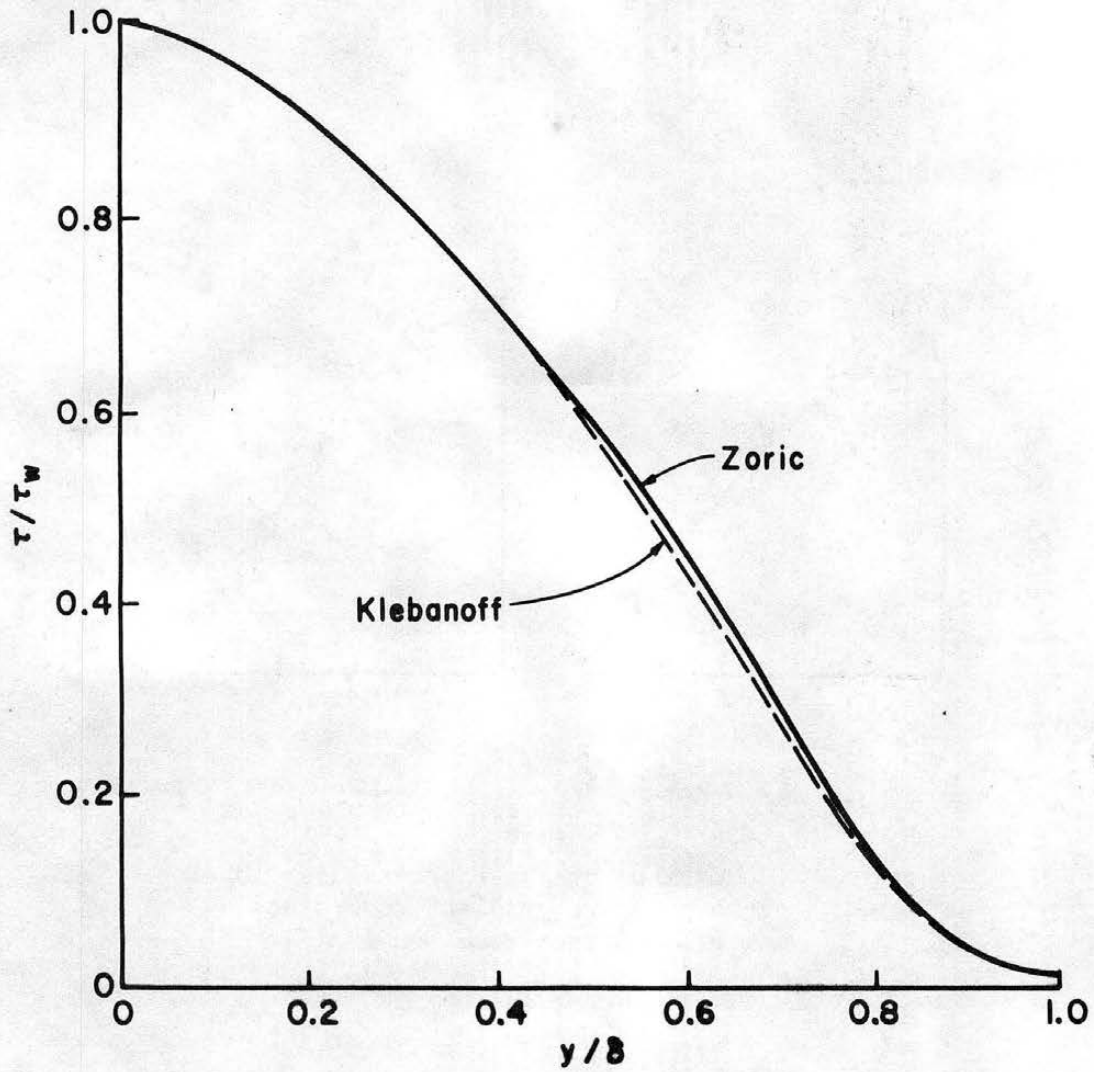
Figure 4. Comparison of shear stress measurements by
Klebanoff and Zoric (10).
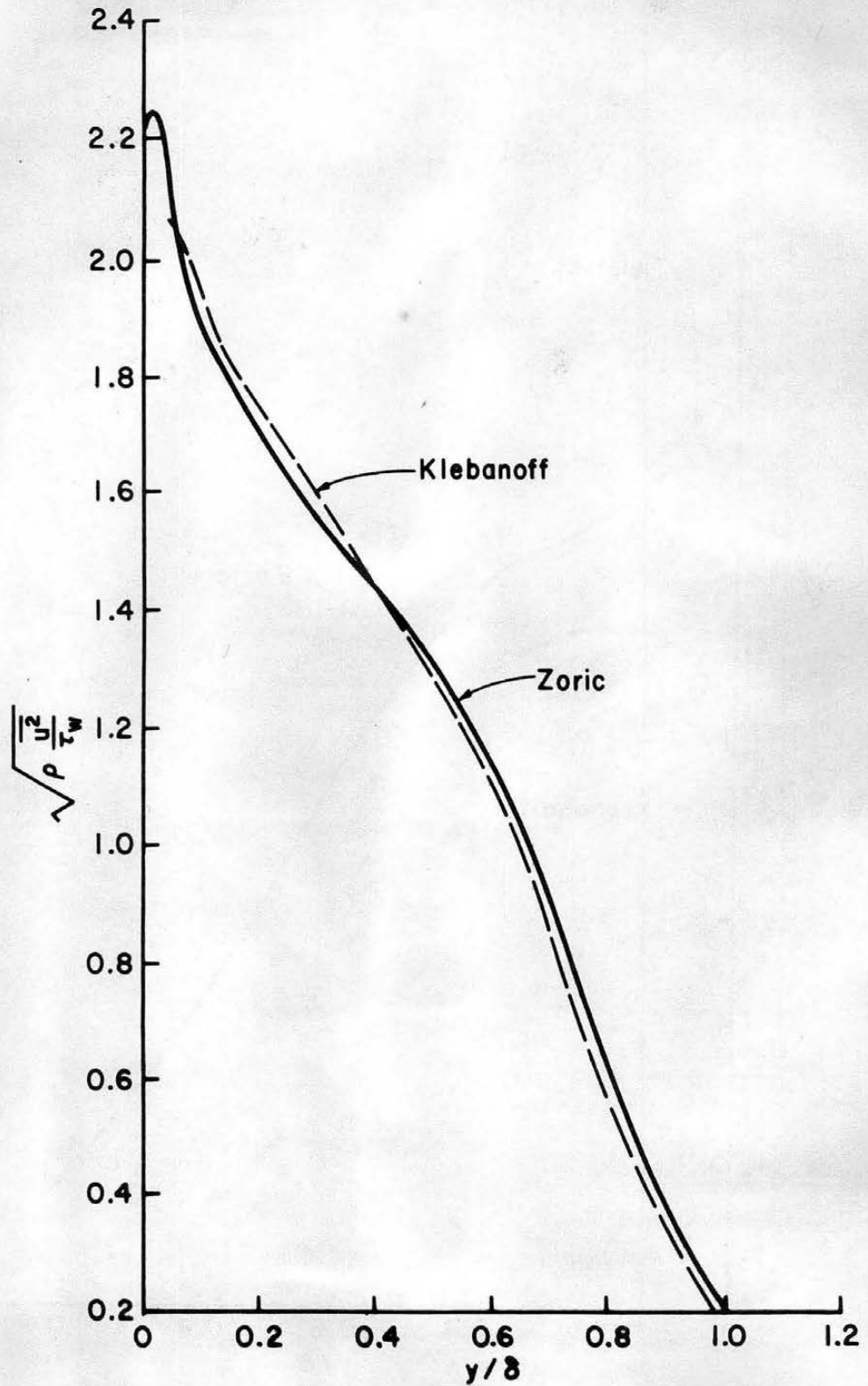
Figure 5. Comparison of flat plate longitudinal
turbulent velocity distribution of
Klebanoff and Zoric (10).
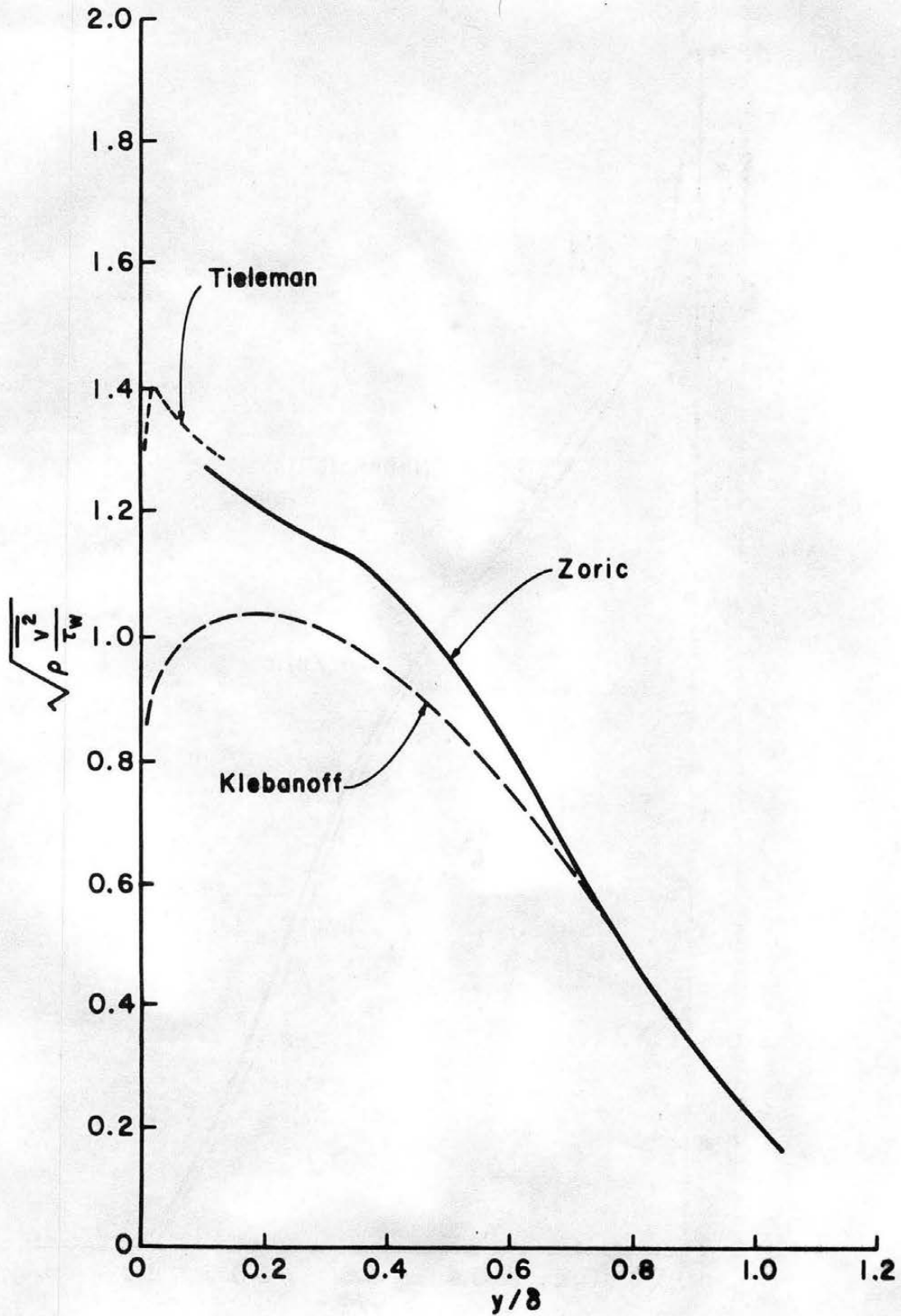
Figure 6. Comparison of flat plate vertical turbulent
velocity distribution of Klebanoff, Zoric
and Tieleman (10).
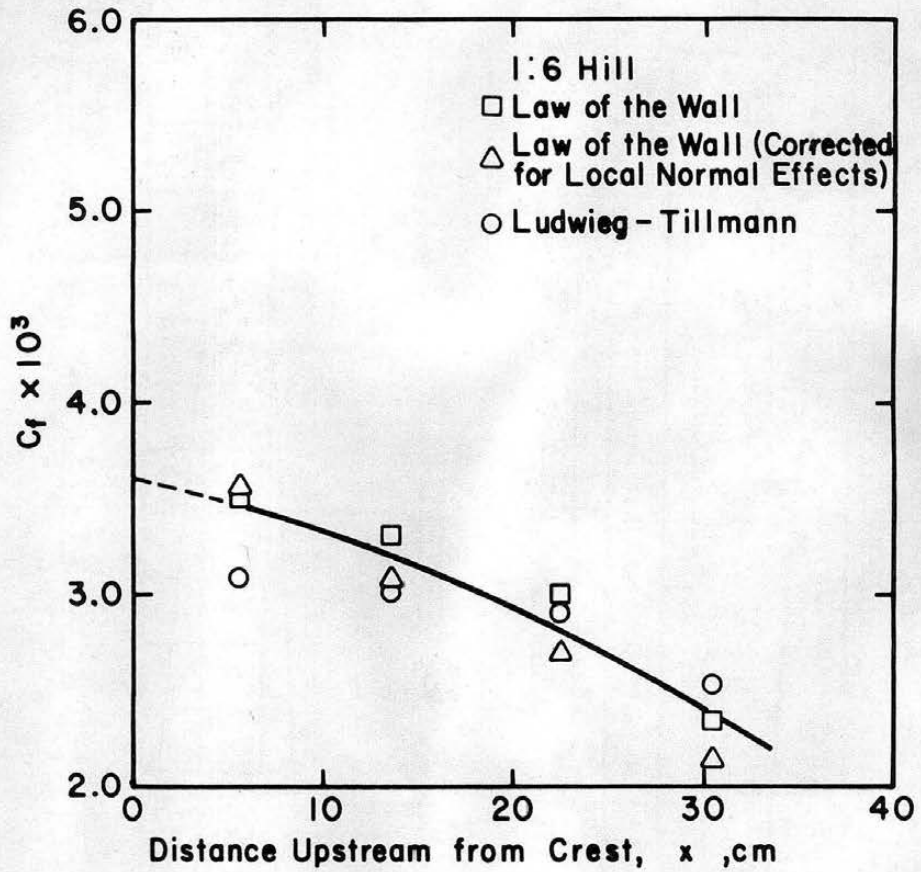
Figure 7. Shear stress evaluated by the "law of the wall" for standard coordinates and curvilinear coordinates.
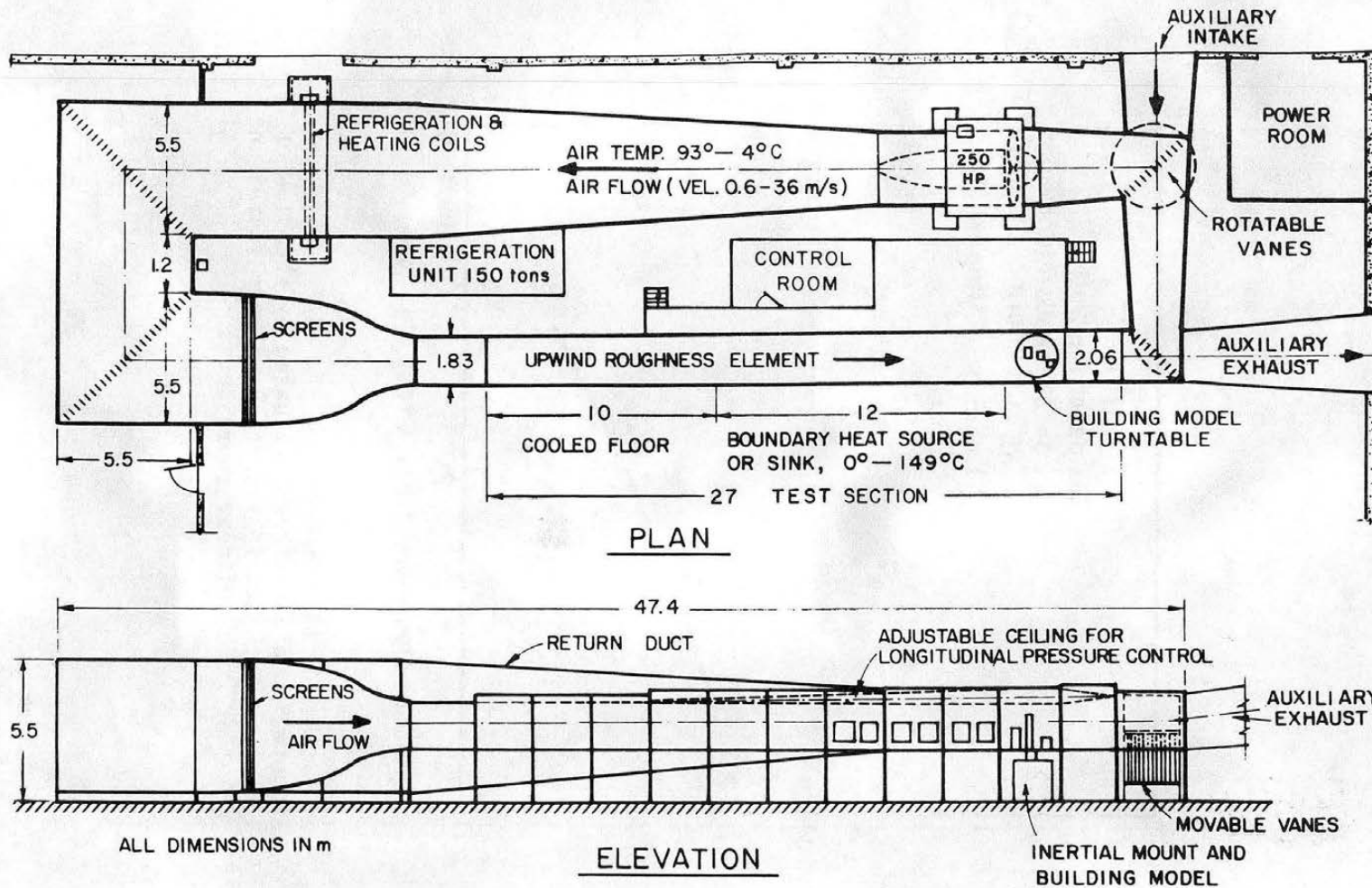
Figure 8.   METEOROLOGICAL WIND TUNNEL (Completed in 1963)

BOUNDARY-LAYER TRIP

FLOW

5.6 m

START OF UP RAMP - FALSE FLOOR

1.3 m

START OF HORIZONTAL FLOOR
END OF UP RAMP

7.1 m

HILL

CREST OF MODELS

1.45 m

START OF DOWN RAMP
END OF HORIZONTAL FLOOR

.9 m

END OF DOWN RAMP - FALSE FLOOR
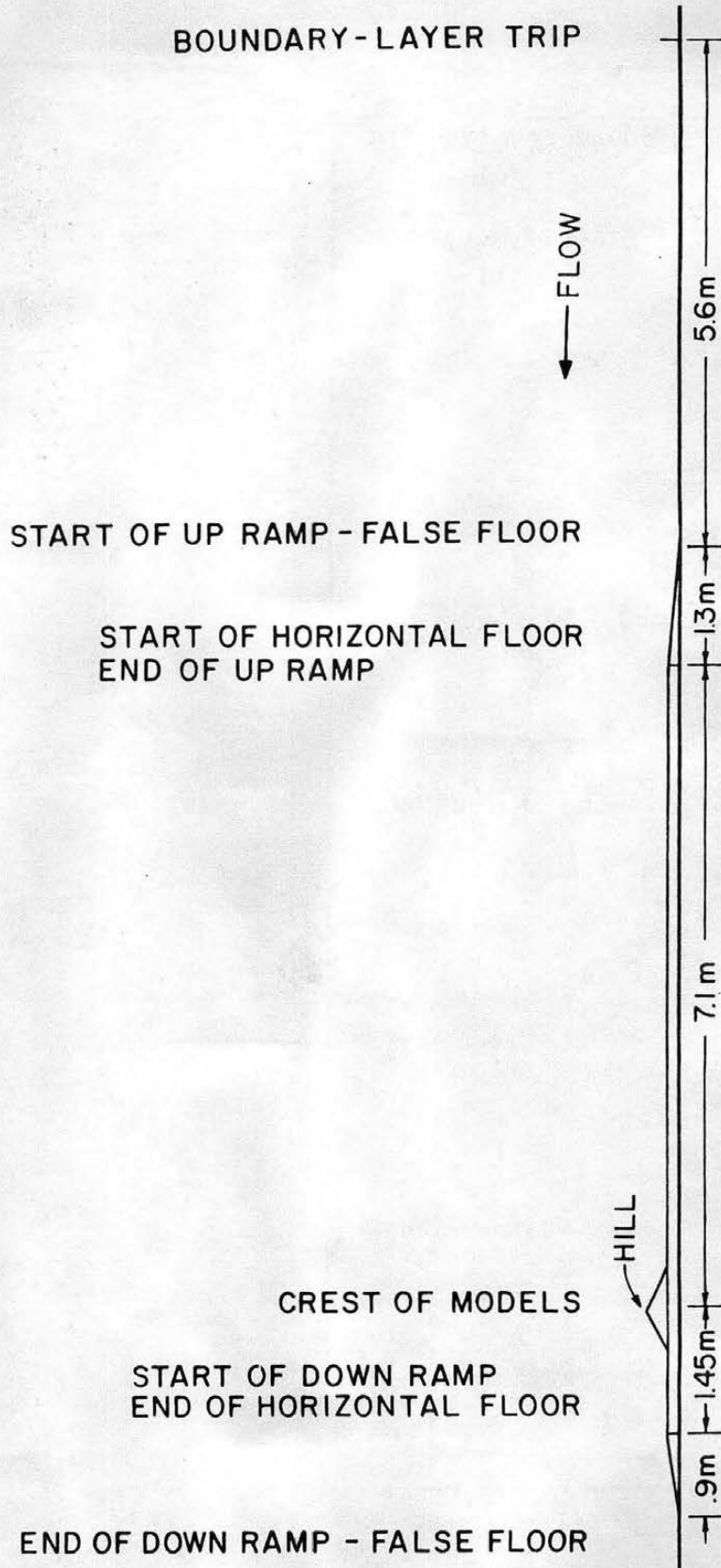
Figure 9. Tunnel setup for flow case I.

38

Boundary-Layer Trip

Start of Roughness

Flow

1.8m

9.6m

End of Roughness

7.2m

Crest of Models
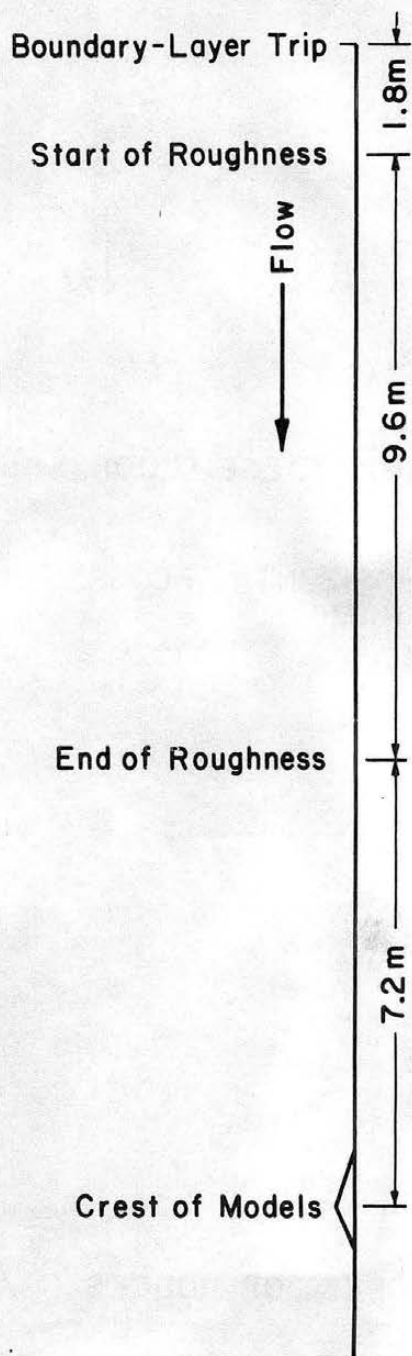
Figure 10.   Tunnel setup for flow case II.
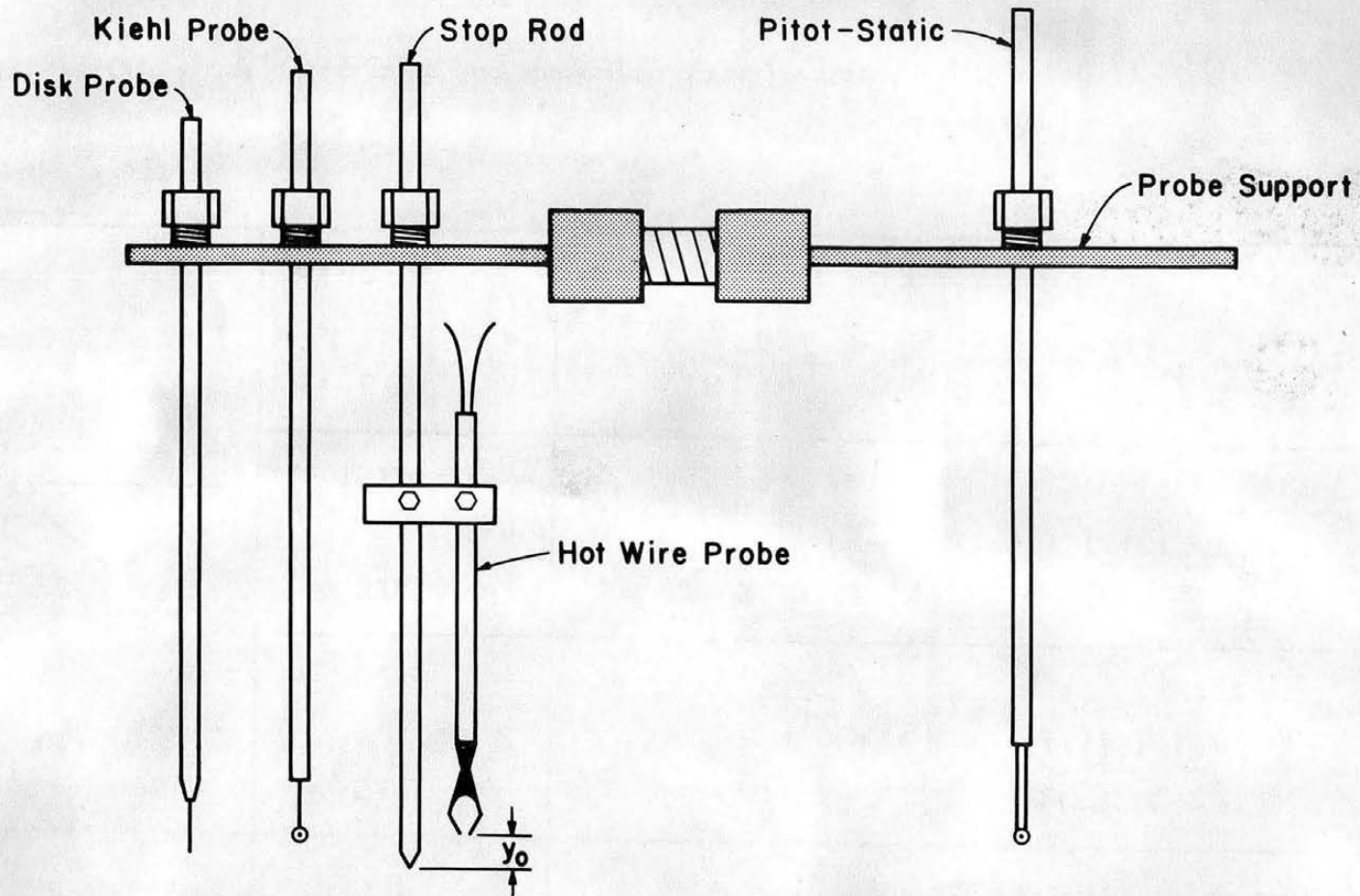
Figure 11. Schematic of probes.

39

(Dimensions in centimeters)

Hill Shape	Height-Length Ratio	Location of Static Pressure Taps along Surface of Hill ⟵ $\overline{U}$
	h = 5.08 1 : 2 b = 20.32	1.91 2.54 1.27 1.27 1.27 1.27 0.64 0.64 0.64 0.64 1.27 1.27 1.27 1.27
	h = 5.08 1 : 4 b = 40.04	2.54 2.54 2.54 2.54 2.54 1.27 1.27 1.27 1.27 1.27 1.27 2.54 2.54 2.54 2.54
	h = 5.08 1 : 6 b = 60.96	5.08 5.08 5.08 2.54 2.54 1.27 1.27 2.54 2.54 2.54 2.54 2.54 2.54 2.54

Crest

Figure 12. Model description and instrumentation location.

40

Figure 13. Schematic of equipment setup.

Pitot-Static
or
Kiehl Disk

Equibar
Pressure
Meter

True
R.M.S.
Voltmeter

D.C.
Integrating
Digital
Voltmeter

Hot Wire
Probe

Hot-Wire
Anemometer
and
Amplifier

True
R.M.S.
Voltmeter

True
R.M.S.
Voltmeter

Analog
Multiplier

D.C.
Integrating
Digital
Voltmeter

D.C.
Integrating
Digital
Voltmeter

D.C.
Integrating
Digital
Voltmeter

———— Horizontal Wire
— — — Cross Wire

41

Flow Case I (a)

Hill
○ 1:2
△ 1:4
□ 1:6

y/δ

$U(y)/U_{F.S.}$

Flow Case II (b)

Hill
○ 1:2
□ 1:6

y/δ

$U(y)/U_{F.S.}$

42

Figure 14. Velocity similarity profiles for both flow cases.
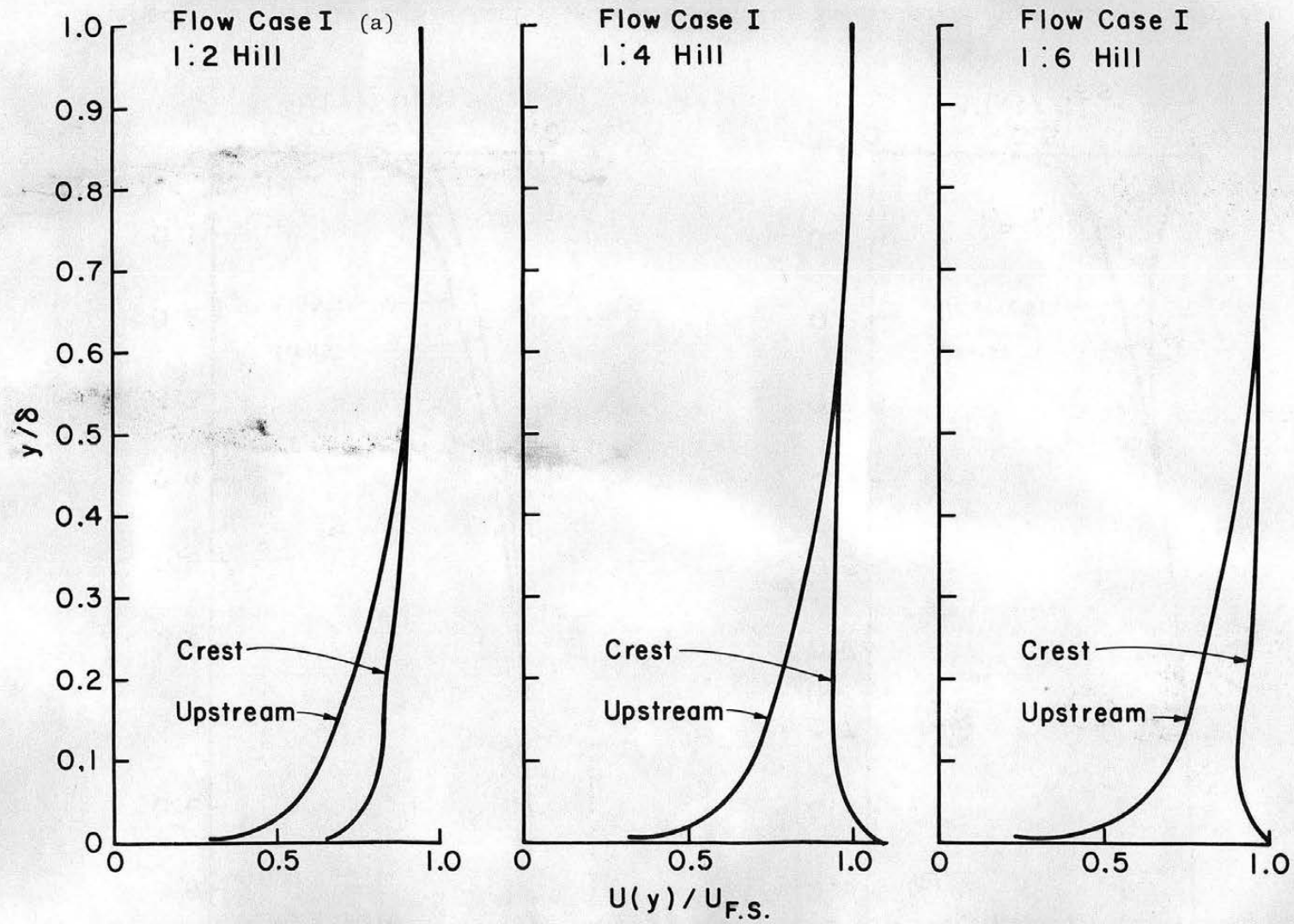
Figure 15a.   Upstream similarity velocity profiles and velocity profiles at the crest.

43
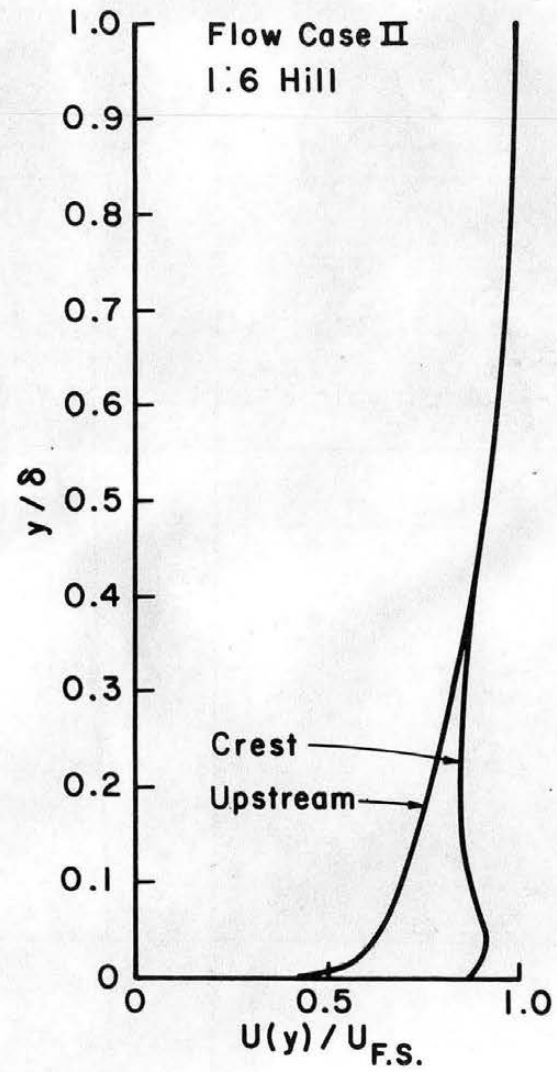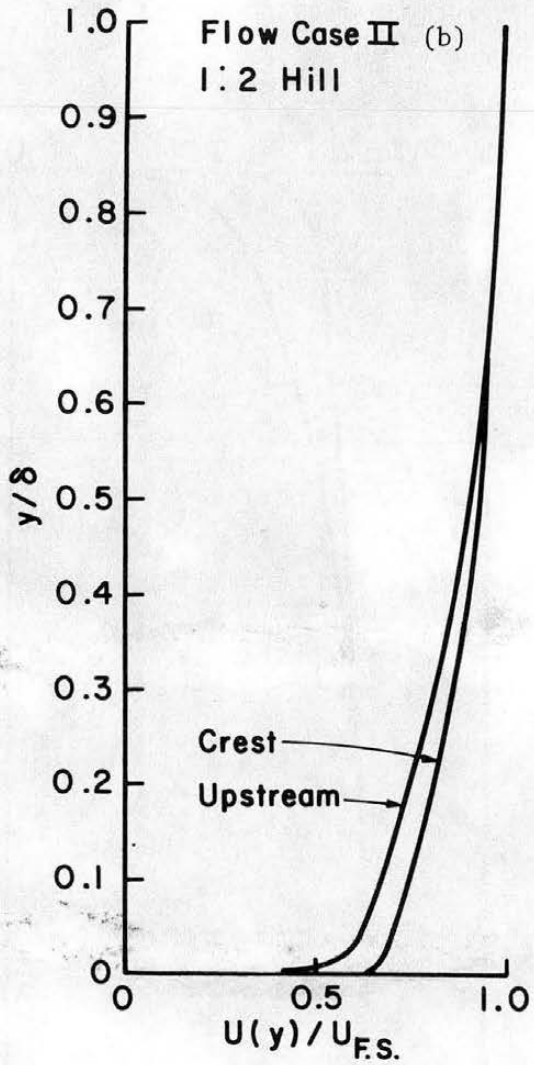
Figure 15b. Upstream similarity velocity profiles and velocity profiles at the crest.
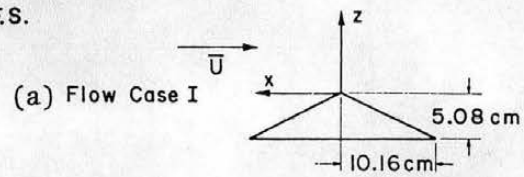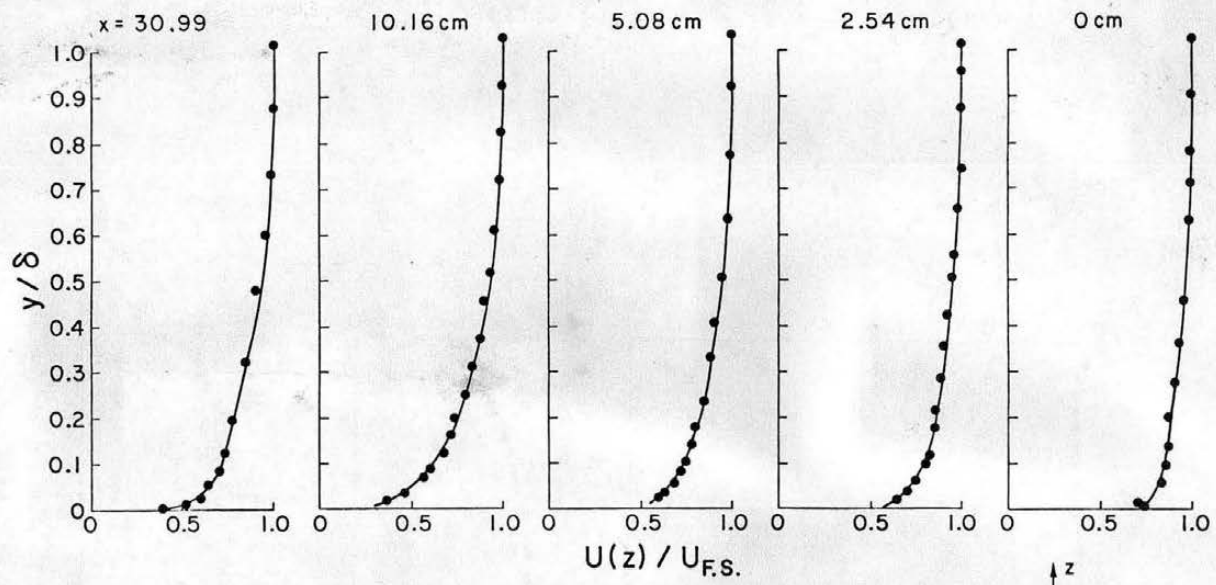
Figure 16a. Velocity profiles flow case I.
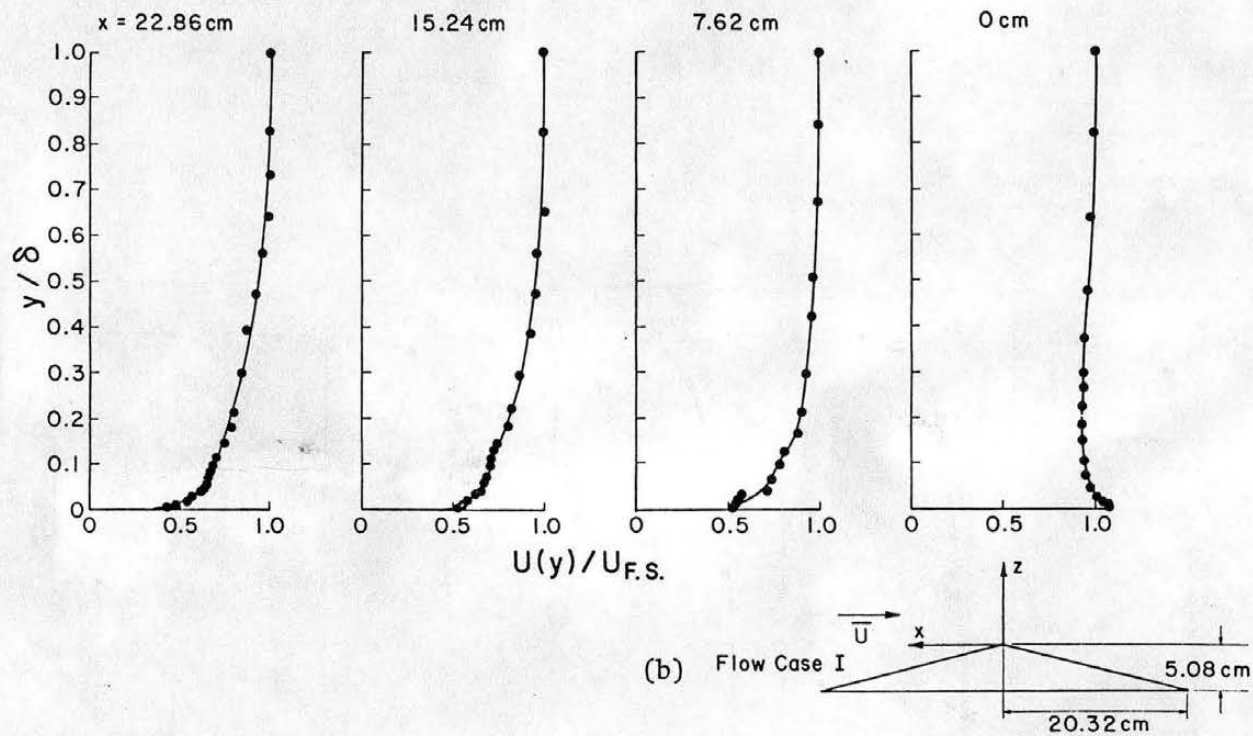
Figure 16b.   Velocity profiles flow case I.
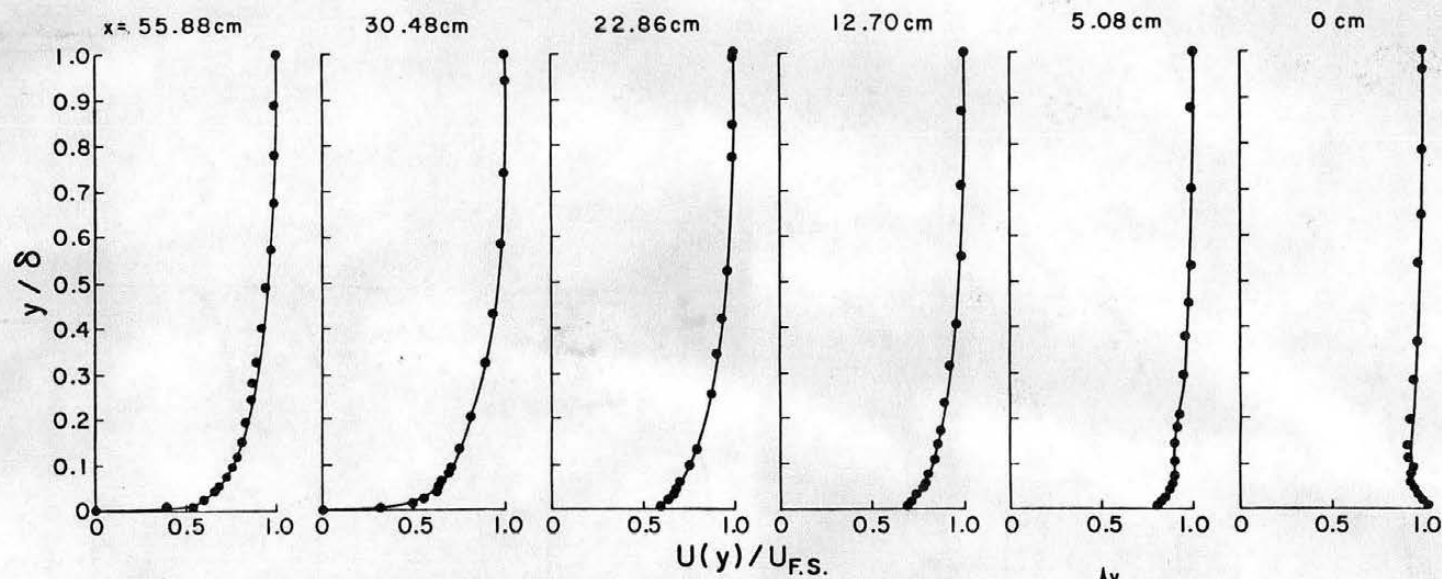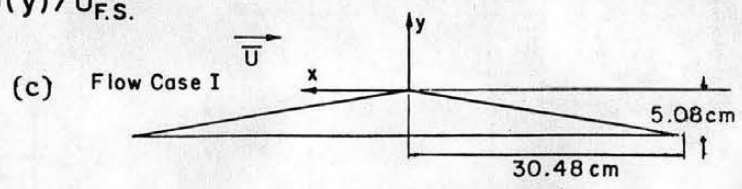
Figure 16c. Velocity profiles flow case I.

x = 50.80 cm   15.24 cm   10.16 cm   7.62 cm   2.54 cm   0 cm

y/δ

$U(y)/U_{F.S.}$

(a)   Flow Case II

$\overline{U}$ x   y

5.08 cm

10.16 cm
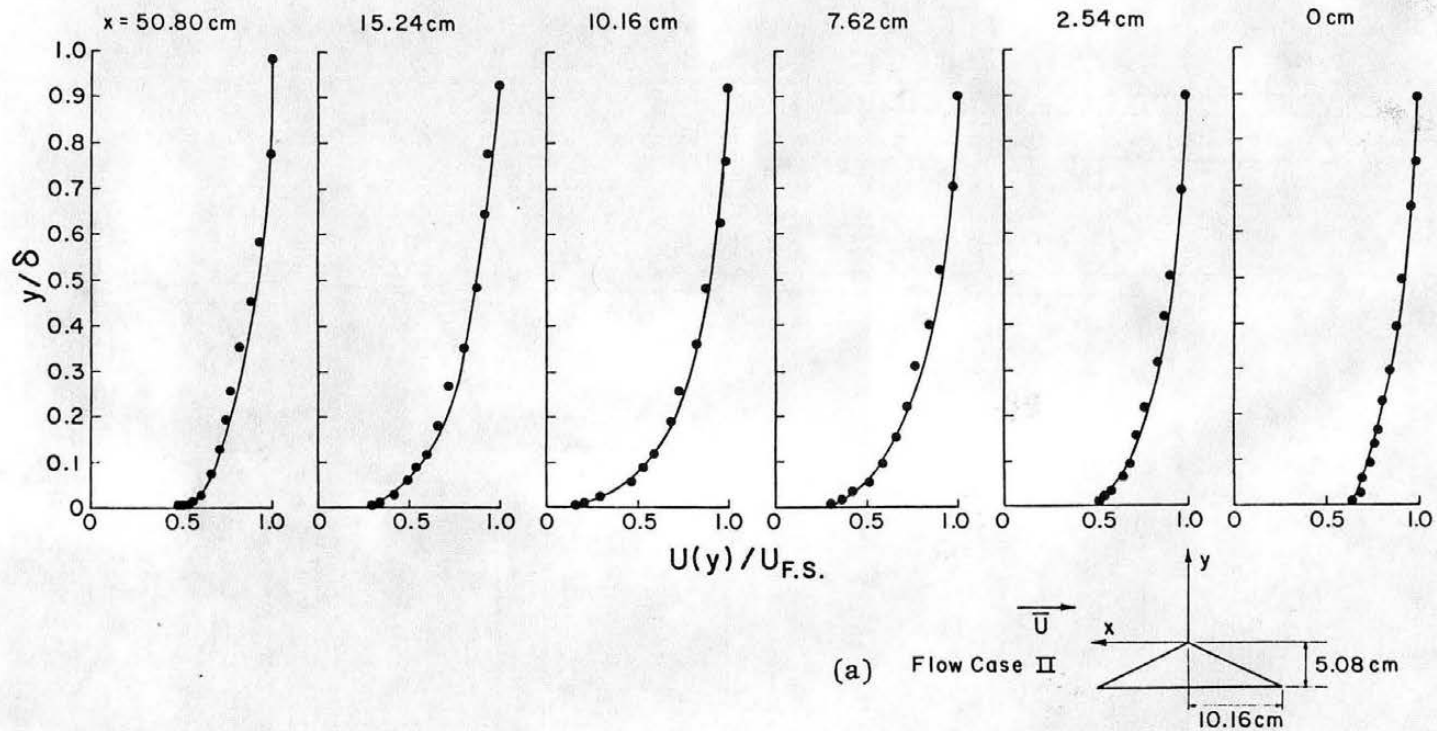
Figure 17a. Velocity profiles flow case II.

48
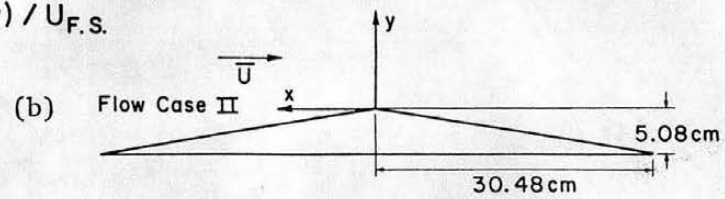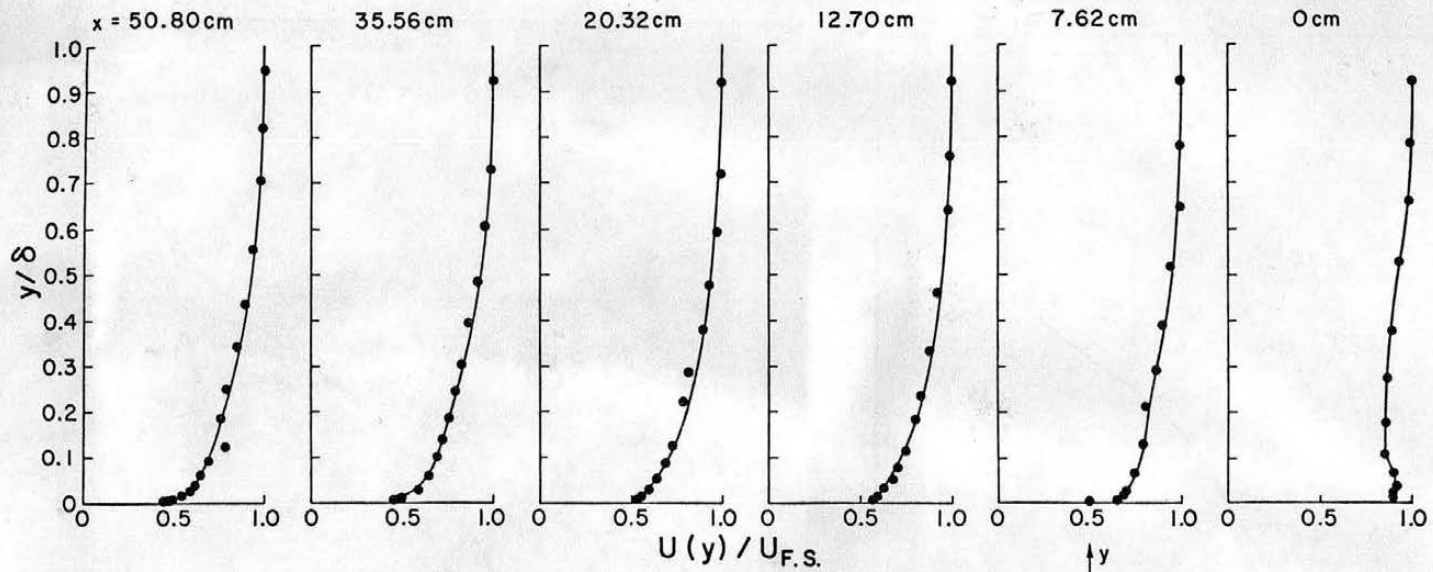
Figure 17b. Velocity profiles flow case II.
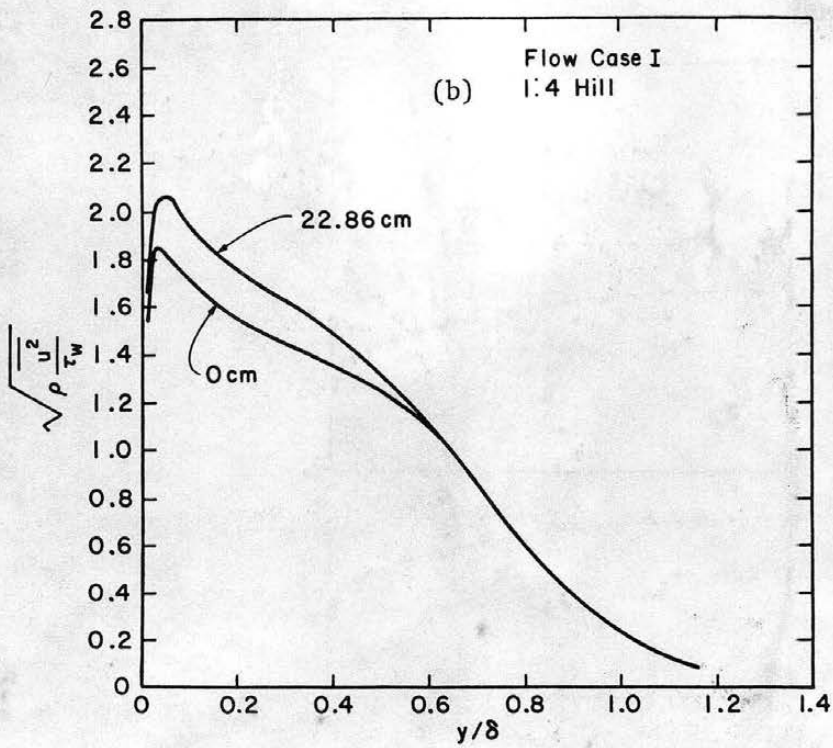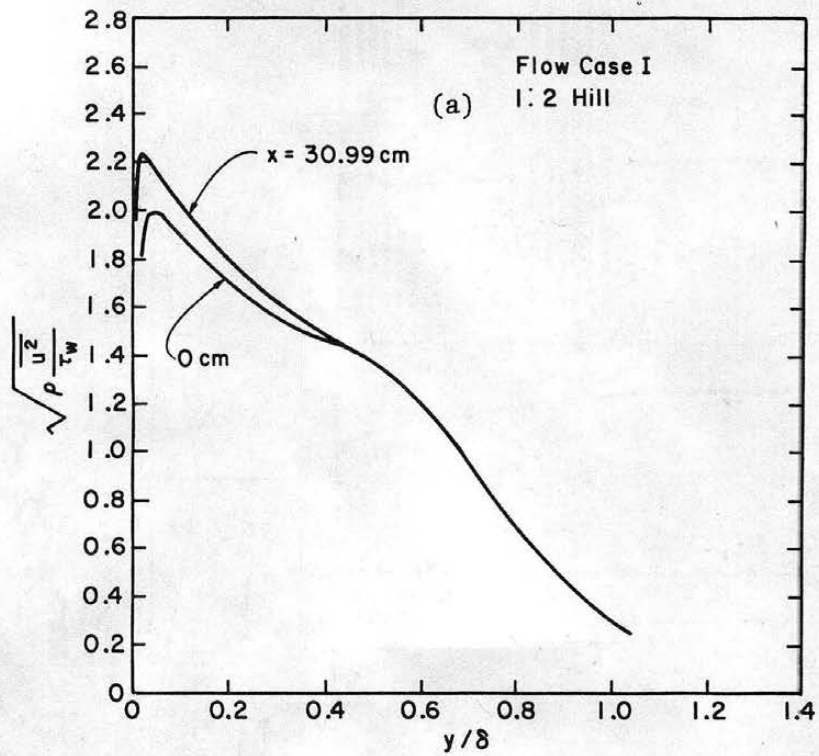
Figure 18. Upstream $\sqrt{\rho \dfrac{\overline{u^2}}{\tau_w}}$ measurements compared to $\sqrt{\rho \dfrac{\overline{u^2}}{\tau_w}}$ measurements at crest. Flow case I.
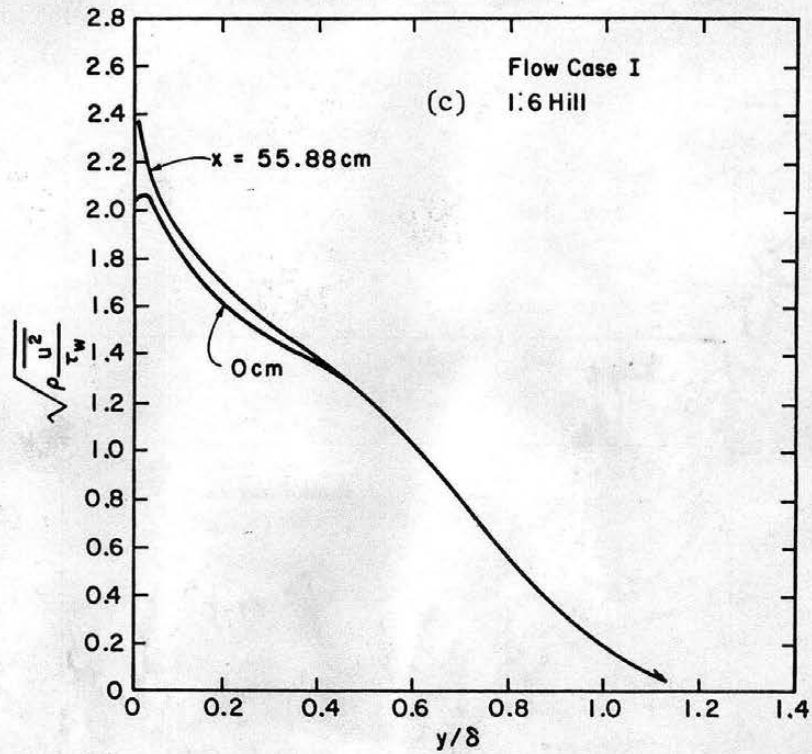
Figure 18 continued. Upstream $\sqrt{\rho \frac{\overline{u^2}}{\tau_w}}$ measurements compared to $\sqrt{\rho \frac{\overline{u^2}}{\tau_w}}$ measurements at crest. Flow case I.
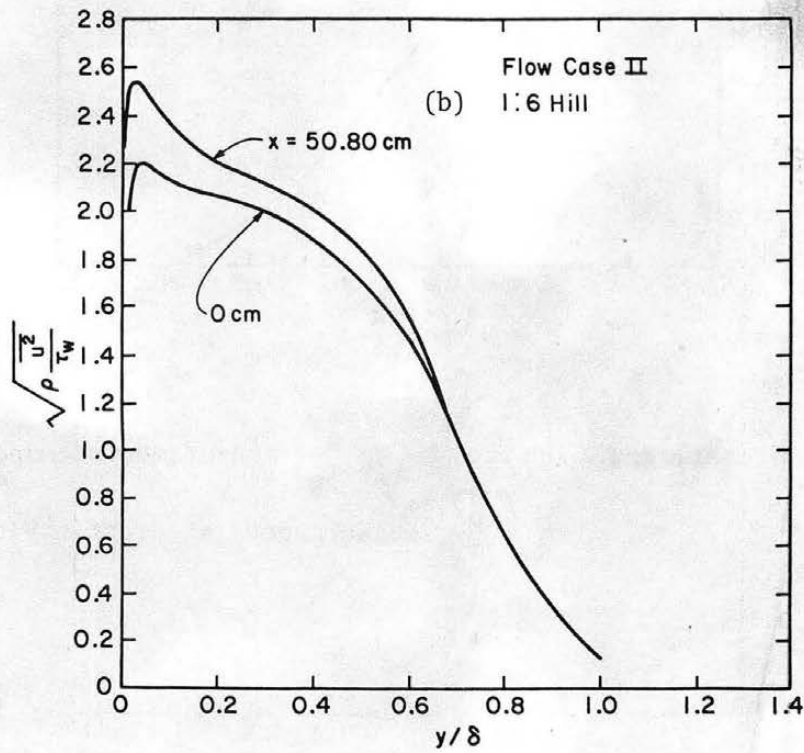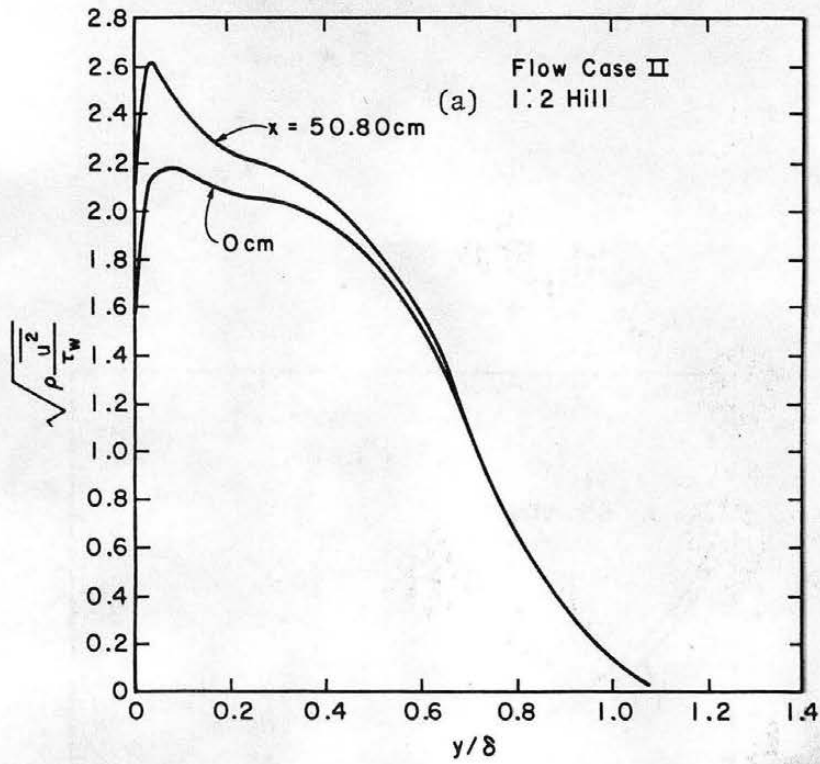
Figure 19. Upstream $\sqrt{\rho \dfrac{\overline{u^2}}{\tau_w}}$ measurements compared to $\sqrt{\rho \dfrac{\overline{u^2}}{\tau_w}}$ measurements at crest. Flow case II.
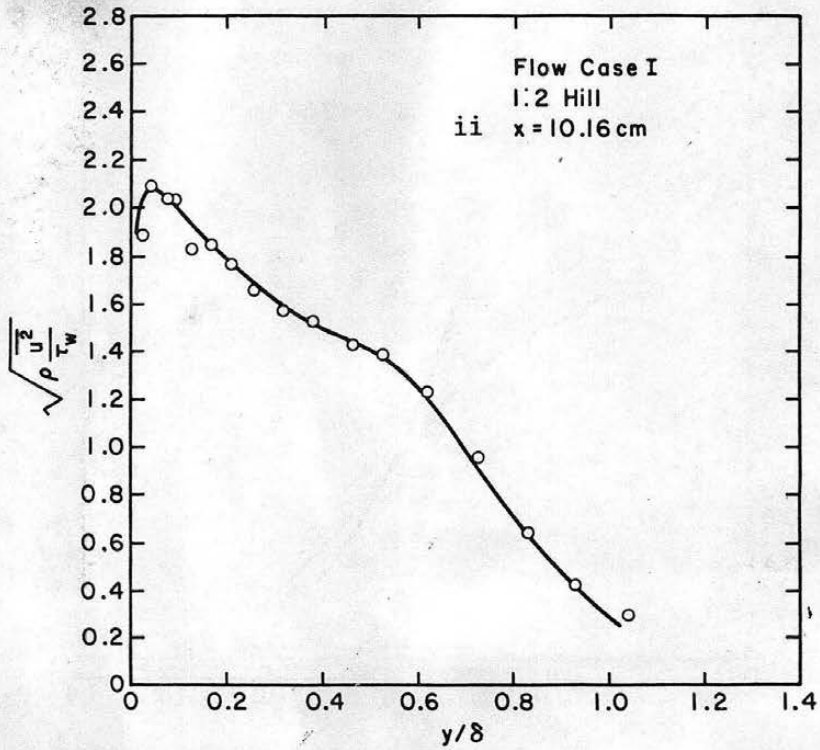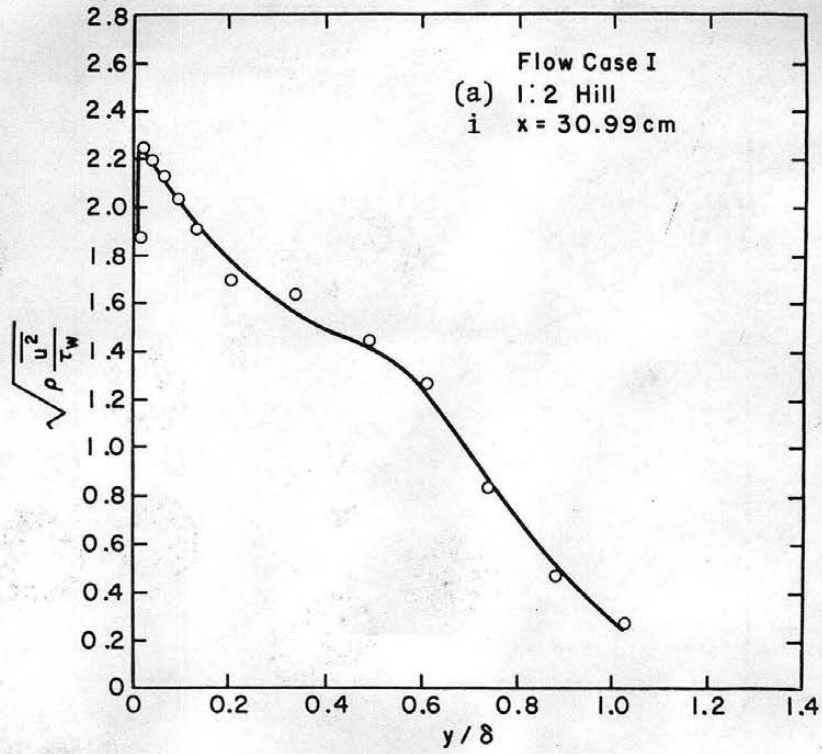
Figure 20. $\sqrt{\rho \dfrac{\overline{u^2}}{\tau_w}}$ profiles flow case I.

Figure 20. $\sqrt{\rho \dfrac{\overline{u^2}}{\tau_w}}$ profiles flow case I (continued).
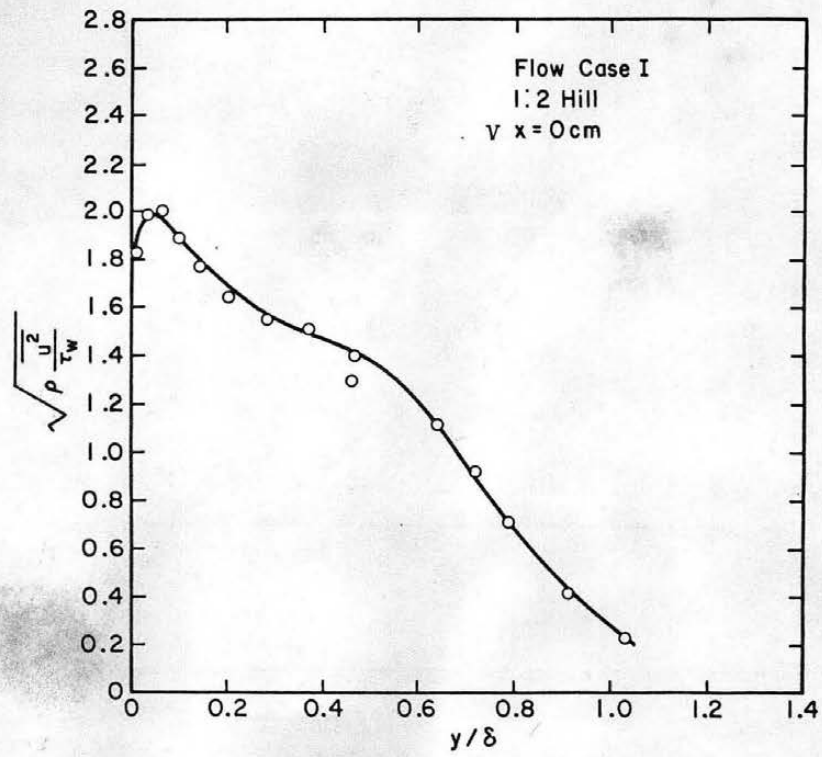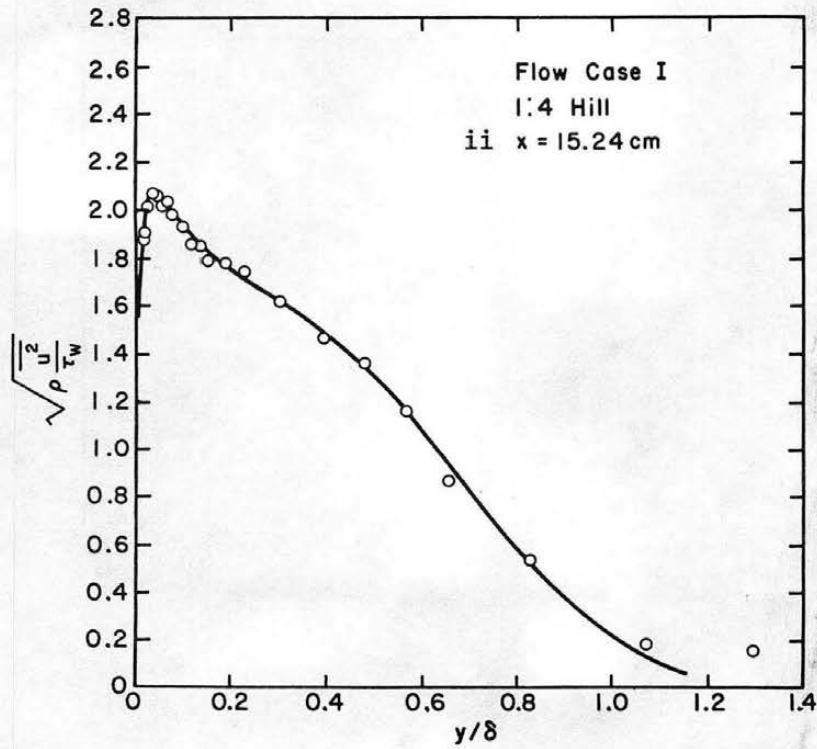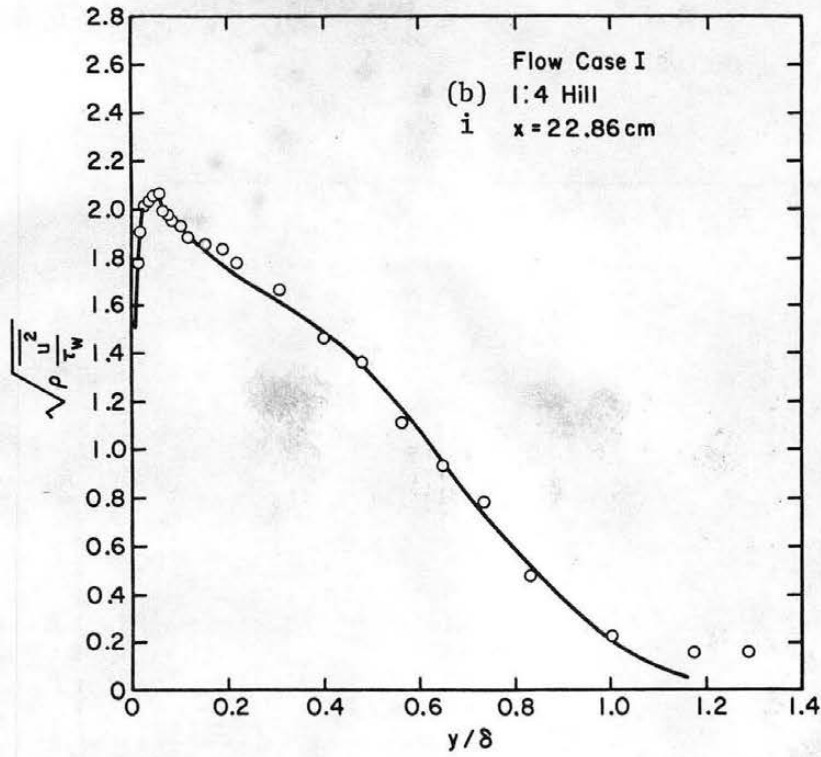
55

Figure 20. $\sqrt{\rho \dfrac{\overline{u^2}}{\tau_w}}$ profiles flow case I (continued).

Figure 20. $\sqrt{\rho \dfrac{\overline{u^2}}{\tau_w}}$ profiles flow case I (continued).

Figure 20. $\sqrt{\rho \dfrac{\overline{u^2}}{\tau_w}}$ profiles flow case I (continued).

58

Figure 20. $\sqrt{\rho \dfrac{\overline{u^2}}{\tau_w}}$ profiles flow case I (continued).

Figure 20. $\sqrt{\rho \dfrac{\overline{u^2}}{\tau_w}}$ profiles flow case I (continued).

Figure 20. $\sqrt{\rho \dfrac{\overline{u^2}}{\tau_w}}$ profiles flow case I (completed).

61
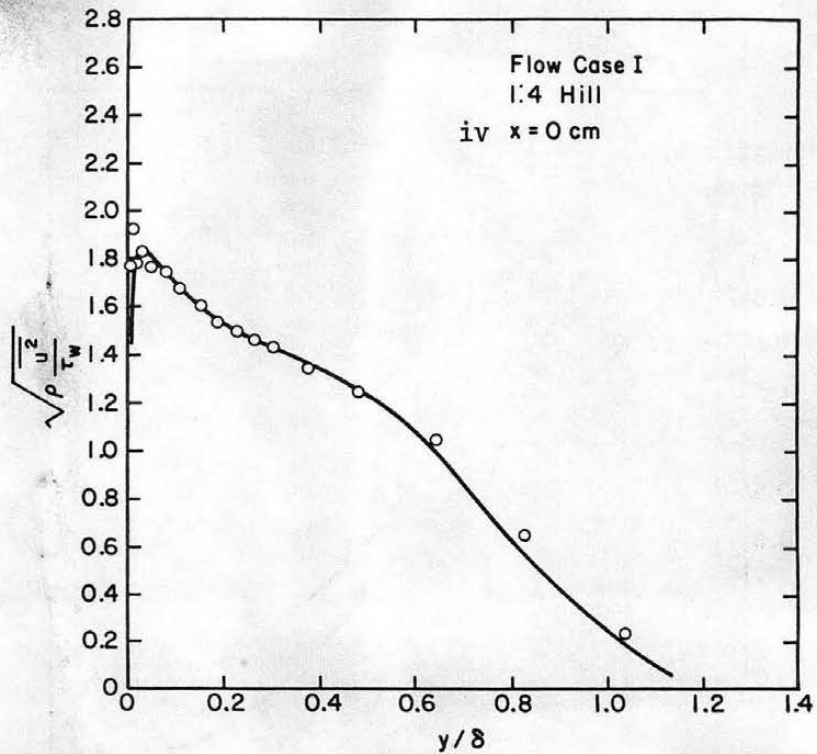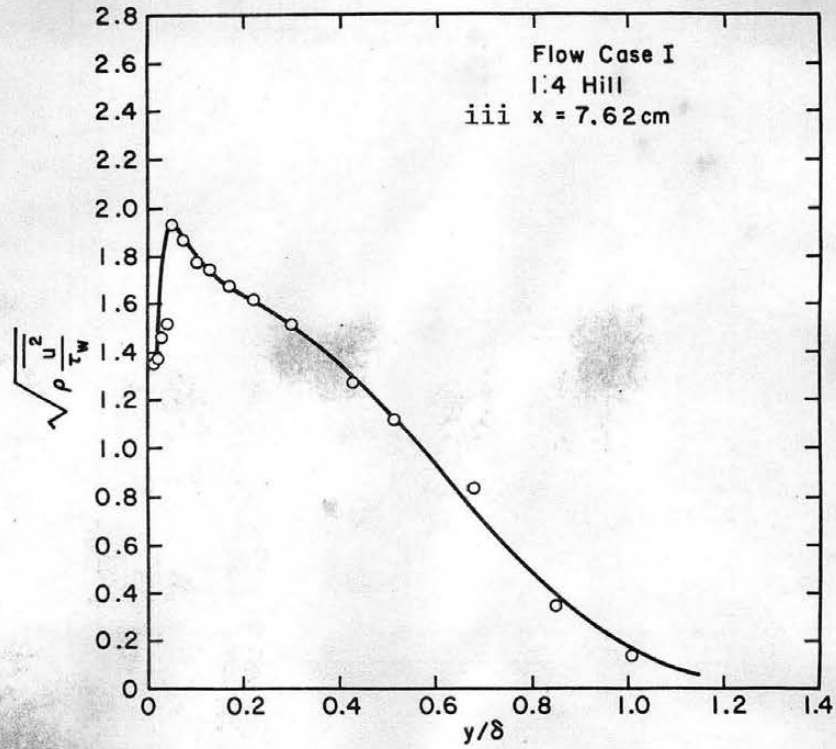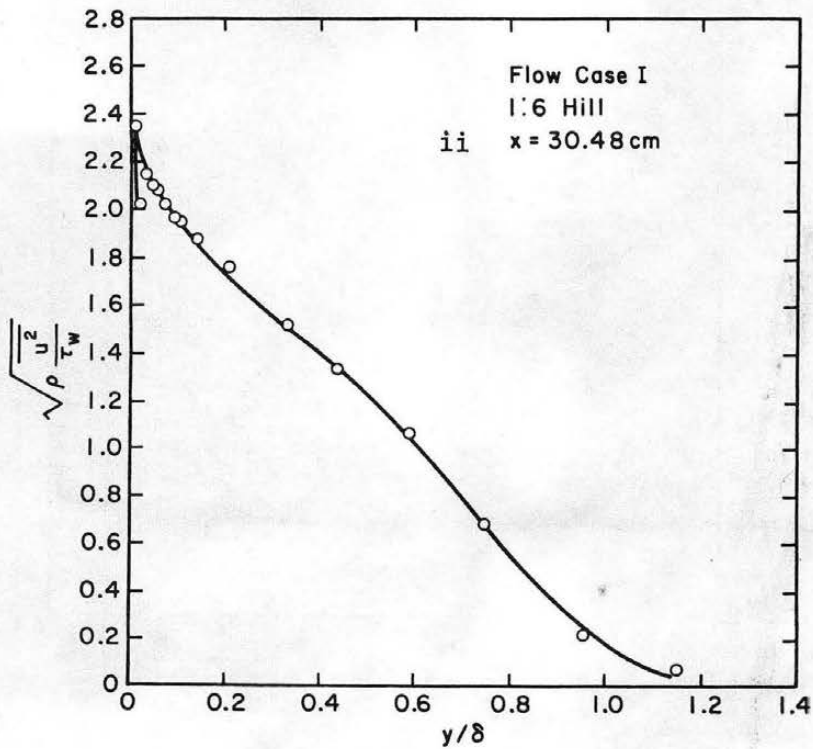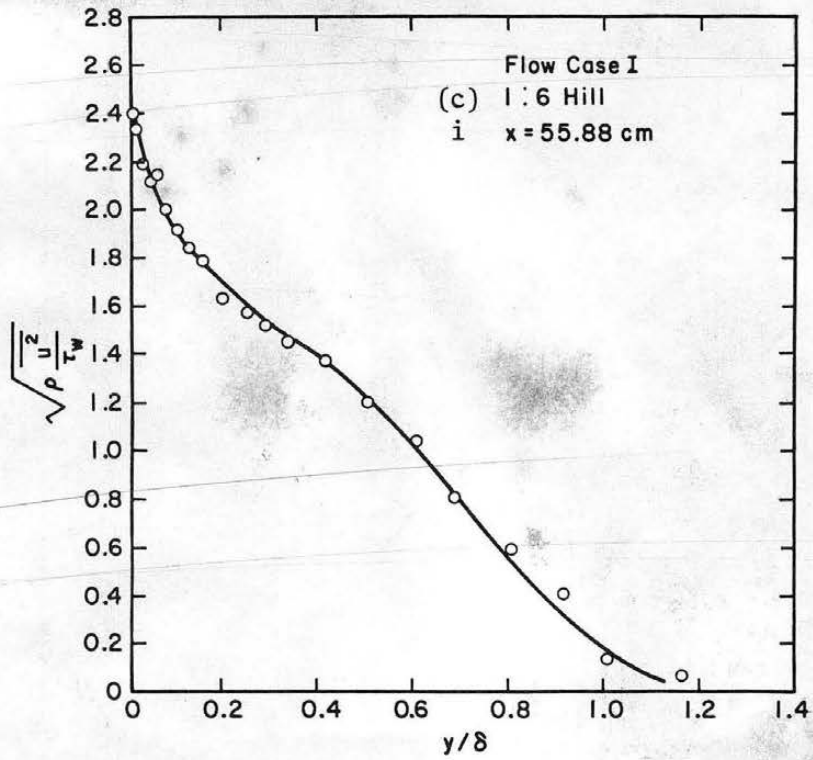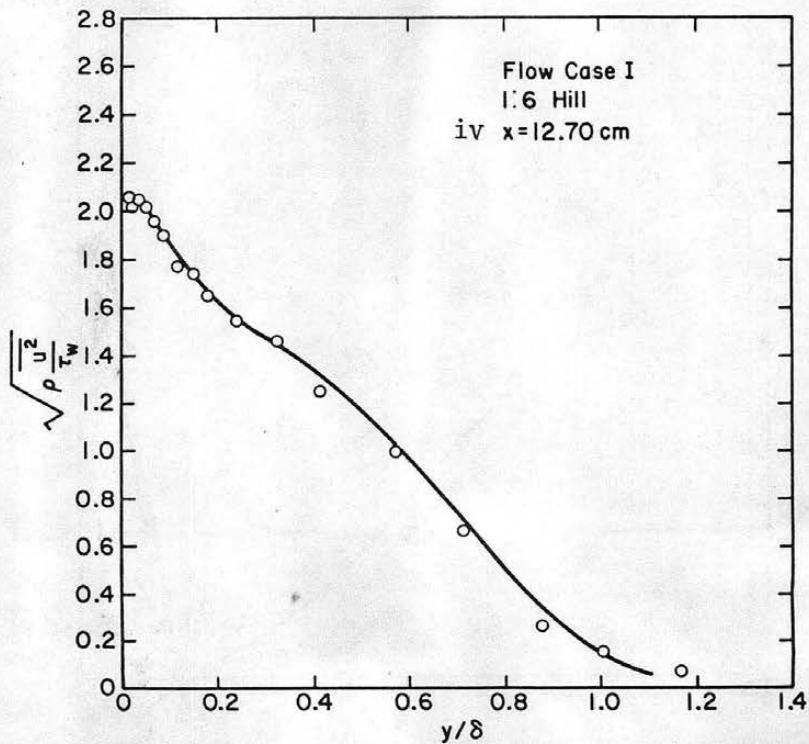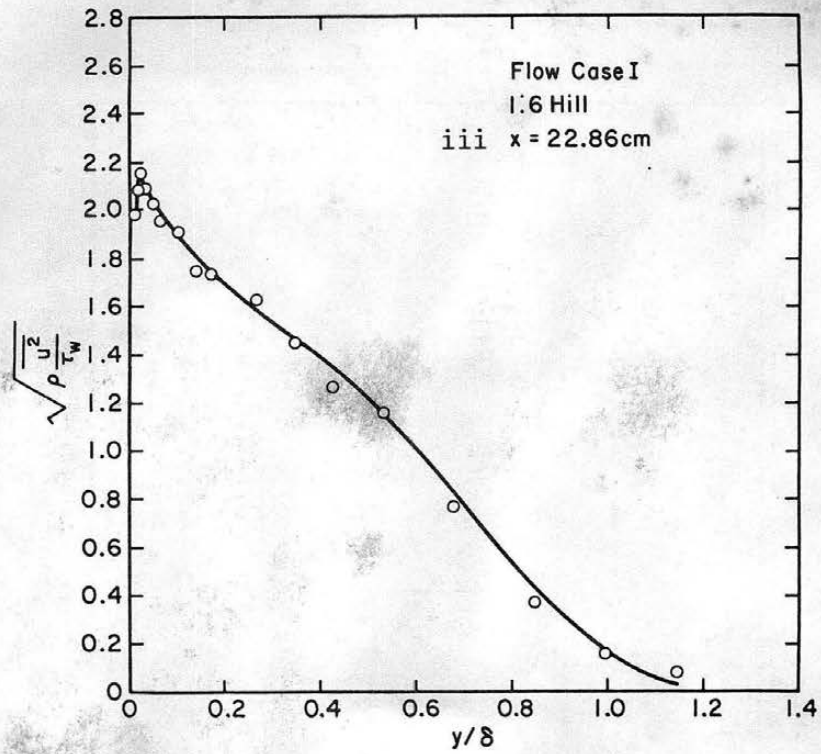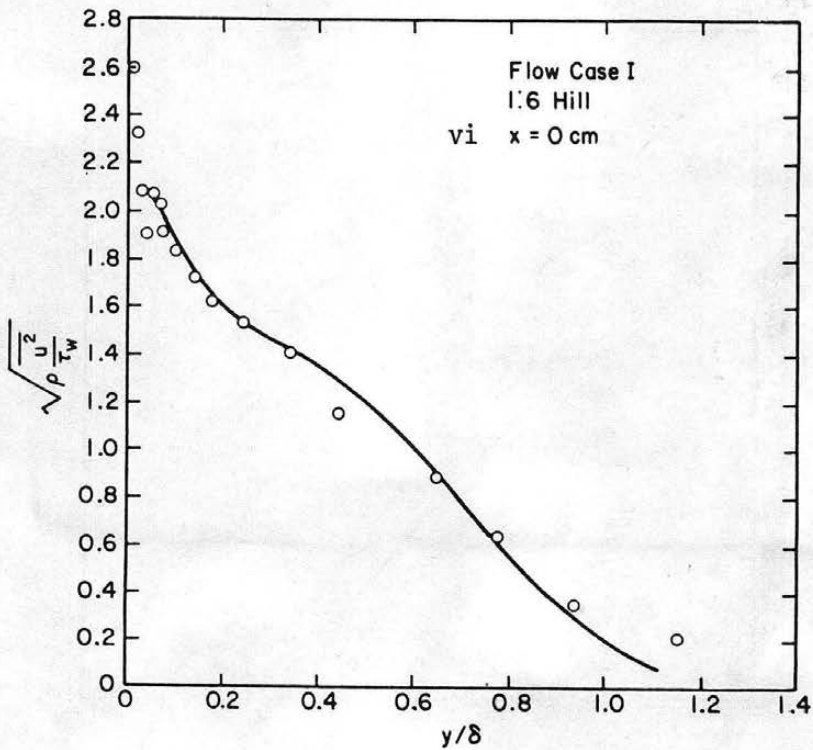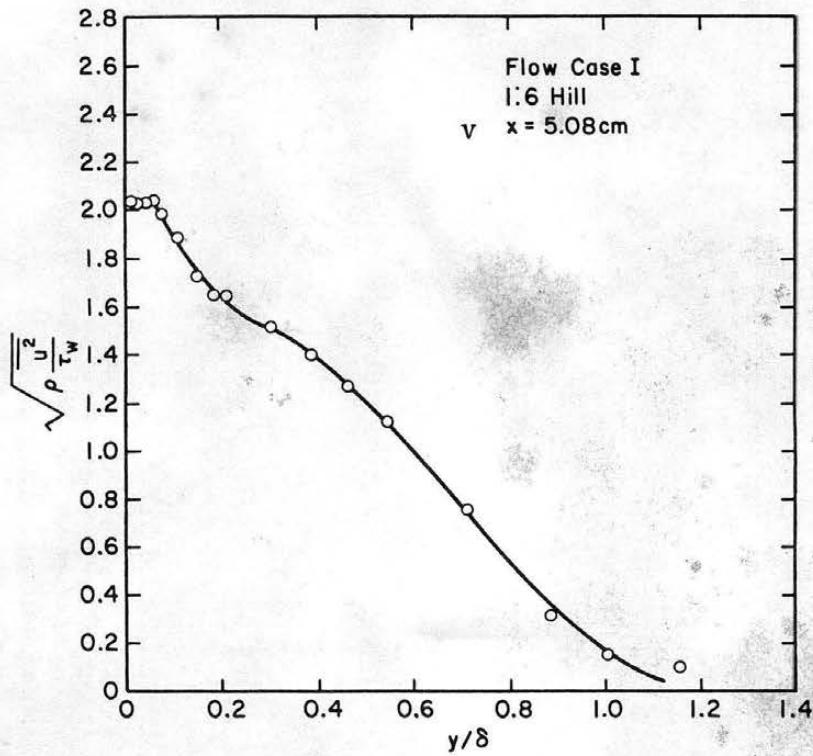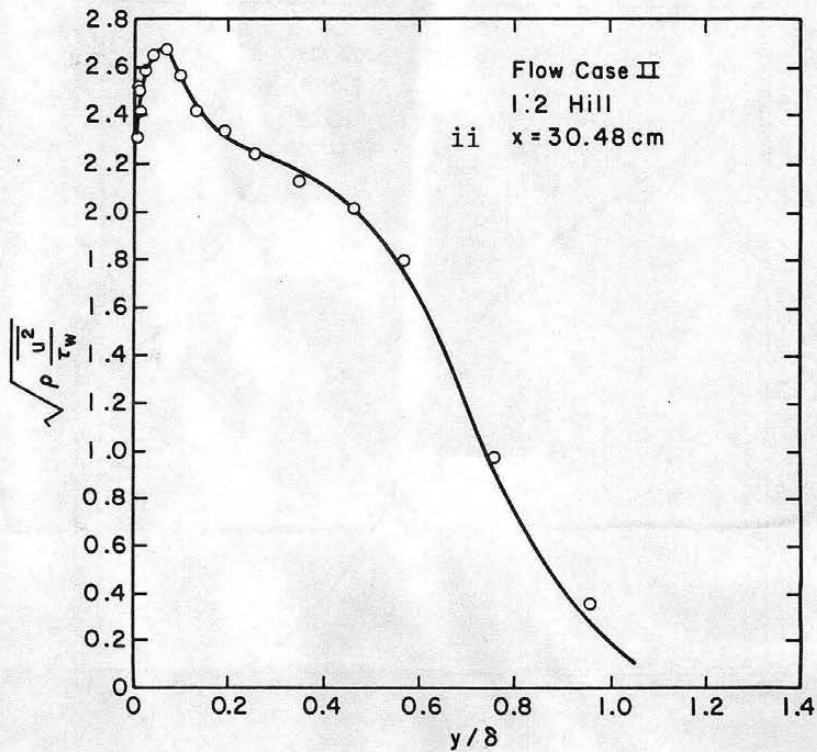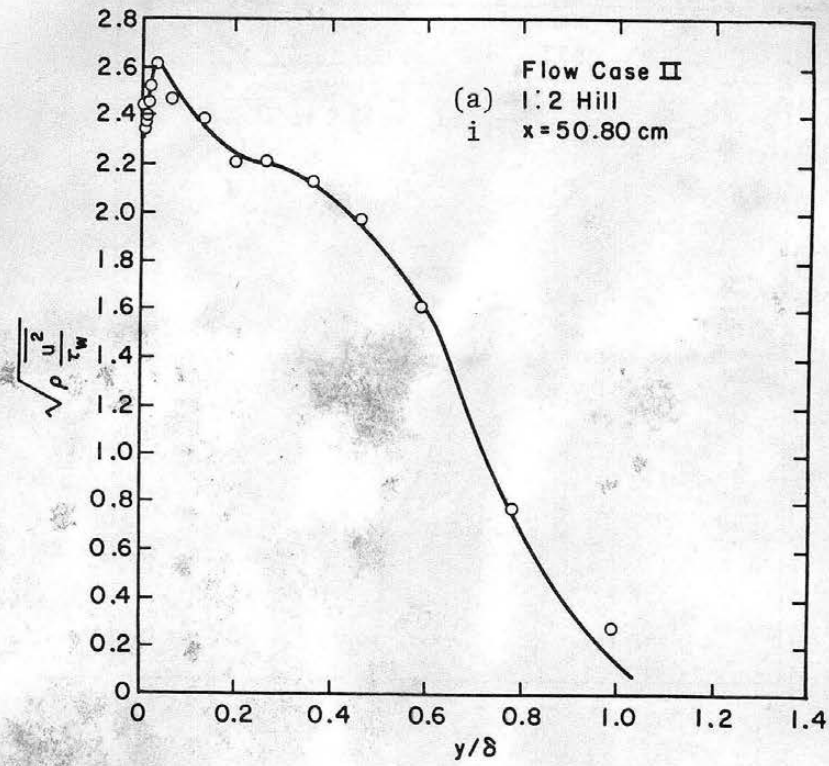
Figure 21. $\sqrt{\rho \dfrac{\overline{u^2}}{\tau_w}}$ profiles flow case II.

Figure 21. $\sqrt{\rho \dfrac{\overline{u^2}}{\tau_w}}$ profiles flow case II (continued).
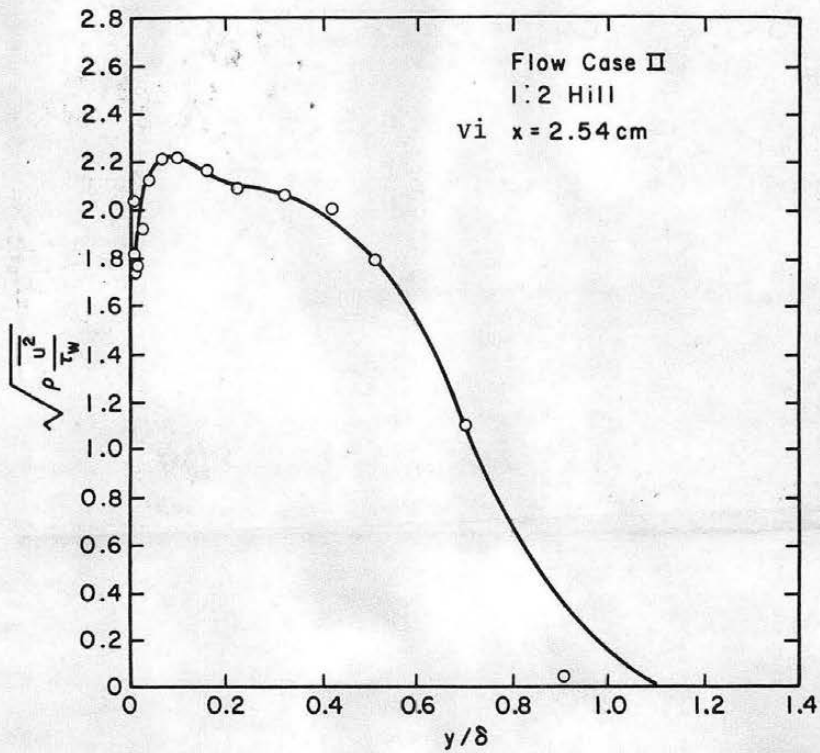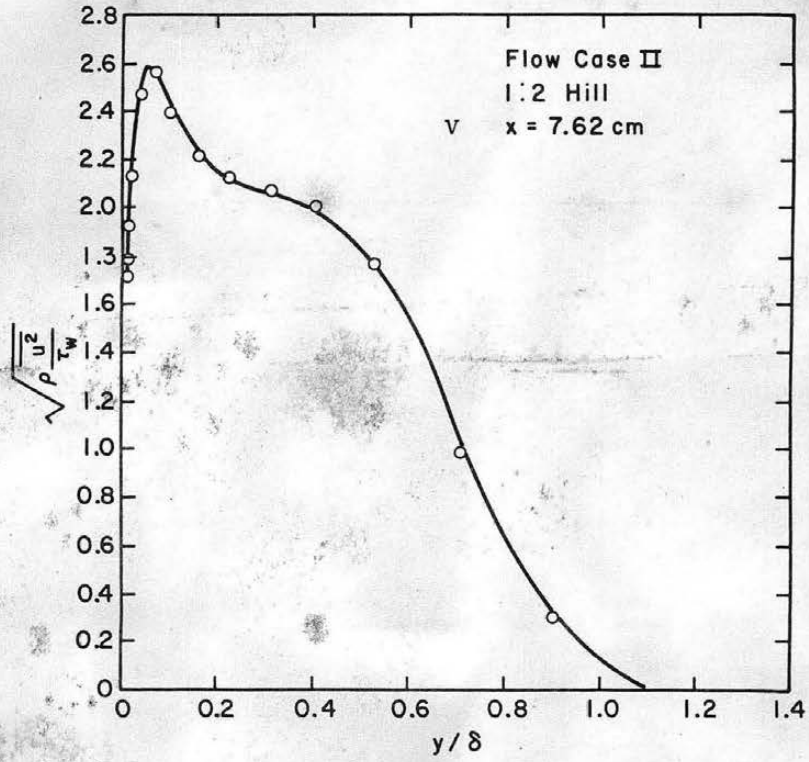
Figure 21. $\sqrt{\rho \dfrac{\overline{u^2}}{\tau_w}}$ profiles flow case II (continued).

Figure 21. $\sqrt{\rho \dfrac{\overline{u^2}}{\tau_w}}$ profiles flow case II (continued).

65
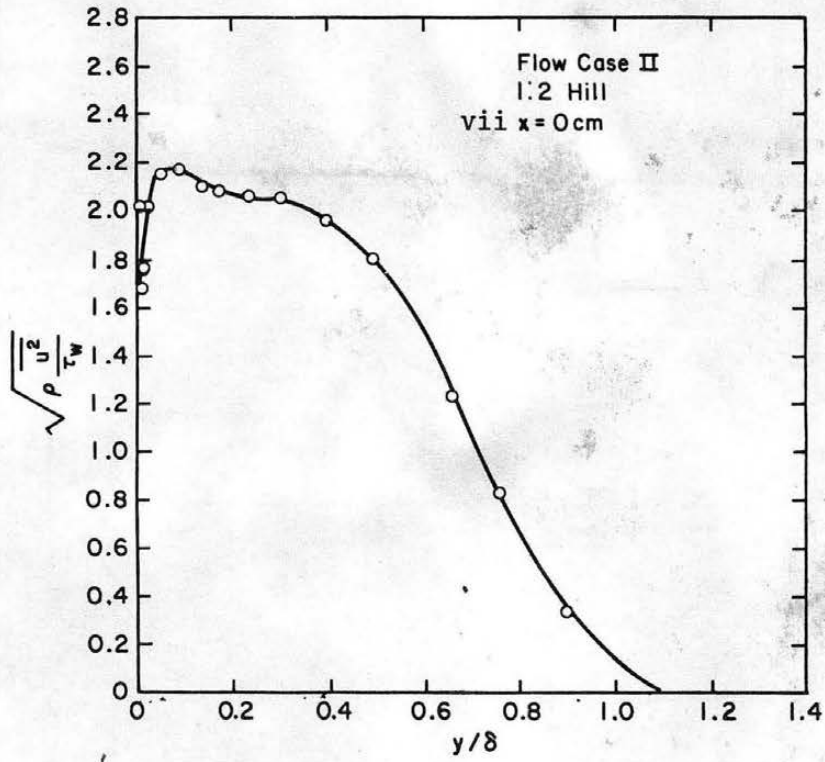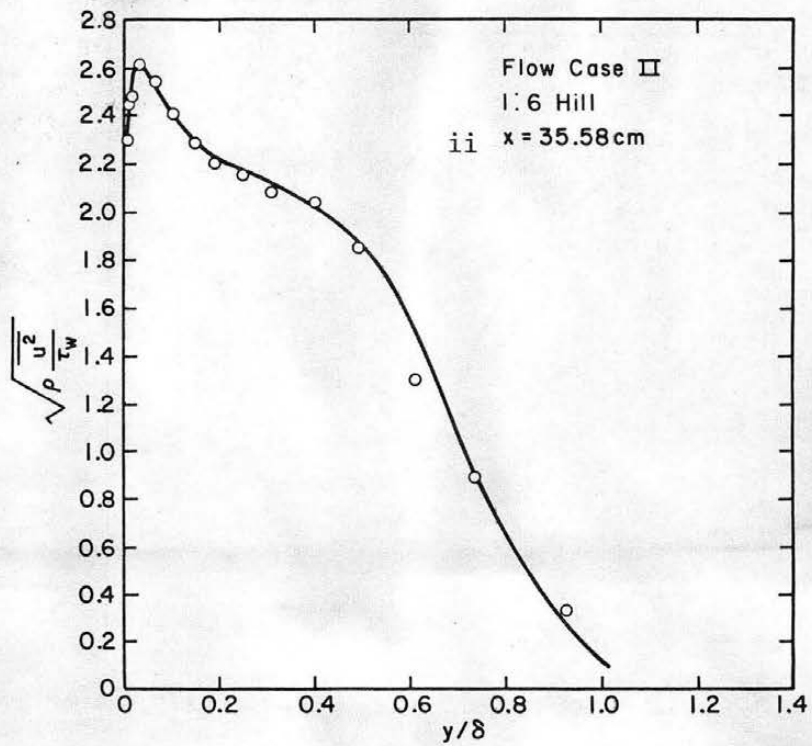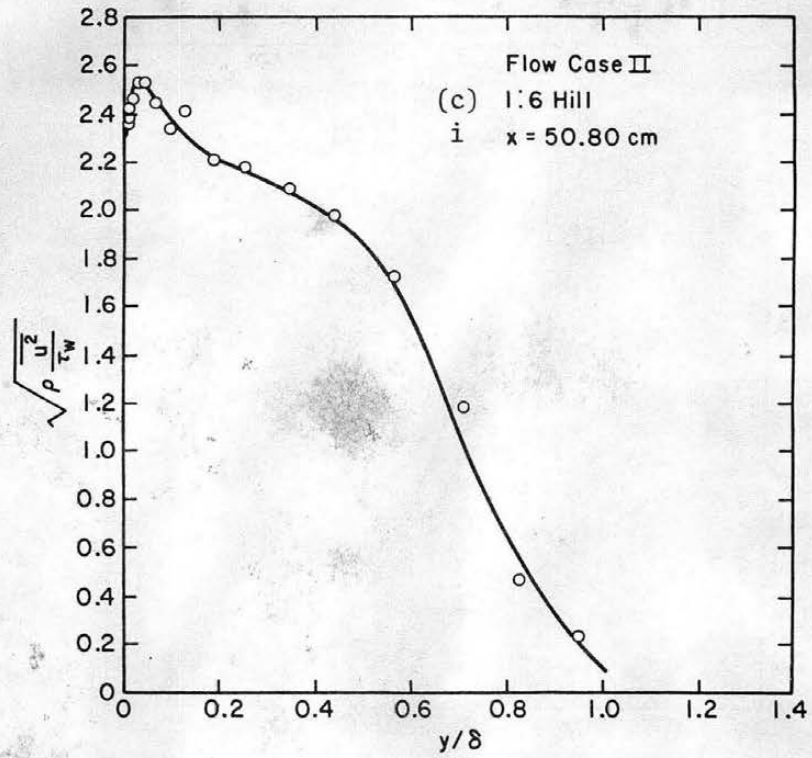
Figure 21. $\sqrt{\rho \dfrac{\overline{u^2}}{\tau_w}}$ profiles flow case II (continued).
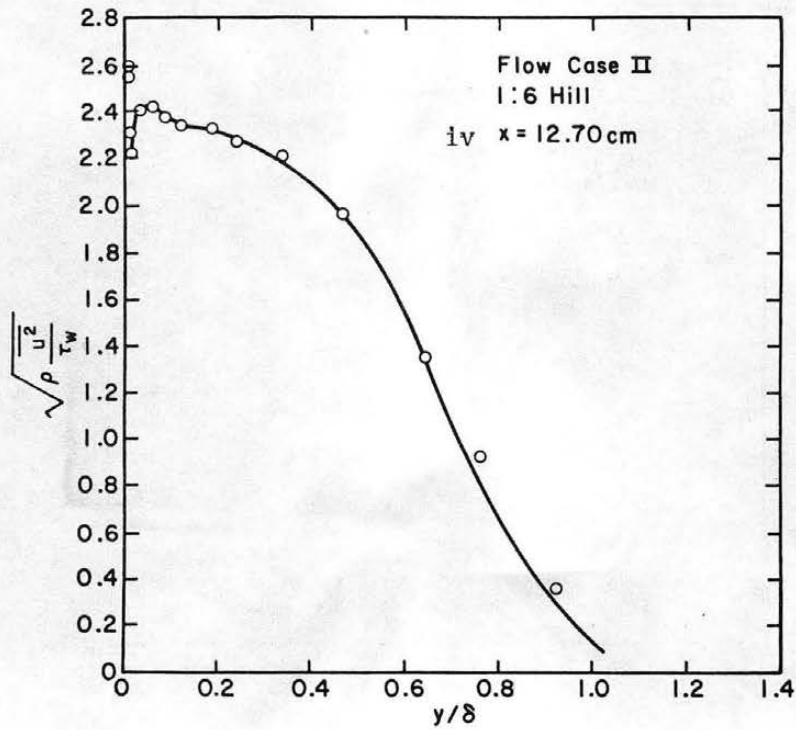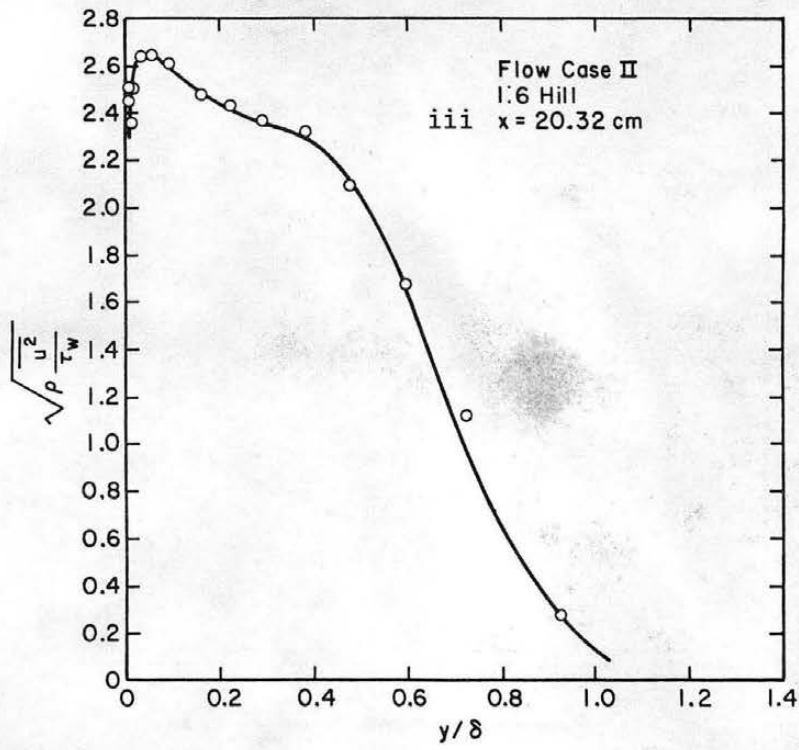
Figure 21. $\sqrt{\rho \dfrac{\overline{u^2}}{\tau_w}}$ profiles flow case II (continued).
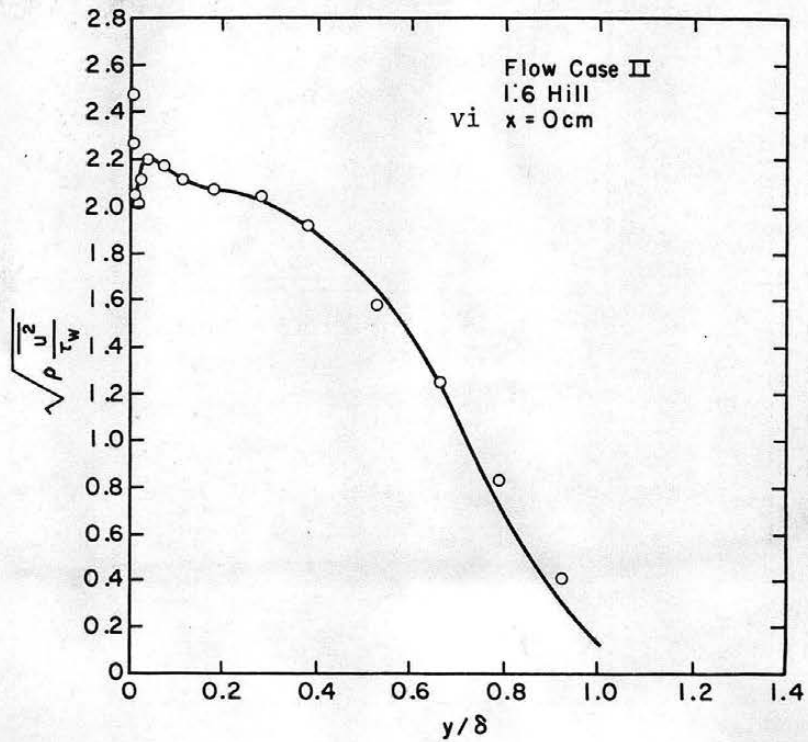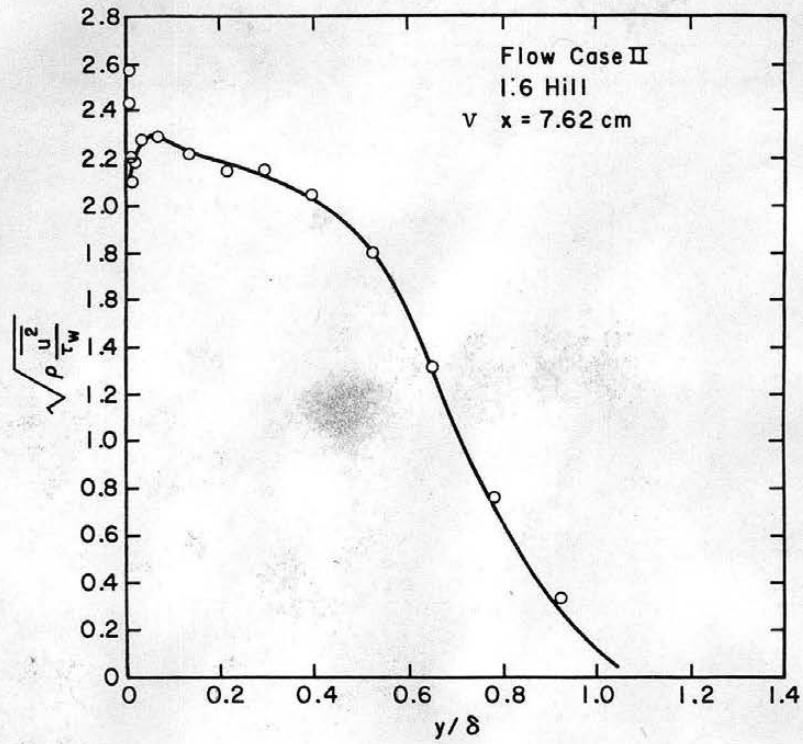
Figure 21. $\sqrt{\rho \dfrac{\overline{u^2}}{\tau_w}}$ profiles flow case II (completed).
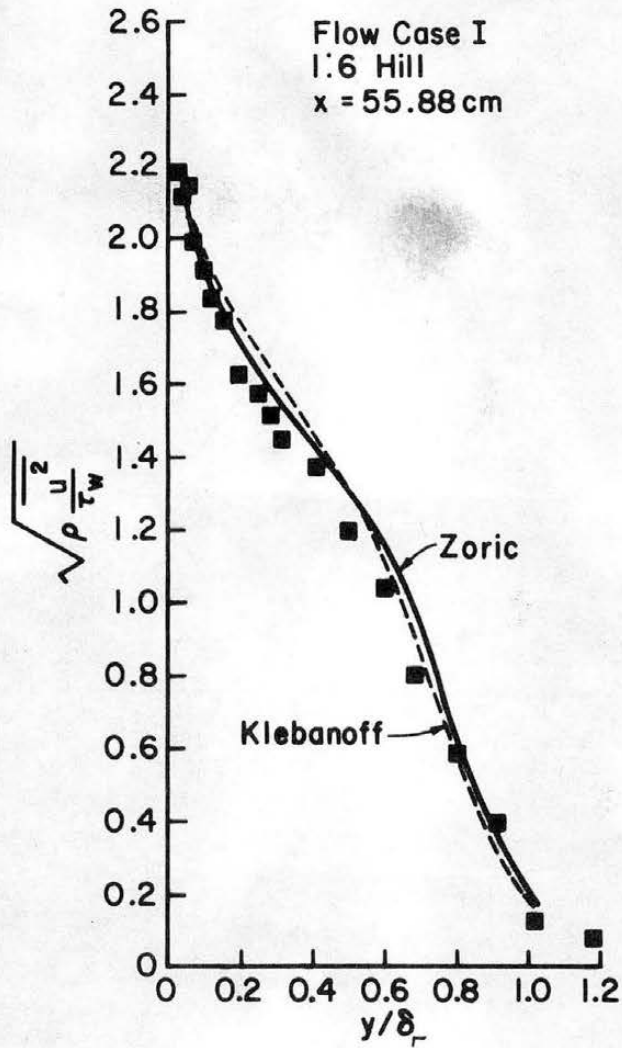
Figure 22. Comparison of upstream $\sqrt{\rho \dfrac{\overline{u^2}}{\tau_w}}$ measurements to those of Zoric and Klebanoff. Flow case I.
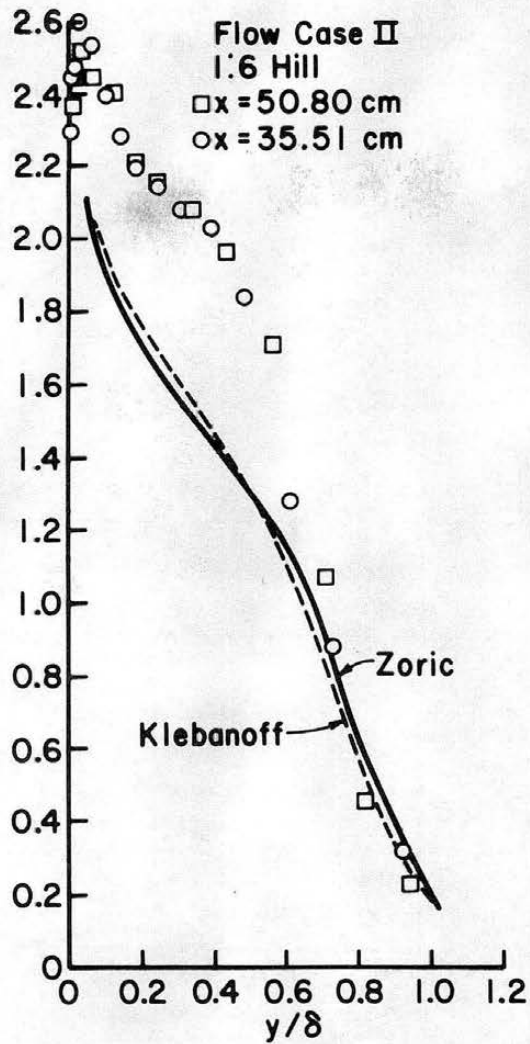
Figure 23. Comparison of upstream $\sqrt{\rho \frac{\overline{u^2}}{\tau_w}}$ measurements to those of Zoric and Klebanoff. Flow case II.
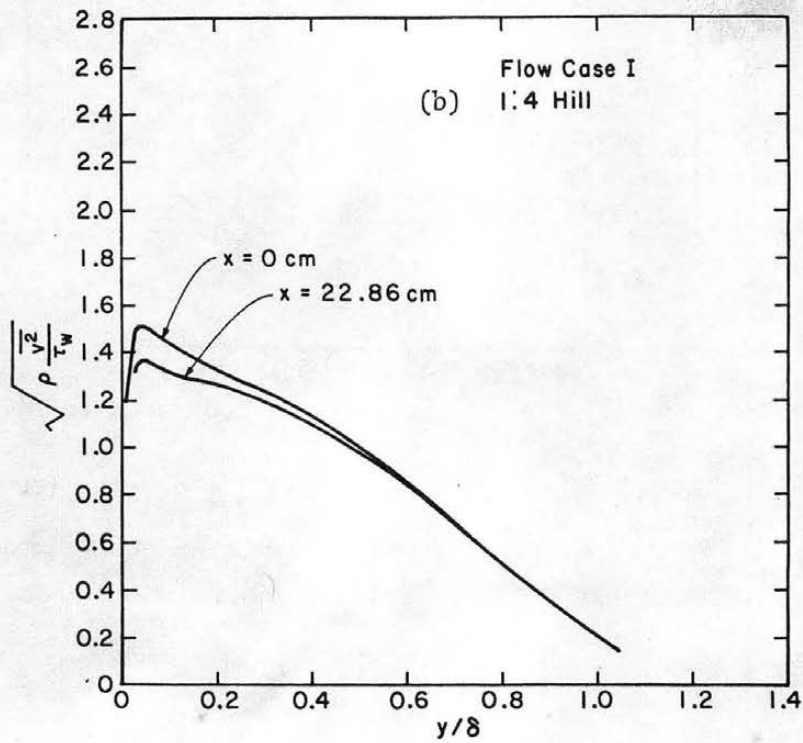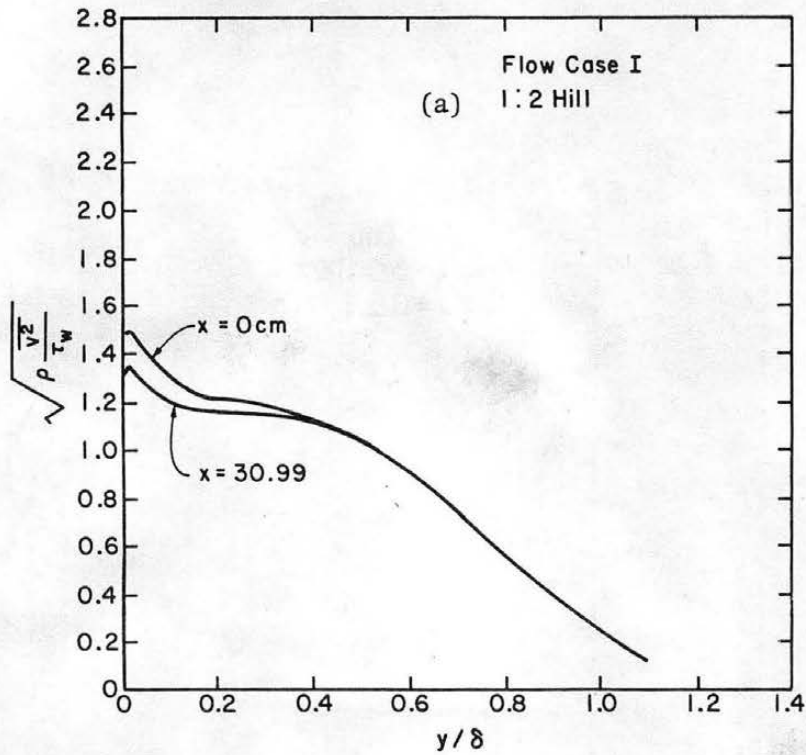
Figure 24. Upstream $\sqrt{\rho \dfrac{\overline{v^2}}{\tau_w}}$ measurements compared to $\sqrt{\rho \dfrac{\overline{v^2}}{\tau_w}}$ measurements at crest. Flow case I.
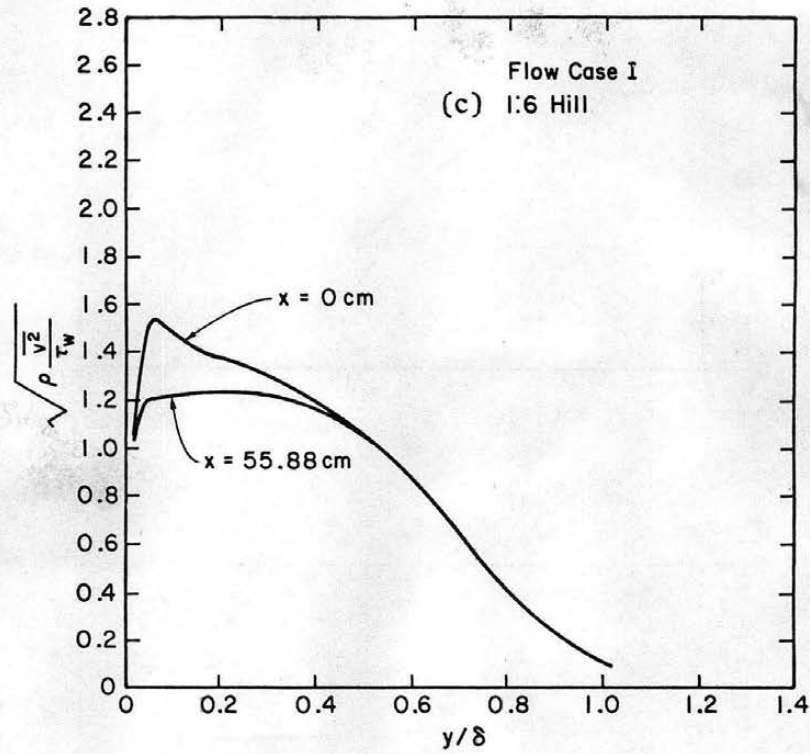
Figure 24. Upstream $\sqrt{\rho \dfrac{\overline{v^2}}{\tau_w}}$ measurements compared to $\sqrt{\rho \dfrac{\overline{v^2}}{\tau_w}}$ measurements at crest. Flow case (continued).
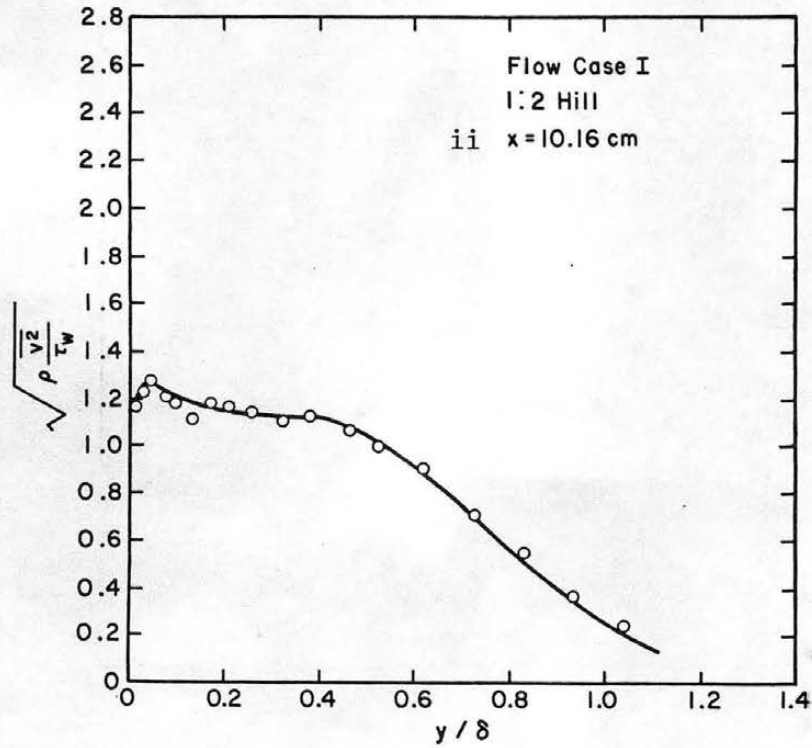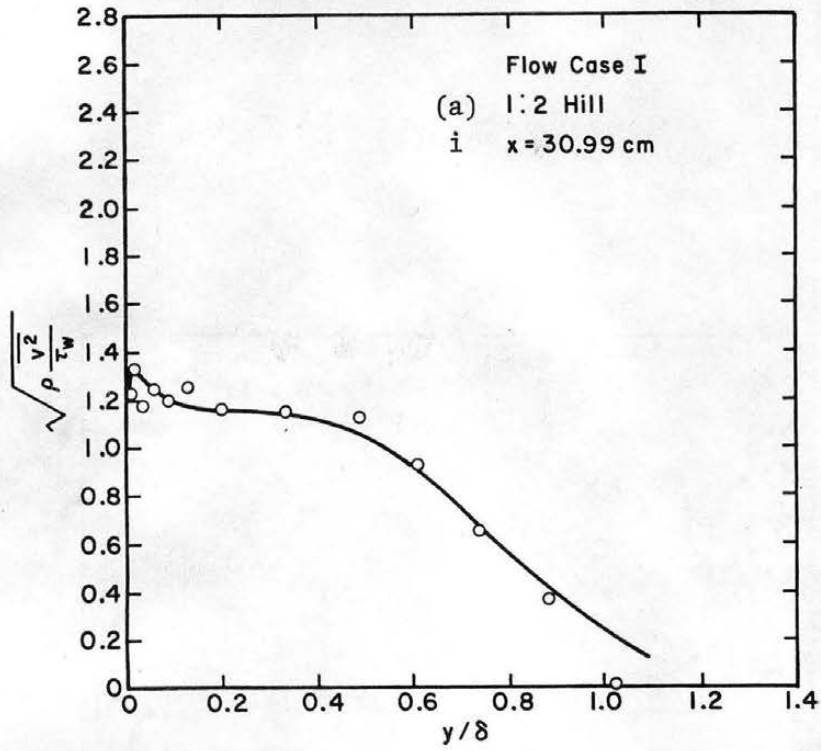
Figure 25. $\sqrt{\rho \dfrac{\overline{v^2}}{\tau_w}}$ profiles flow case I.
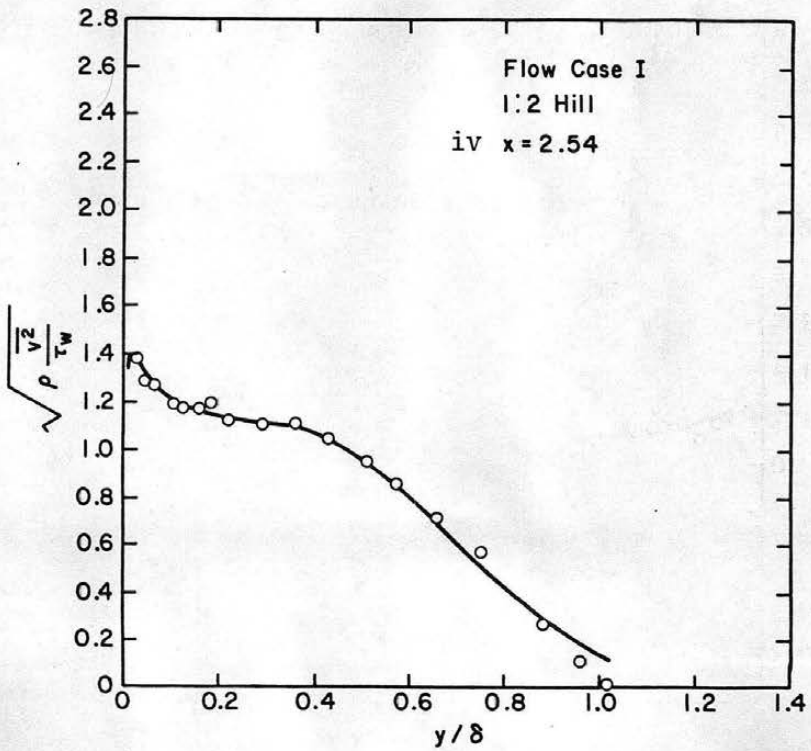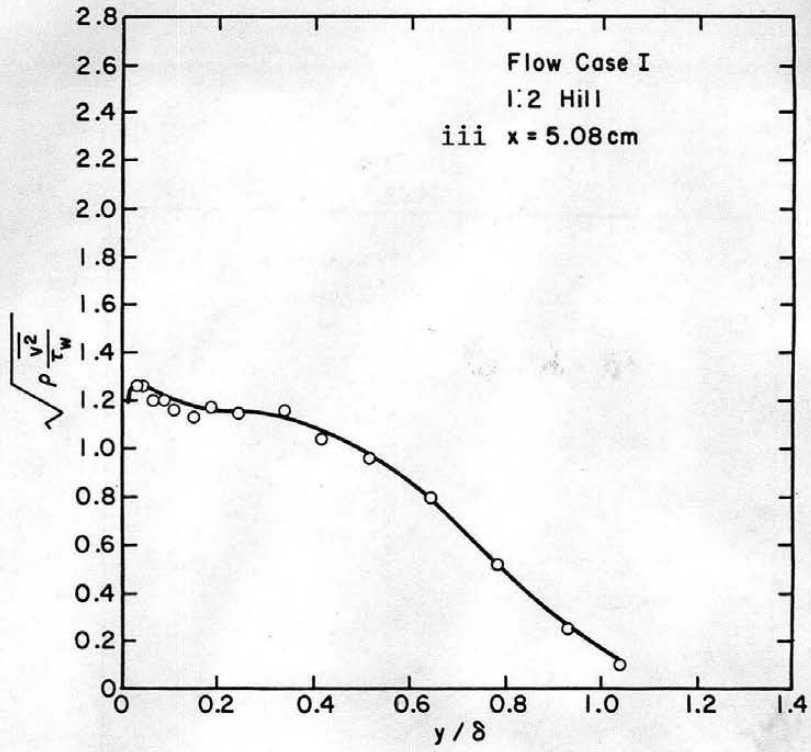
Figure 25. $\sqrt{\rho \dfrac{\overline{v^2}}{\tau_w}}$ profiles flow case I (continued).
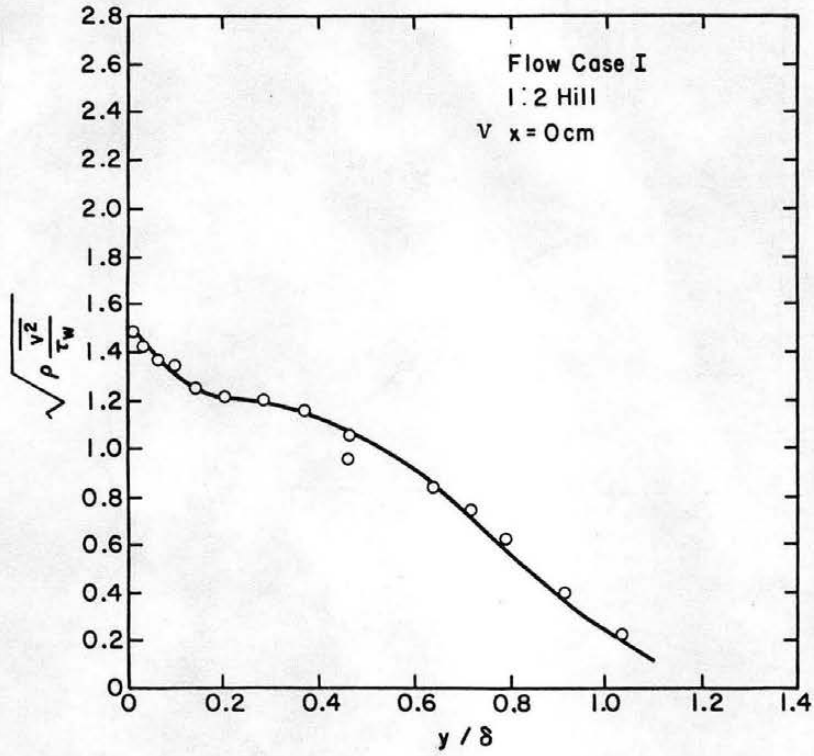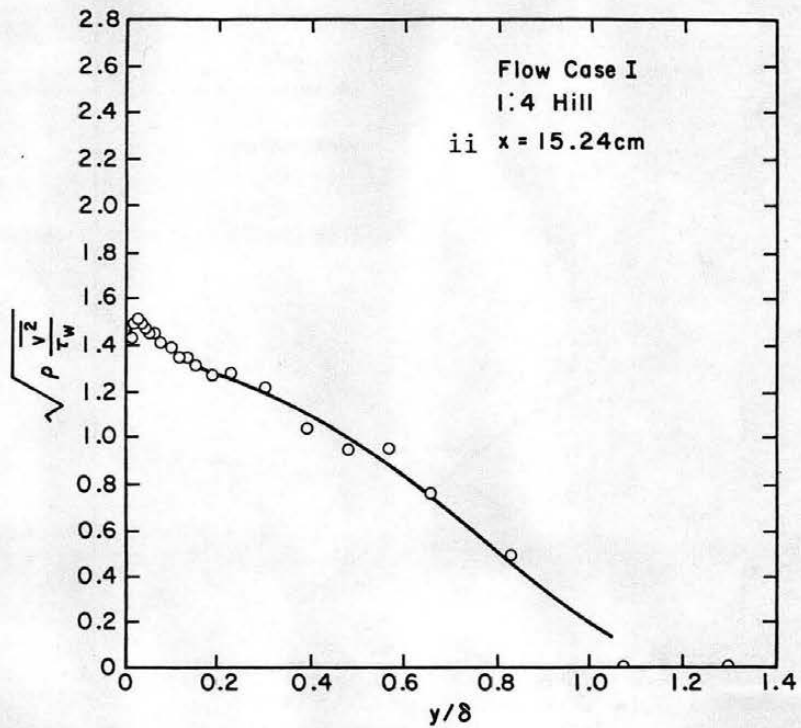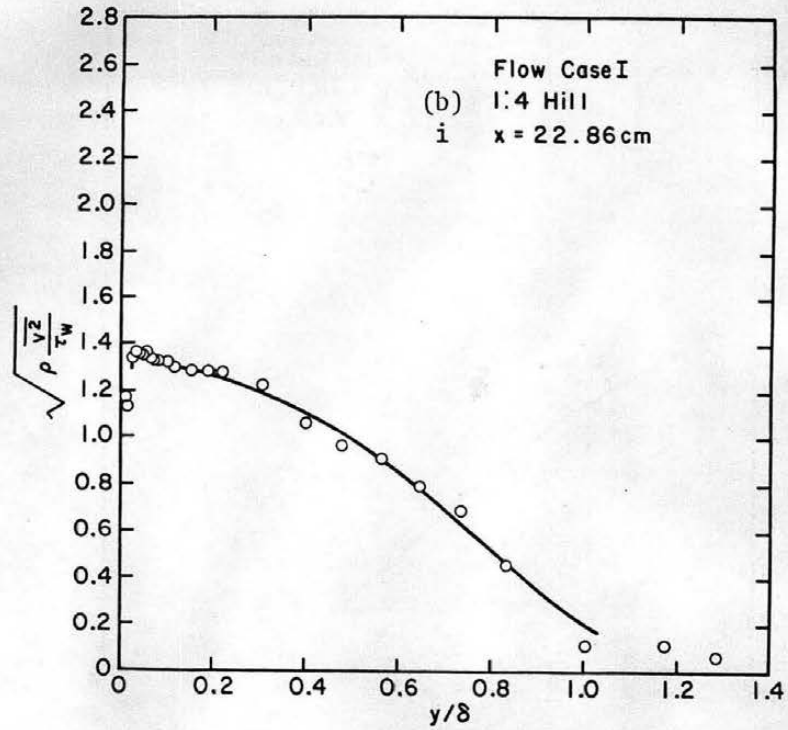
Figure 25. $\sqrt{\rho\,\dfrac{\overline{v^2}}{\tau_w}}$ profiles flow case I (continued).

Figure 25. $\sqrt{\rho\, \dfrac{\overline{v^2}}{\tau_w}}$ profiles flow case I (continued).
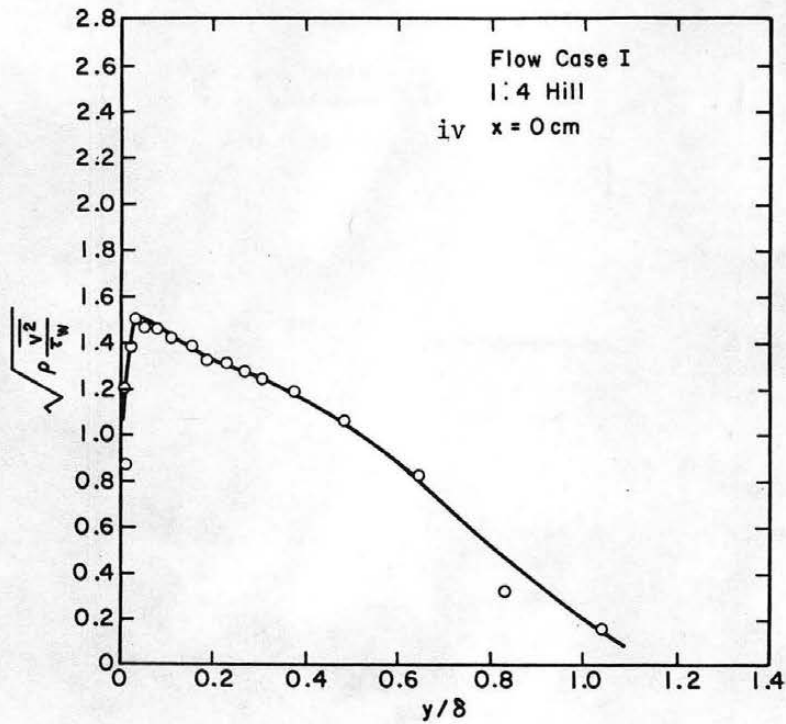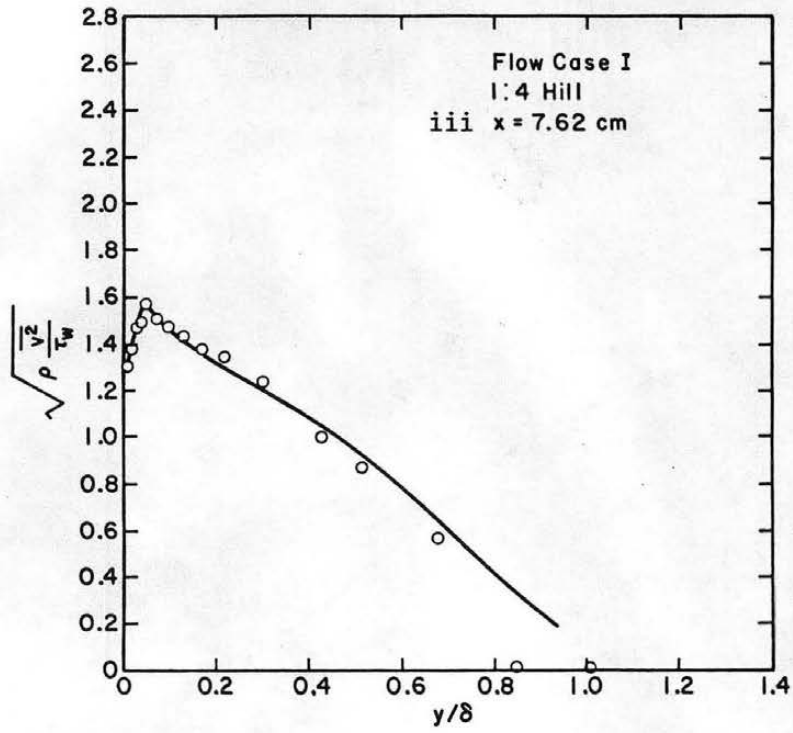
Figure 25. $\sqrt{\rho \dfrac{\overline{v^2}}{\tau_w}}$ profiles flow case I (continued).
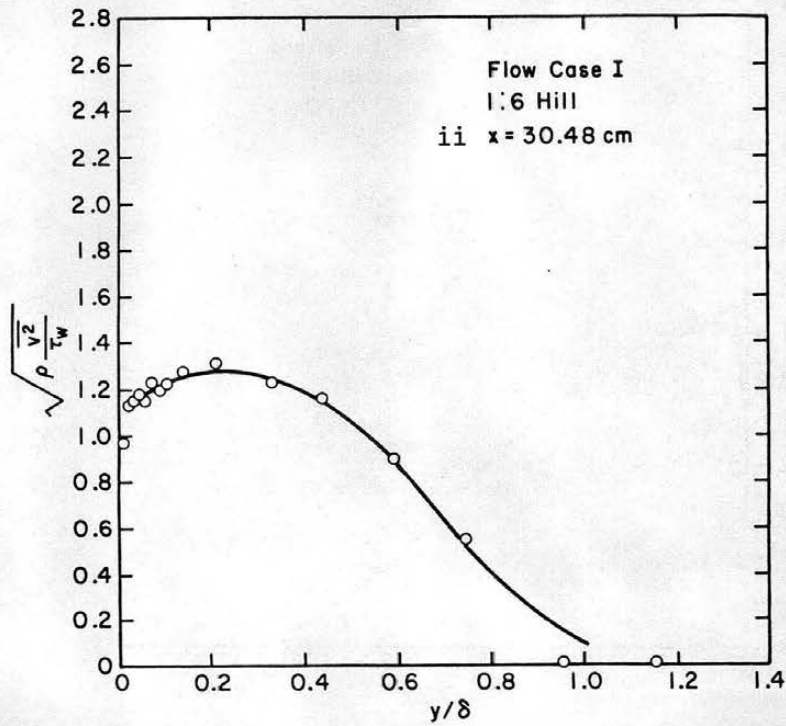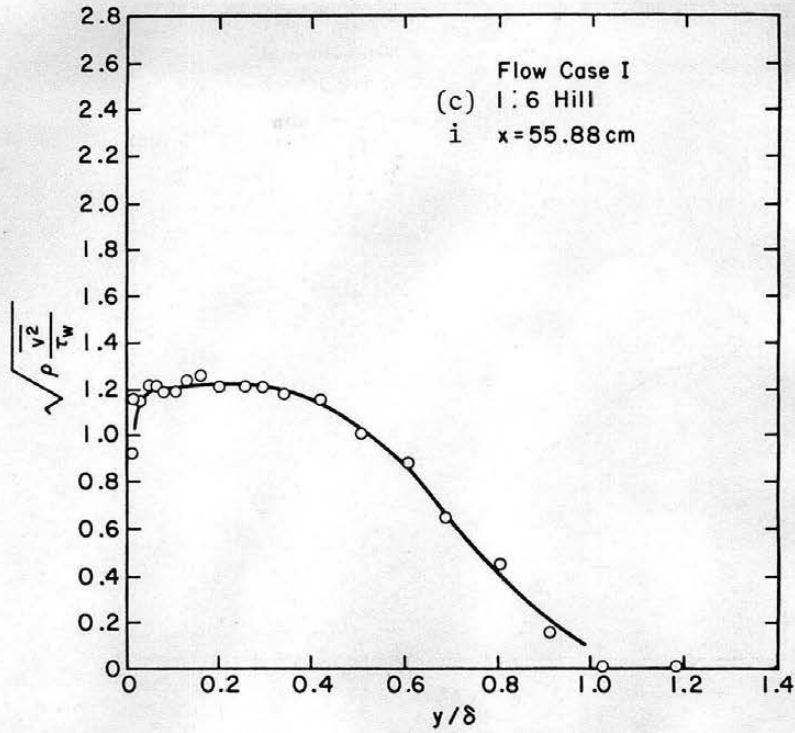
Figure 25. $\sqrt{\rho \dfrac{\overline{v^2}}{\tau_w}}$ profiles flow case I (continued).
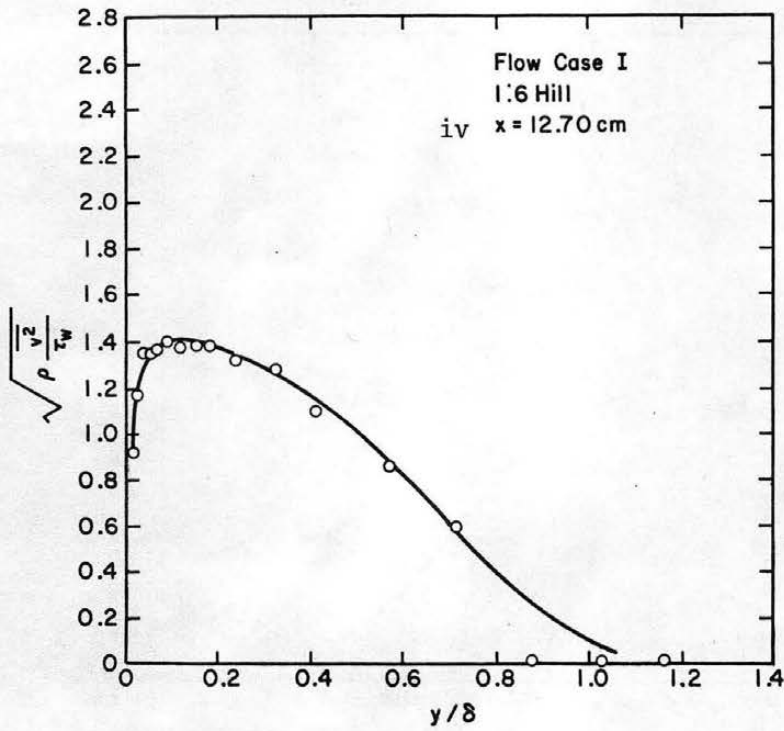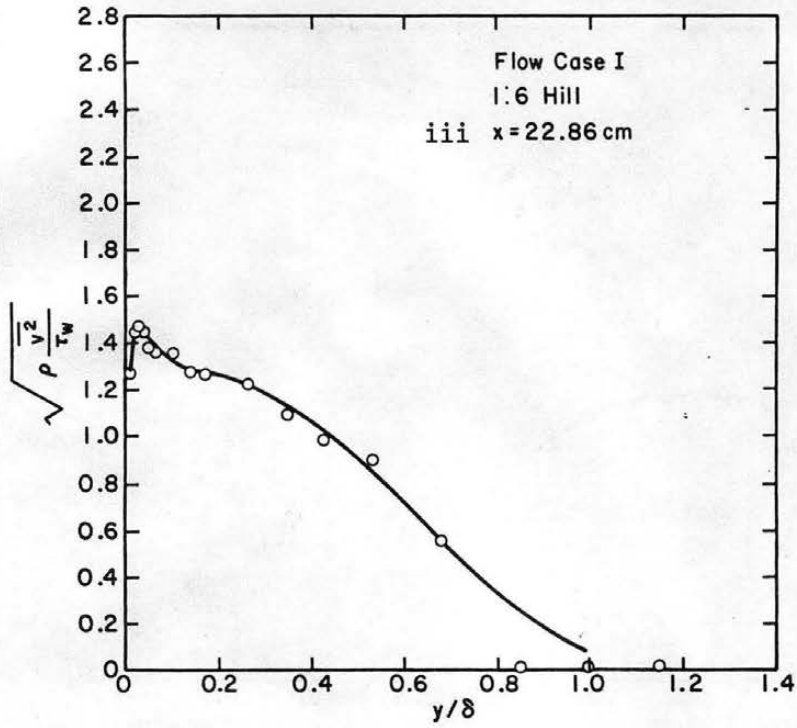
Figure 25. $\sqrt{\rho \dfrac{\overline{v^2}}{\tau_w}}$ profiles flow case I (continued).
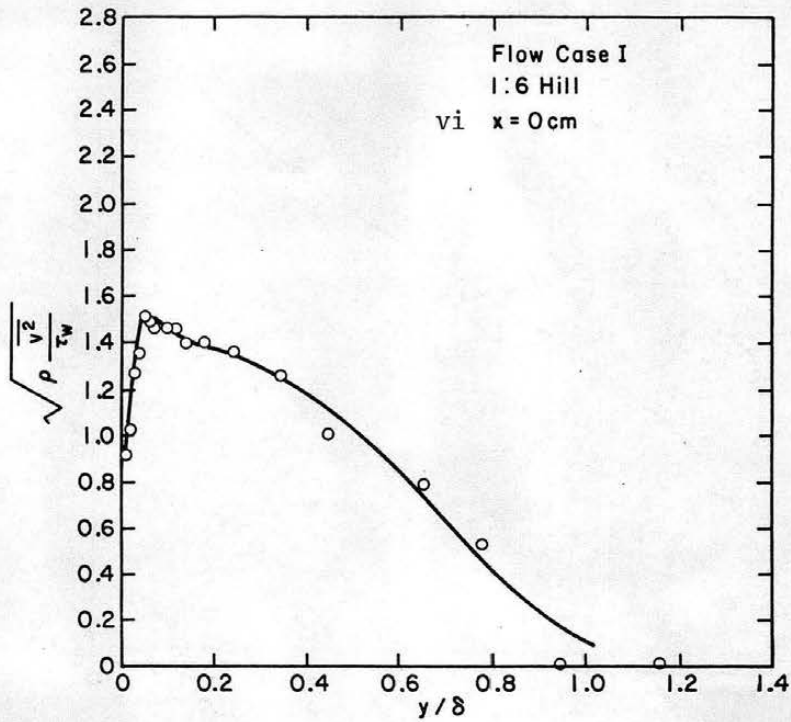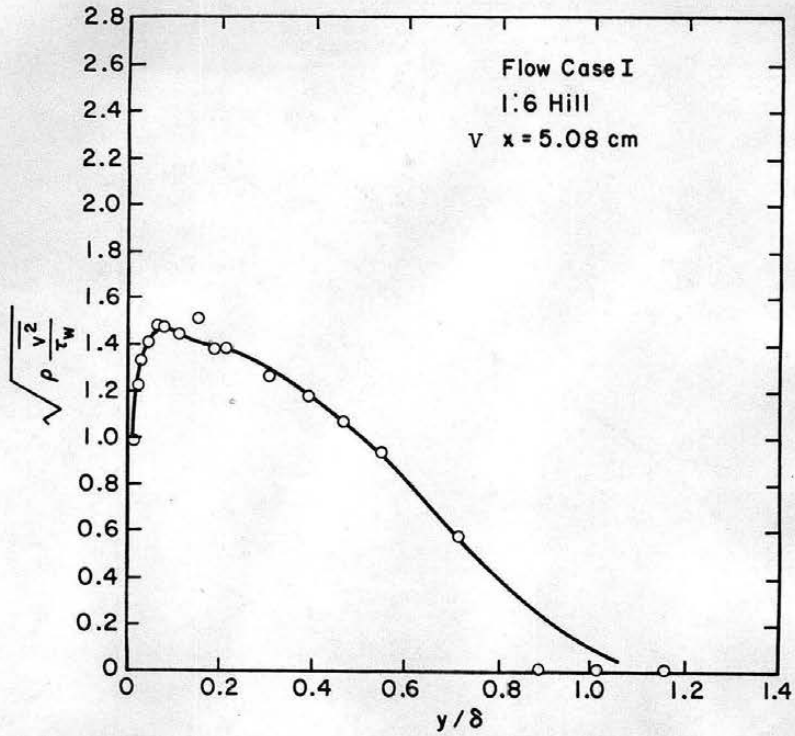
Figure 25. $\sqrt{\rho \frac{\overline{v^2}}{\tau_w}}$ profiles flow case I (completed).
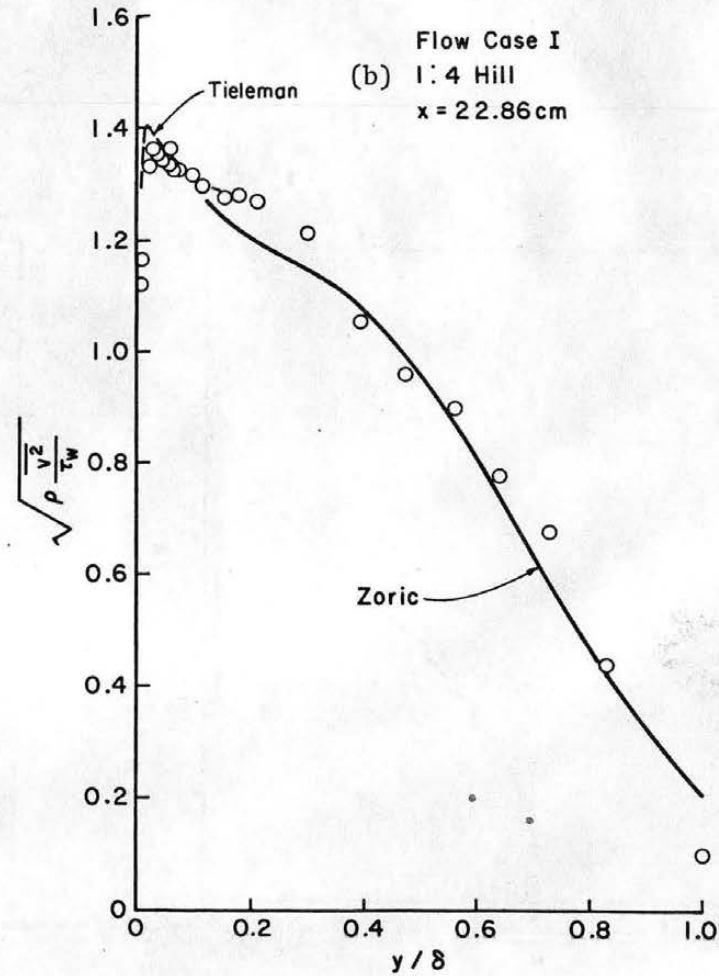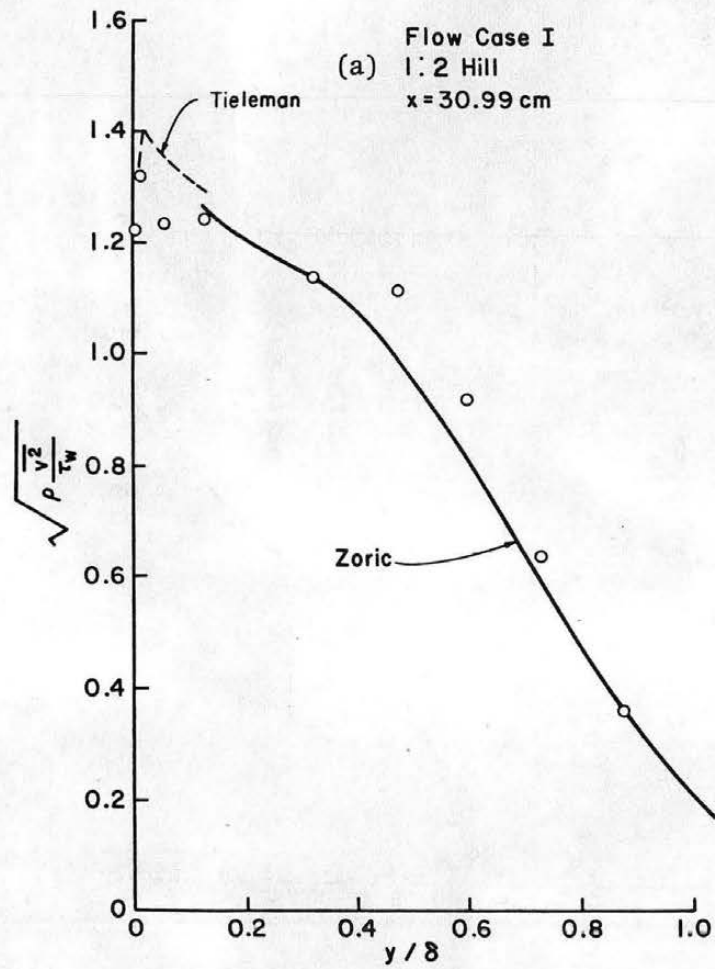
Figure 26. Comparison of $\sqrt{\rho \frac{\overline{v^2}}{\tau_w}}$ measurements to those of Zoric and Tieleman. Flow case I.
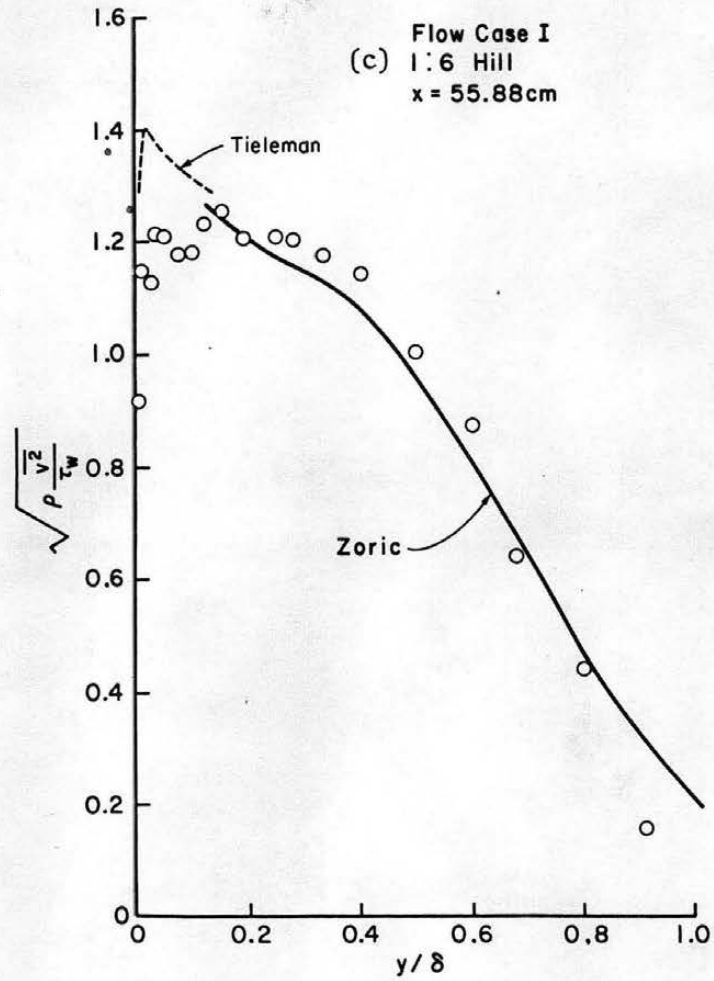
Figure 26. Comparison of $\sqrt{\rho \dfrac{\overline{v^2}}{\tau_w}}$ measurements to those of Zoric and Tieleman. Flow case I (continued).
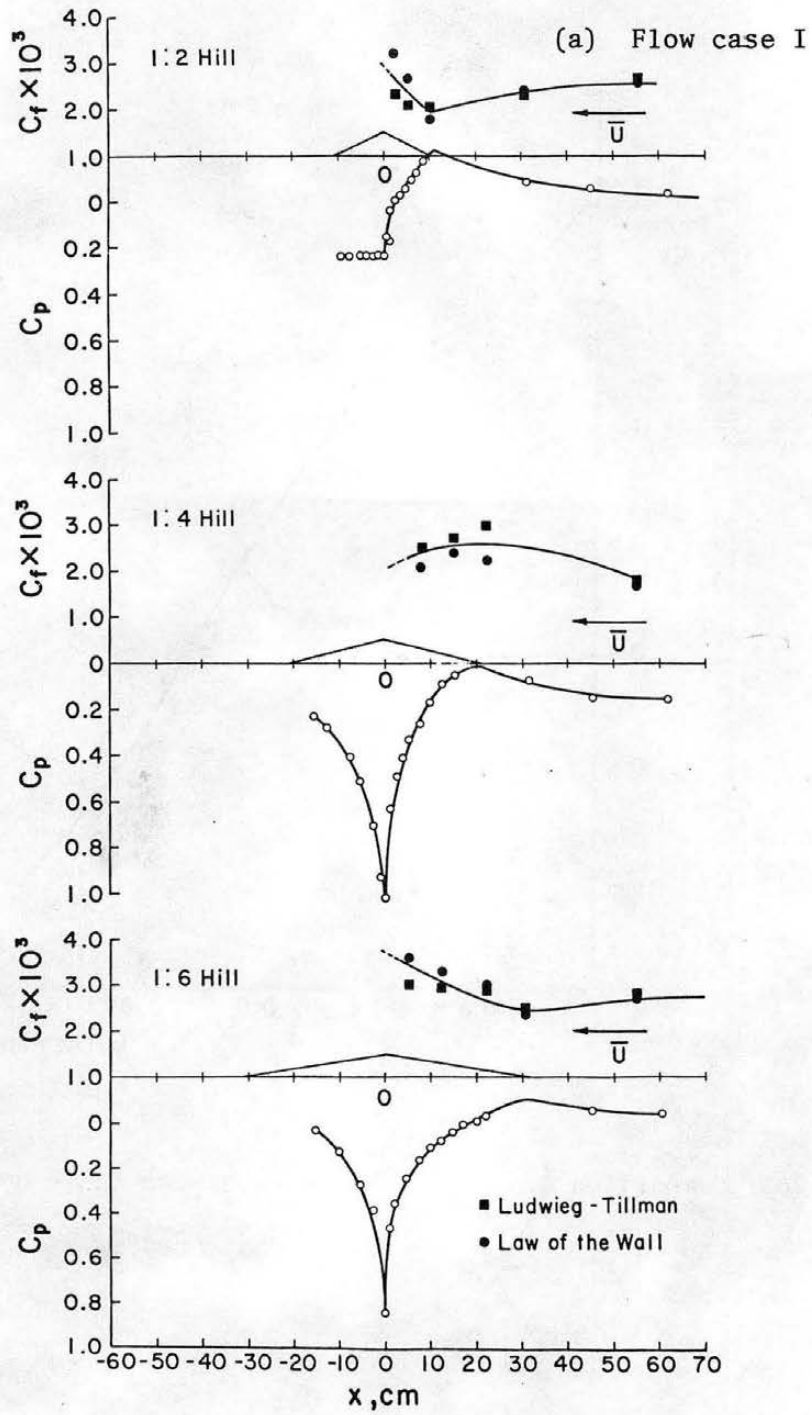
Figure 27. Wall, shear stress, and static pressure distribution.
Flow case I.
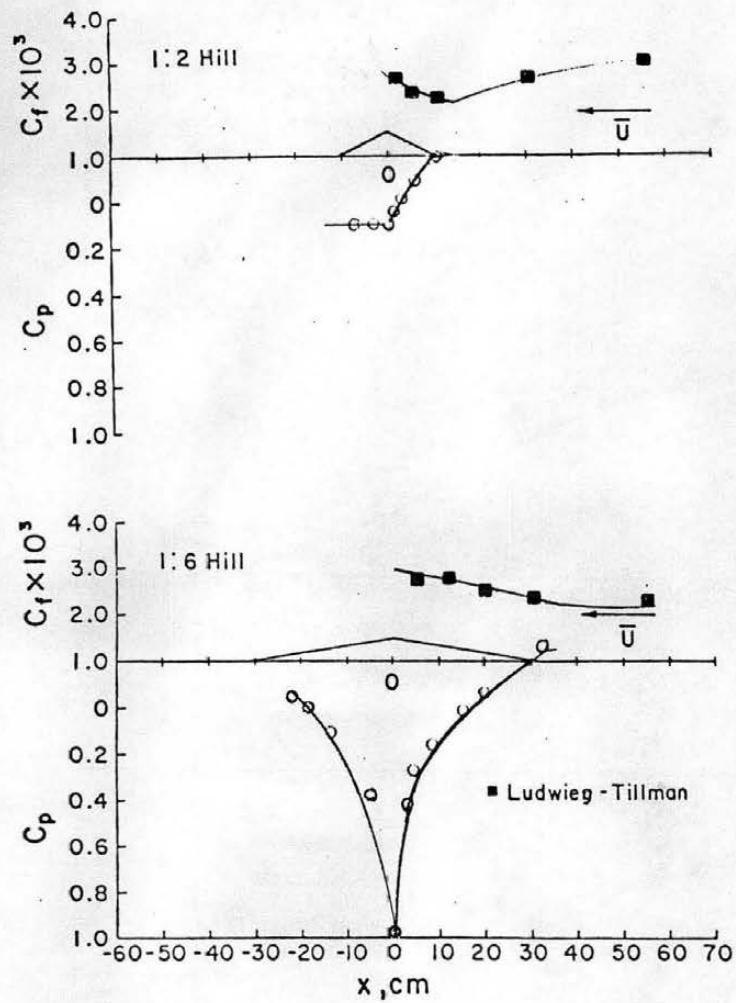
Figure 27. Wall, shear stress, and static pressure distribution. Flow case II.
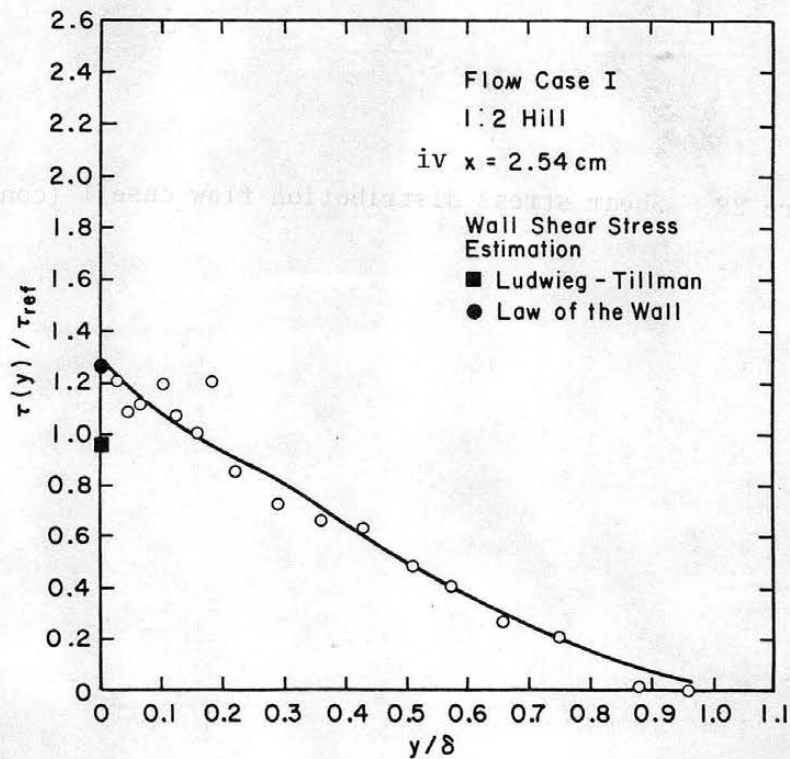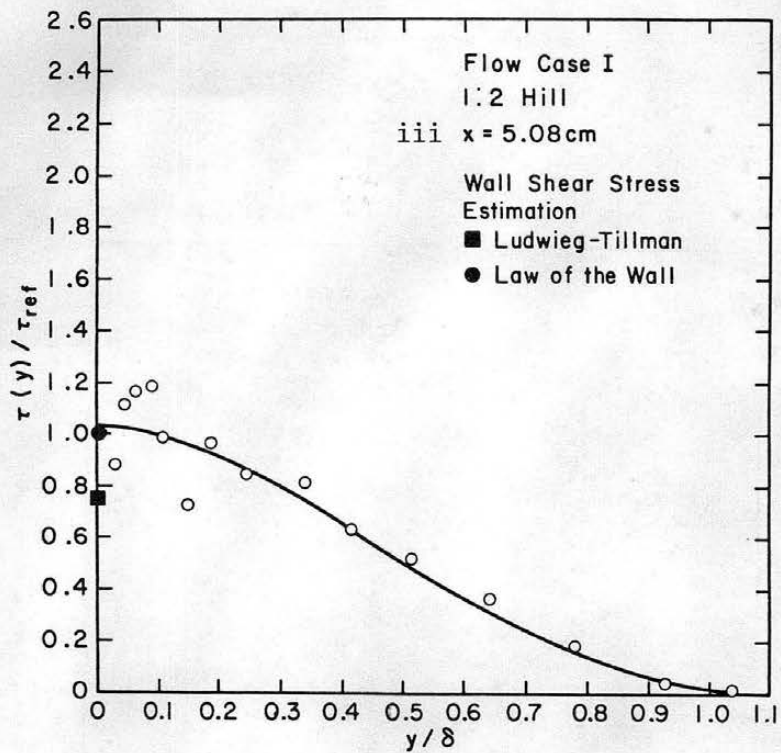
84

Figure 28. Shear stress distribution flow case I.

Figure 28.   Shear stress distribution flow case I (continued).
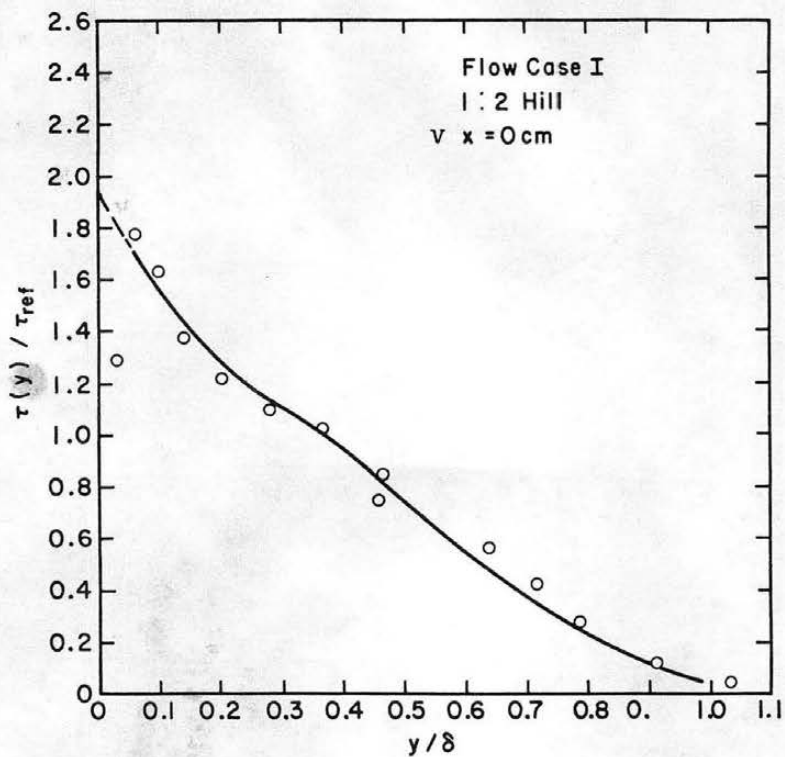
Figure 28. Shear stress distribution flow case I (continued).

Figure 28.   Shear stress distribution flow case I (continued).

88
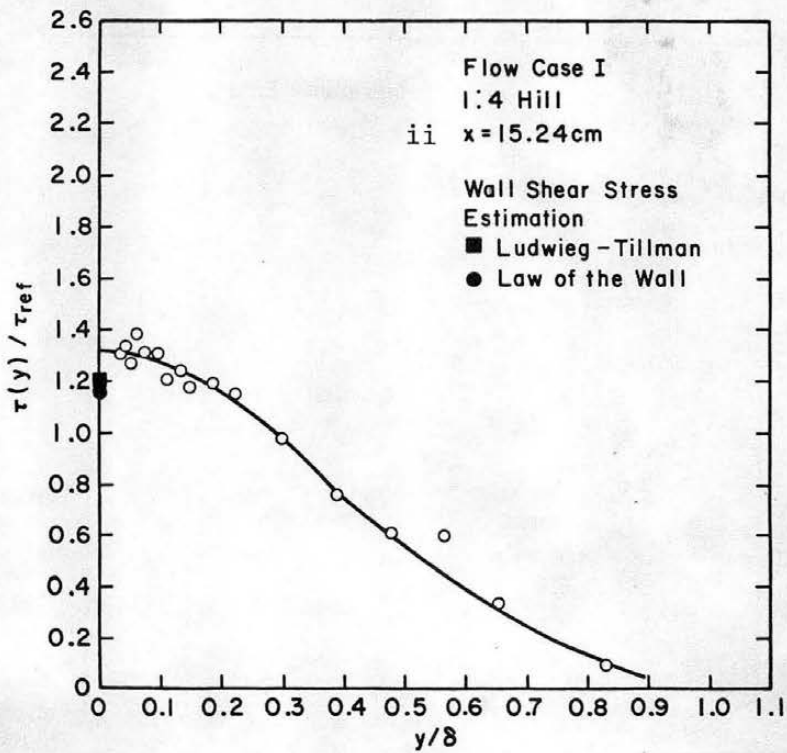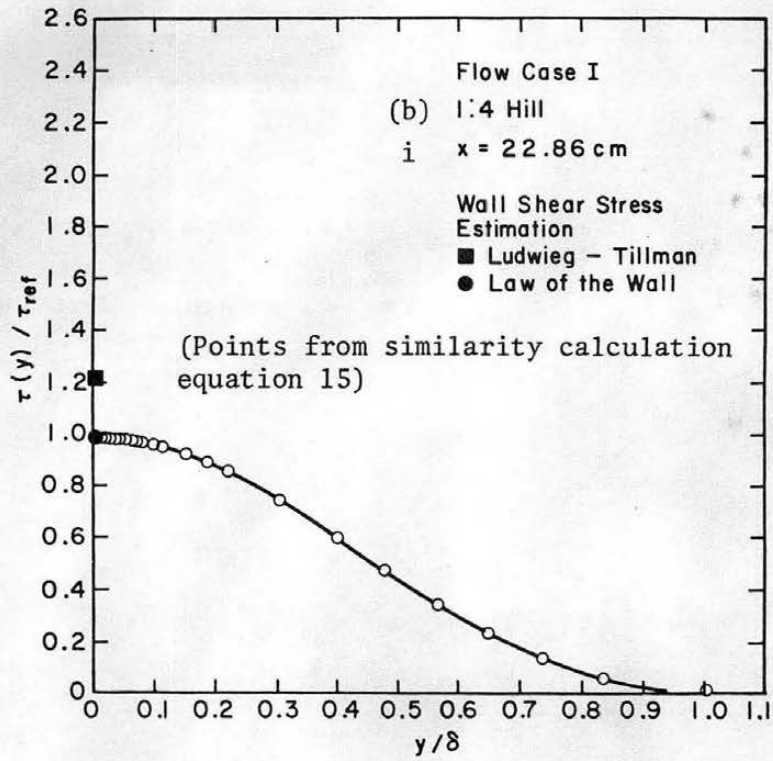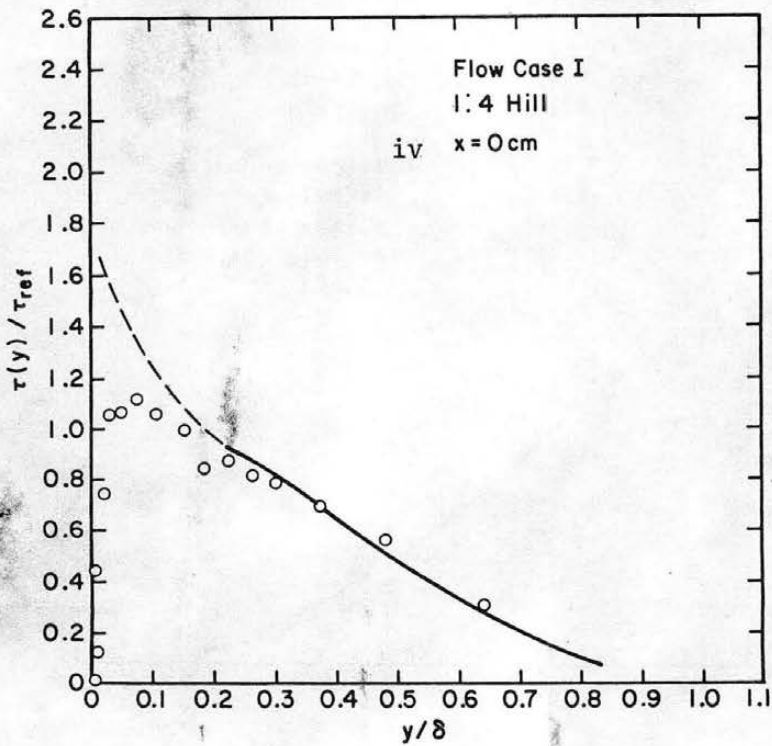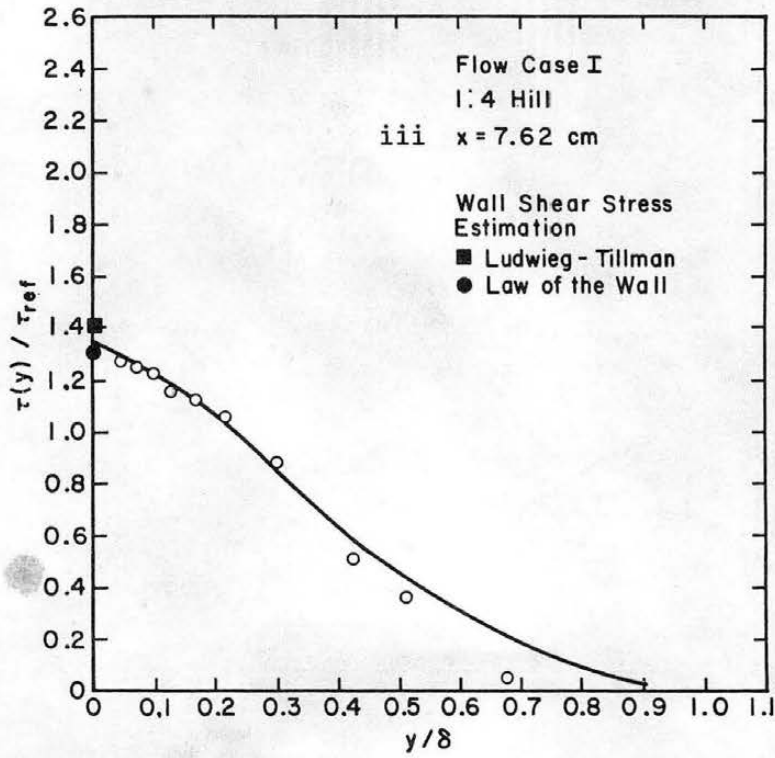
Figure 28.   Shear stress distribution flow case I (continued).
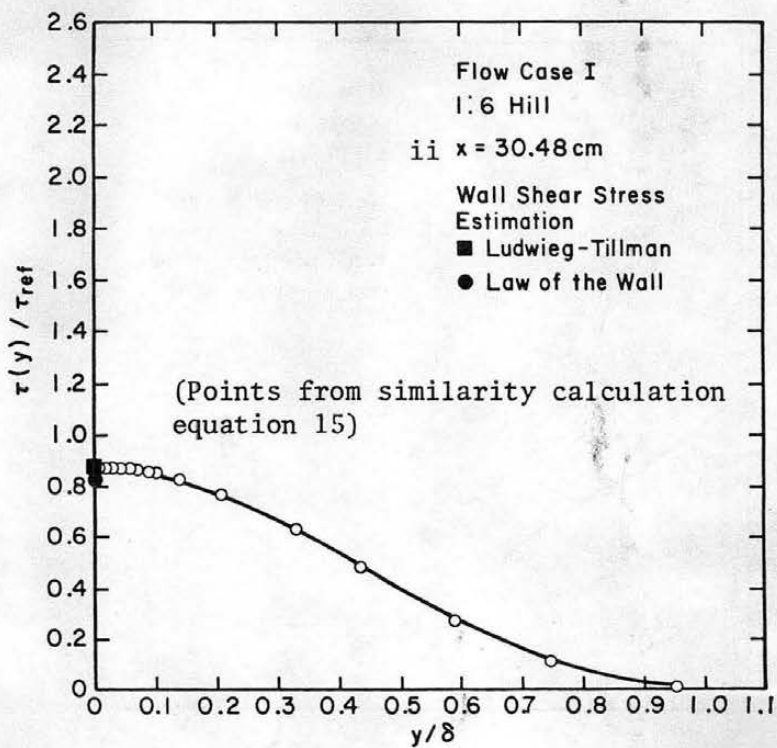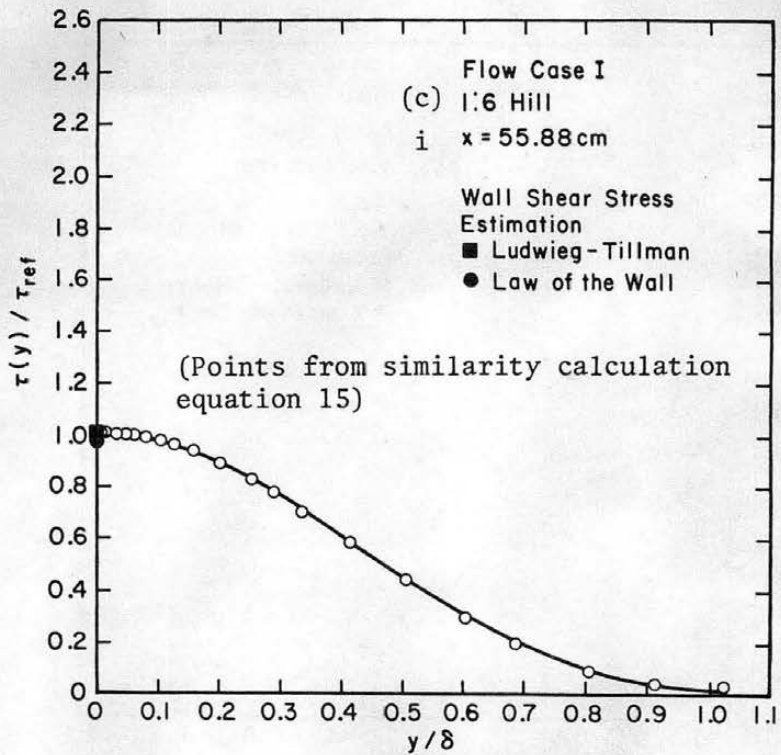
Figure 28.   Shear stress distribution flow case I (continued).
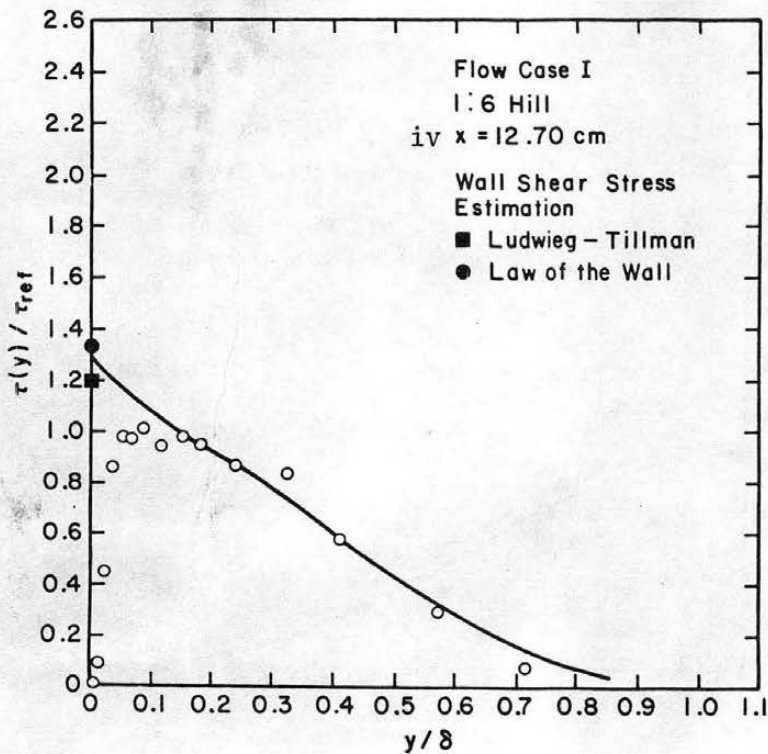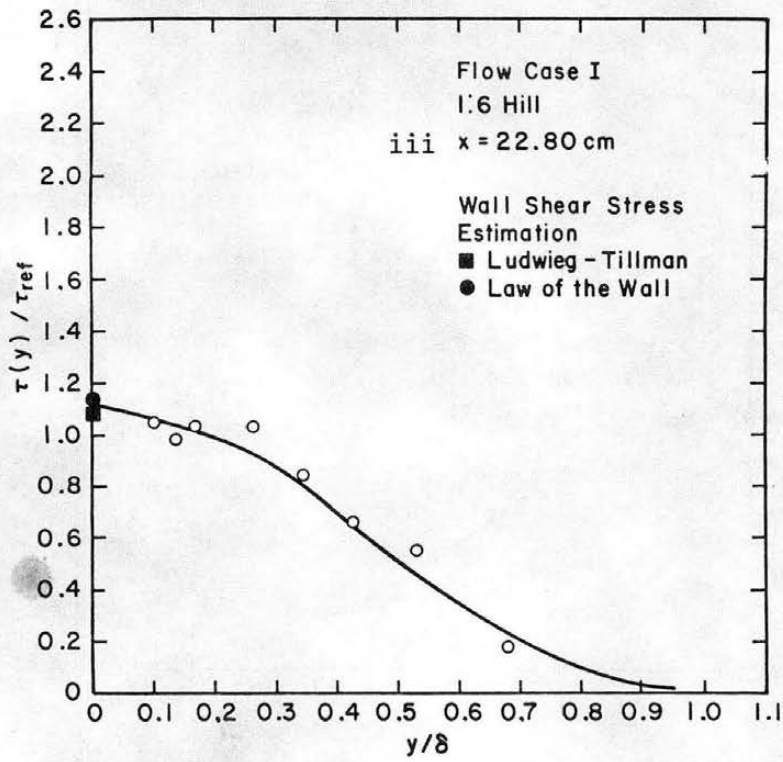
Figure 28.   Shear stress distribution flow case I (continued).
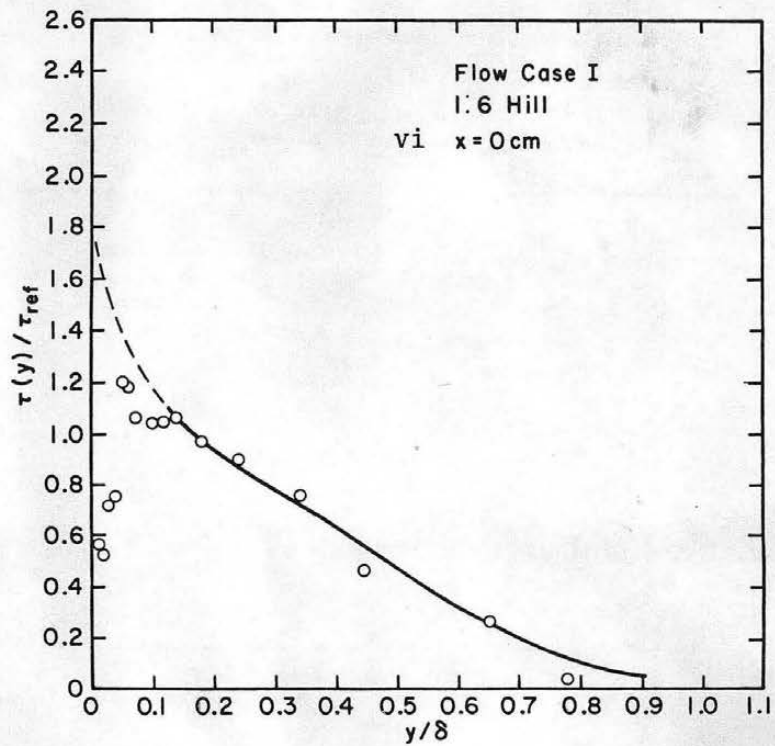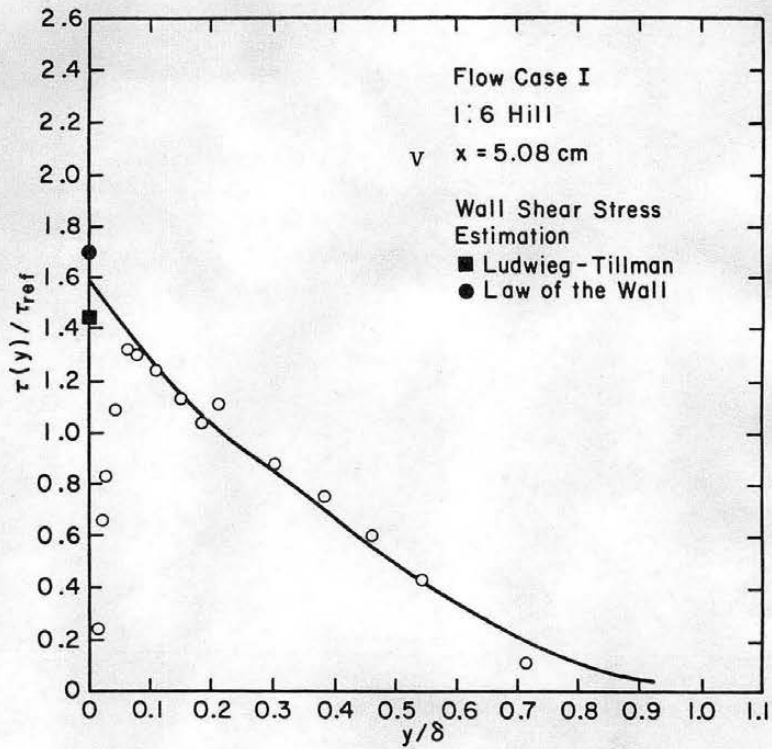
Figure 28. Shear stress distribution flow case I (completed).
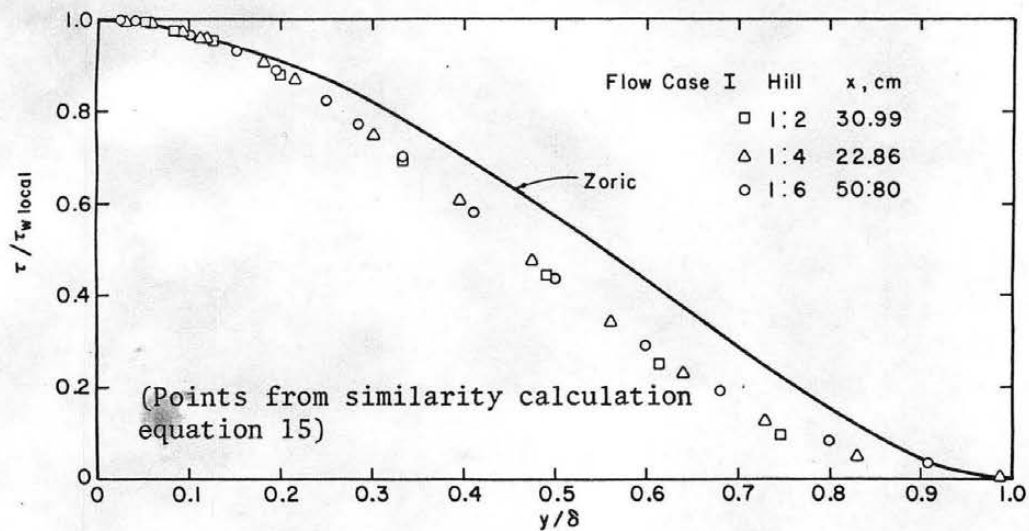
Figure 29.   Comparison of upstream shear stress distribution to that of Zoric.   Flow case I.
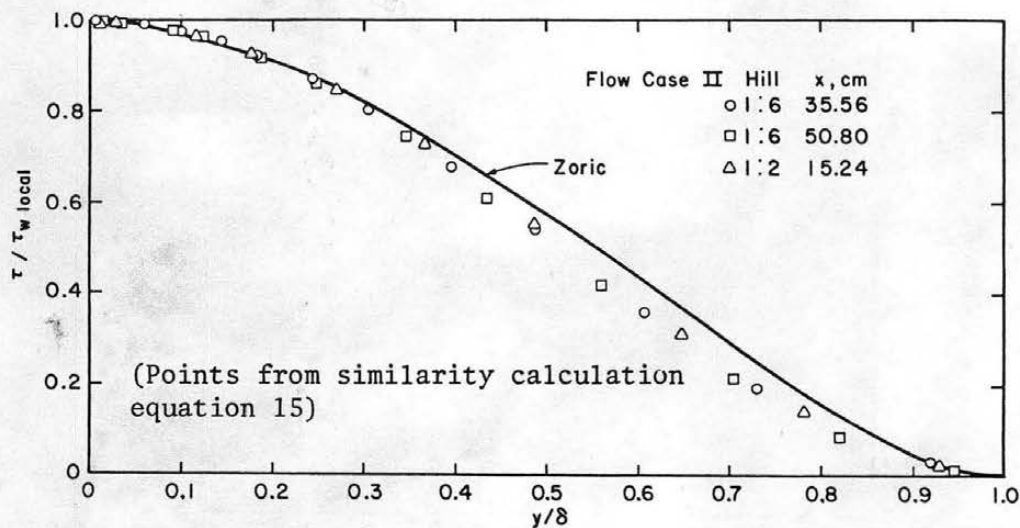
Figure 30.   Comparison of upstream shear stress distribution to that of Zoric.   Flow case II.
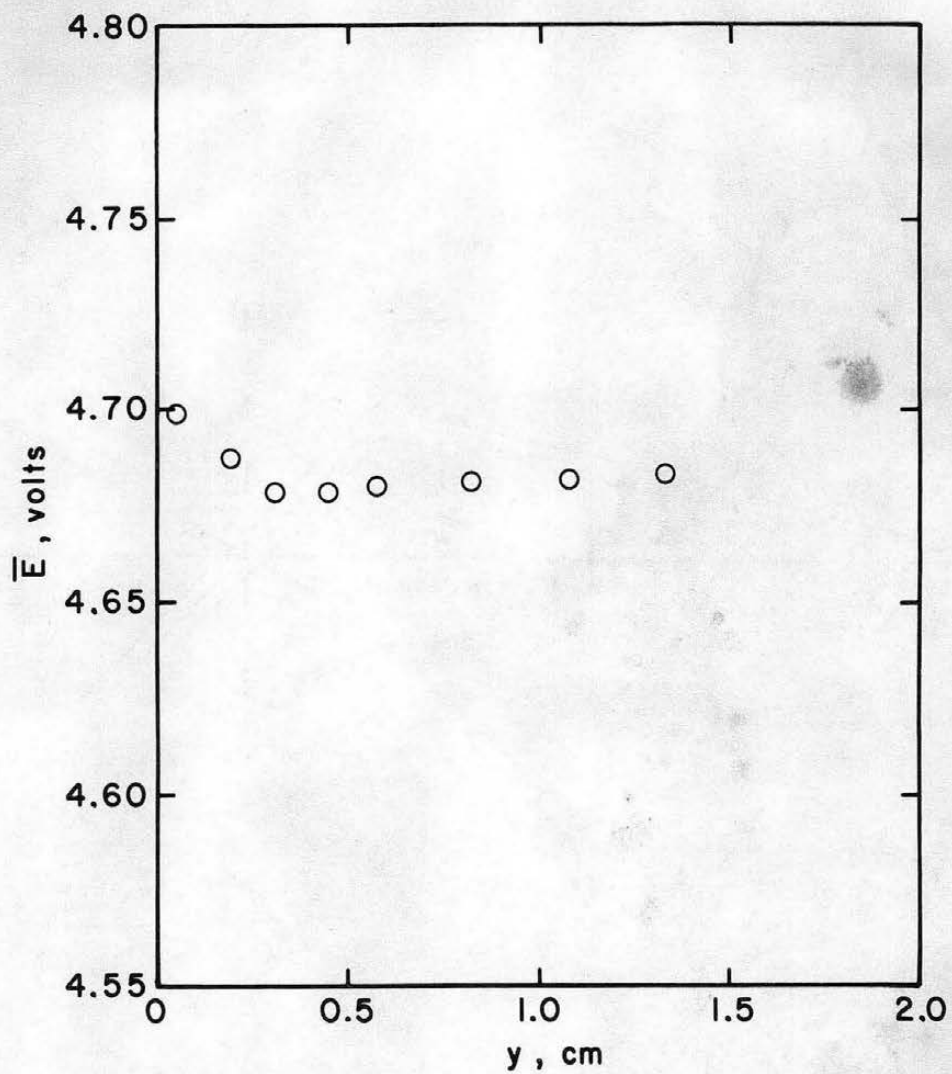
Figure 31. Effect of the wall as a heat sink.

94
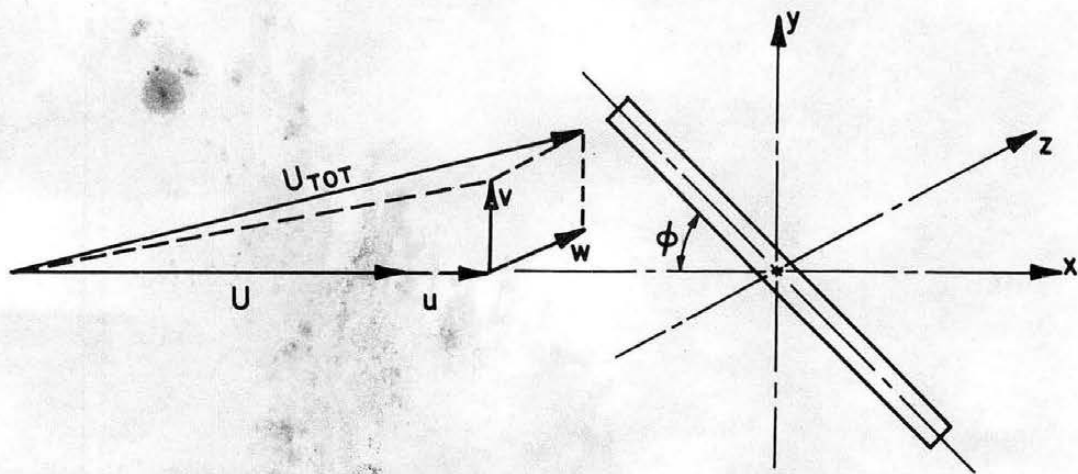
Figure 32. Hot wire with respect to the coordinate system.
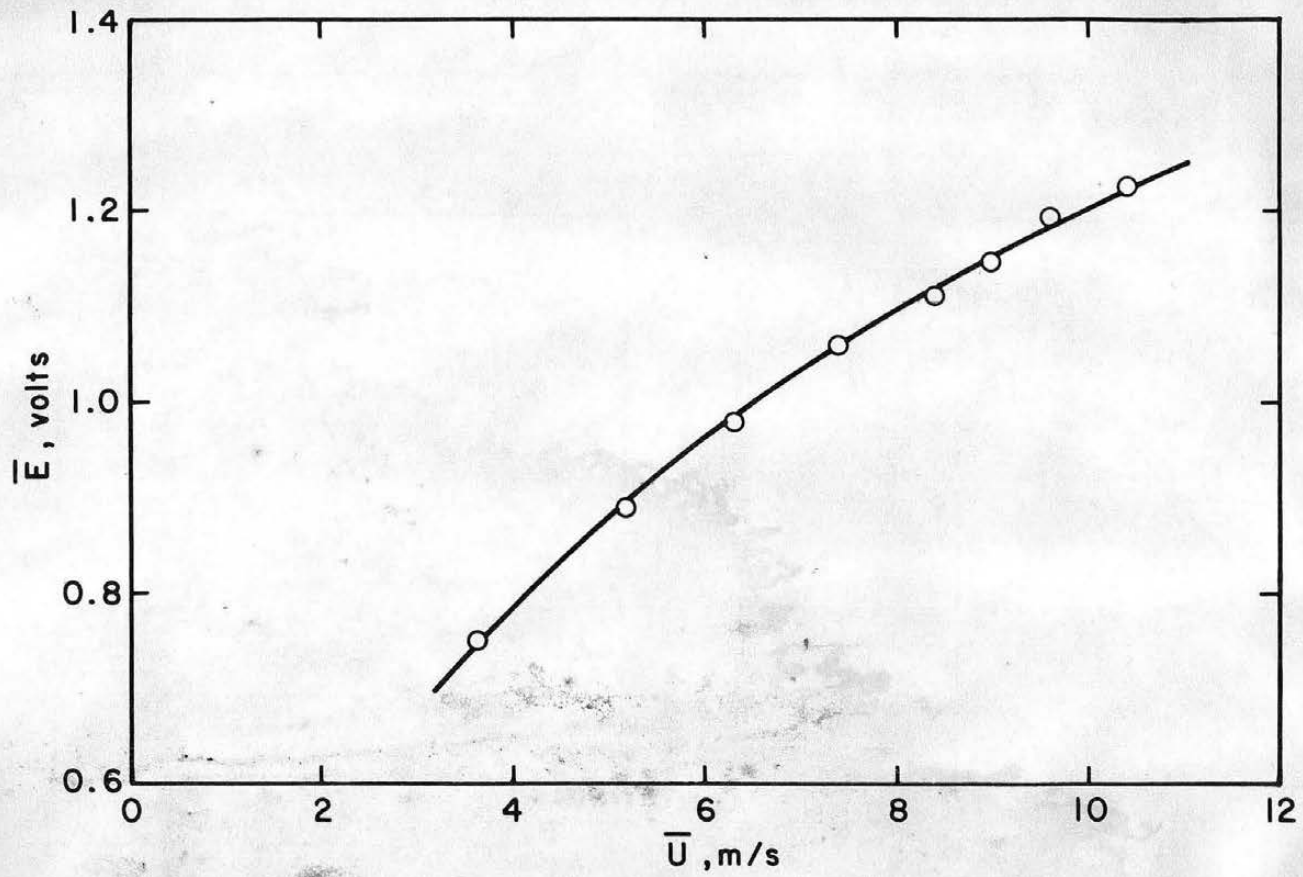
Figure 33. Typical hot wire calibrator curve.
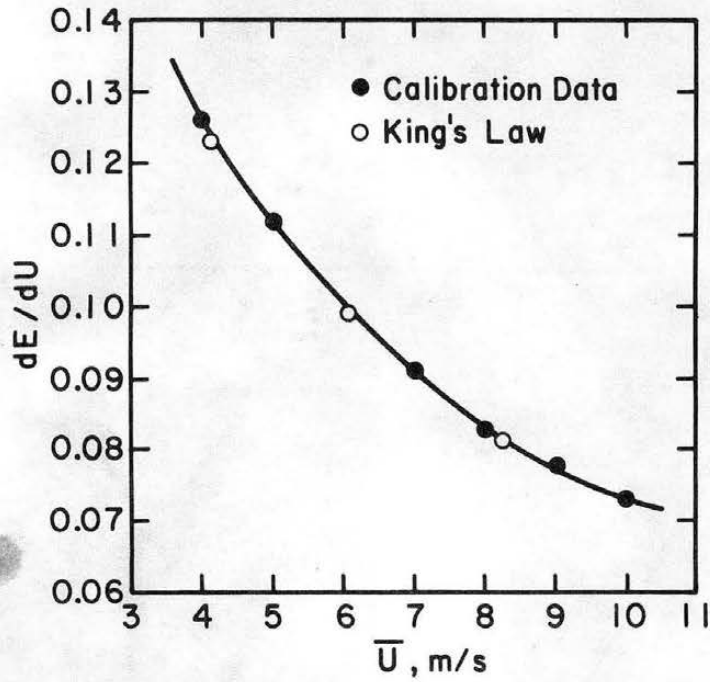
Figure 34.   Typical hot wire sensitivity curve to velocity.
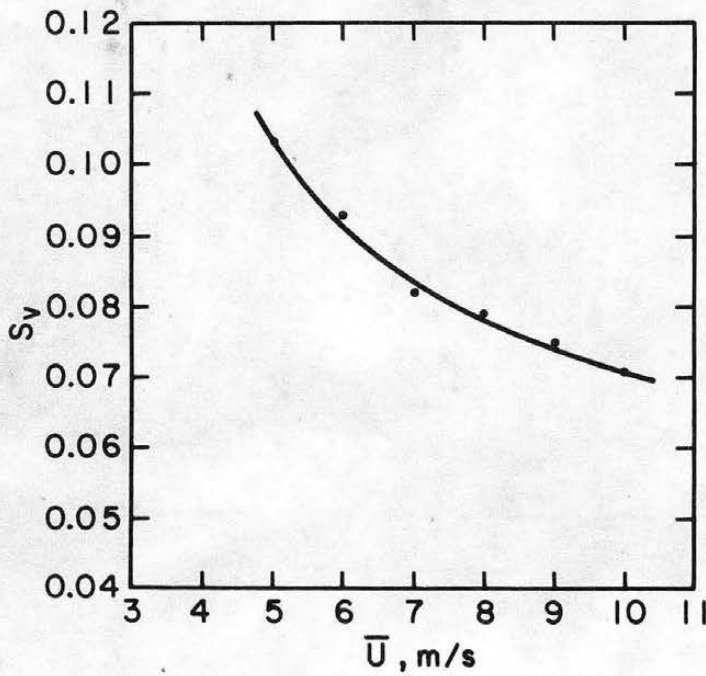
Figure 35.   Typical hot wire sensitivity curve to yaw.

TABLES

Table Ia. Tabulated data for flow case I: 1:2 Hill model.

FOR HILL 1/2   POSITION 30.99CM FROM CREST   FREE STREAM VELOCIT 9.09M/S

Y/DELTA	U(y)/U F.S.	RMSU(ROE/T)**.5	RMSV(ROE/T)**.5	T(y)/T REF
.005	.380	1.850	1.222	.792
.012	.519	2.223	1.323	.792
.029	.595	2.170	1.170	.790
.053	.641	2.105	1.237	.786
.084	.694	2.010	1.189	.775
.124	.728	1.881	1.245	.755
.196	.771	1.668	1.151	.699
.326	.842	1.606	1.144	.557
.480	.911	1.417	1.115	.359
.602	.949	1.240	.919	.208
.732	.979	.808	.639	.083
.875	.999	.443	.356	.006
1.017	1.000	.246	0.000	-.012

86

Table Ia.   Tabulated data for flow case I: 1:2   Hill model (continued).

FOR HILL 1/2   POSITION 10.16CM FROM CREST   FREE STREAM VELOCIT 9.61M/S

Y/DELTA	U(Y)/U F.S.	RMSU(ROE/T)**.5	RMSV(ROE/T)**.5	T(Y)/T REF
.021	.360	1.877	1.217	.550
.037	.469	2.082	1.260	.549
.070	.568	2.032	1.199	.545
.088	.607	2.026	1.170	.541
.123	.675	1.823	1.102	.531
.162	.738	1.838	1.167	.514
.201	.763	1.754	1.154	.493
.250	.795	1.650	1.133	.461
.314	.831	1.569	1.093	.412
.373	.874	1.519	1.113	.361
.458	.907	1.418	1.055	.282
.520	.931	1.378	.982	.226
.612	.947	1.221	.894	.147
.721	.977	.947	.696	.073
.824	.995	.629	.536	.025
.927	.998	.413	.350	.003
1.033	1.000	.284	.227	-.001

66

Table Ia. Tabulated data for flow case I: 1:2 Hill model (continued).

FOR HILL 1/2   POSITION   2.54CM FROM CREST   FREE STREAM VELOCIT 9.53M/S

Y/DELTA	U(y)/U F.S.	RMSU(ROE/T)**.5	RMSV(ROE/T)**.5	T(y)/T REF
.022	.707	2.086	1.375	1.198
.041	.728	2.004	1.278	1.076
.060	.758	2.007	1.262	1.104
.099	.805	2.002	1.183	1.181
.120	.823	1.899	1.163	1.061
.153	.841	1.817	1.159	.992
.177	.853	1.907	1.185	1.194
.215	.857	1.694	1.110	.845
.285	.881	1.614	1.096	.720
.356	.899	1.545	1.101	.656
.425	.916	1.471	1.035	.626
.505	.944	1.376	.939	.475
.568	.958	1.307	.846	.394
.653	.978	1.100	.705	.254
.746	.993	.926	.559	.200
.874	1.000	.492	.253	.003
.954	1.000	.369	.099	-.011
1.012	1.000	.275	0.000	-.029

Table Ia. Tabulated data for flow case I: 1:2 Hill model (continued).

FOR HILL 1/2   POSITION   5.08CM FROM CREST   FREE STREAM VELOCIT 9.67M/S

Y/DELTA	U(y)/U F.S.	RMSU(ROE/T)**.5	RMSV(ROE/T)**.5	T(y)/T REF
.025	.595	1.936	1.256	.878
.038	.628	2.069	1.251	1.104
.057	.688	2.103	1.196	1.159
.082	.721	1.982	1.196	1.177
.102	.752	1.884	1.153	.979
.143	.789	1.655	1.125	.719
.181	.808	1.808	1.162	.960
.237	.851	1.689	1.141	.839
.333	.883	1.631	1.150	.805
.410	.912	1.521	1.031	.621
.507	.942	1.381	.954	.504
.636	.975	1.162	.781	.355
.775	.990	.866	.508	.171
.924	1.000	.453	.243	.033
1.034	1.000	.292	.090	-.002

Table Ia. Tabulated data for flow case I: 1:2 Hill model (continued).

FOR HILL 1/2   POSITION   0.00CM FROM CREST   FREE STREAM VELOCIT 9.68M/S

Y/DELTA	U(y)/U F.S.	RMSU(ROE/T)**.5	RMSV(ROE/T)**.5	T(y)/T REF
.005	.723	1.819	1.479	.791
.026	.714	1.980	1.419	1.283
.056	.825	1.997	1.359	1.766
.095	.845	1.882	1.333	1.622
.136	.860	1.763	1.241	1.365
.198	.868	1.634	1.208	1.207
.277	.898	1.547	1.194	1.090
.363	.920	1.500	1.145	1.015
.460	.946	1.388	1.044	.837
.455	.959	1.289	.947	.731
.632	.979	1.108	.828	.554
.712	.993	.911	.737	.415
.783	.999	.696	.614	.269
.909	.999	.405	.391	.108
1.028	1.000	.217	.221	.031

Table Ib. Tabulated data for flow case I: 1:4 Hill model.

FOR HILL 1/4   POSITION 22.86CM FROM CREST   FREE STREAM VELOCIT*IO*.00M/S

Y/DELTA	U(y)/U F.S.	RMSU(ROE/T)**.5	RMSV(ROE/T)**.5	T(y)/T REF
.005	.428	1.770	1.166	.979
.010	.484	1.899	1.122	.979
.019	.540	2.003	1.331	.979
.028	.570	2.018	1.358	.978
.039	.610	2.046	1.351	.976
.046	.622	2.049	1.343	.974
.054	.644	2.058	1.357	.972
.062	.640	1.984	1.331	.969
.071	.652	1.972	1.323	.966
.080	.660	1.945	1.323	.962
.096	.676	1.925	1.314	.953
.113	.692	1.879	1.292	.943
.147	.745	1.850	1.276	.916
.181	.777	1.829	1.277	.884
.215	.795	1.771	1.267	.848
.300	.836	1.659	1.215	.735
.395	.865	1.452	1.055	.591
.473	.932	1.353	.959	.465
.558	.955	1.099	.901	.334
.641	.995	.922	.782	.220
.729	1.000	.773	.679	.121
.828	.997	.462	.442	.047
.999	1.000	.214	.100	-.000
1.168	.995	.141	.105	-.000
1.280	.990	.140	.056	-.000

103

Table Ib. Tabulated data for flow case I: 1:4 Hill model (continued).

FOR HILL 1/4   POSITION 15.24CM FROM CREST   FREE STREAM VELOCIT 10.05M/S

Y/DELTA	U(y)/U F.S.	RMSU(ROE/T)**.5	RMSV(ROE/T)**.5	T(y)/T REF
.007	.537	1.870	1.421	.708
.011	.542	1.901	1.479	.911
.020	.572	2.010	1.503	1.173
.031	.614	2.067	1.477	1.299
.039	.647	2.049	1.458	1.328
.049	.662	2.008	1.438	1.260
.057	.669	2.031	1.440	1.378
.071	.685	1.976	1.402	1.302
.093	.709	1.920	1.378	1.300
.109	.711	1.850	1.335	1.198
.129	.730	1.838	1.333	1.236
.145	.738	1.781	1.302	1.171
.181	.801	1.769	1.260	1.184
.221	.829	1.739	1.268	1.141
.295	.859	1.612	1.206	.973
.385	.927	1.453	1.032	.752
.472	.960	1.352	.941	.596
.561	.965	1.147	.945	.588
.649	1.005	.857	.750	.324
.823	1.000	.521	.480	.086
1.066	1.000	.364	0.000	-.038
1.289	.995	.136	0.000	-.035

Table Ib. Tabulated data for flow case I: 1:4 Hill model (continued).

FOR HILL 1/4   POSITION   0.00CM FROM CREST   FREE STREAM VELOCIT 9.70M/S

Y/DELTA	U(y)/U F.S.	RMSU(ROE/T)**.5	RMSV(ROE/T)**.5	T(y)/T REF
.005	1.072	1.920	.862	.109
.001	1.070	1.765	1.200	.434
.016	1.052	1.778	1.374	.737
.025	1.014	1.821	1.496	1.044
.045	.977	1.762	1.456	1.055
.072	.957	1.737	1.453	1.105
.104	.941	1.671	1.414	1.046
.148	.934	1.599	1.376	.984
.182	.934	1.531	1.316	.834
.221	.934	1.494	1.310	.861
.260	.932	1.458	1.267	.806
.297	.934	1.426	1.239	.775
.370	.938	1.344	1.182	.685
.477	.954	1.241	1.056	.551
.637	.977	1.035	.815	.291
.822	.994	.643	.311	-.078
1.033	1.000	.220	.148	-.272

Table Ib. Tabulated data for flow case I: 1:4 Hill model (continued).

FOR HILL 1/4 POSITION 7.62CM FROM CREST FREE STREAM VELOCIT 9.95M/S

Y/DELTA	U(y)/U F.S.	RMSU(ROE/T)**.5	RMSV(ROE/T)**.5	T(y)/T REF
.005	.529	1.341	1.289	-.061
.014	.538	1.368	1.368	.114
.021	.553	1.455	1.462	.388
.032	.567	1.509	1.481	.565
.042	.709	1.921	1.567	1.266
.067	.738	1.861	1.497	1.244
.095	.772	1.766	1.460	1.216
.122	.799	1.733	1.421	1.146
.163	.878	1.662	1.366	1.112
.212	.899	1.611	1.333	1.048
.294	.930	1.500	1.229	.875
.421	.953	1.268	.990	.495
.505	.965	1.114	.859	.351
.671	.989	.822	.558	.039
.842	1.000	.333	0.000	-.236
1.001	.993	.129	0.000	-.292

Table Ic. Tabulated data for flow case I: 1:6 Hill model.

FOR HILL 1/6   POSITION 55.88CM FROM CREST   FREE STREAM VELOCIT 9.48M/S

Y/DELTA	U(y)/U F.S.	RMSU(ROE/T)**.5	RMSV(ROE/T)**.5	T(y)/T REF
.004	.396	2.395	.916	1.000
.010	.530	2.332	1.150	1.000
.027	.608	2.182	1.138	.998
.043	.655	2.110	1.208	.995
.057	.688	2.143	1.209	.991
.075	.730	1.992	1.183	.984
.100	.760	1.907	1.186	.971
.122	.788	1.835	1.228	.956
.153	.814	1.784	1.252	.930
.196	.825	1.624	1.202	.887
.248	.869	1.569	1.206	.823
.285	.869	1.510	1.205	.773
.333	.899	1.444	1.174	.701
.409	.923	1.366	1.144	.580
.500	.950	1.196	1.000	.436
.599	.975	1.033	.875	.289
.682	.988	.802	.643	.187
.799	.997	.585	.441	.083
.908	.999	.394	.150	.035
1.020	1.000	.123	0.000	.025
1.178	1.000	.075	0.000	.025

107

Table Ic. Tabulated data for flow case I: 1:6 Hill model (continued).

FOR HILL 1/6   POSITION 30.48CM FROM CREST   FREE STREAM VELOCIT 9.50M/S

Y/DELTA	U(y)/U F.S.	RMSU(ROE/T)**.5	RMSV(ROE/T)**.5	T(y)/T REF
.004	.321	2.342	.964	.867
.017	.500	2.015	1.121	.866
.026	.556	2.138	1.139	.865
.041	.594	2.097	1.169	.863
.053	.630	2.074	1.135	.861
.065	.653	2.011	1.220	.857
.084	.697	1.957	1.186	.850
.099	.707	1.941	1.218	.843
.134	.748	1.867	1.267	.822
.204	.813	1.751	1.302	.764
.324	.883	1.510	1.225	.622
.432	.931	1.326	1.150	.472
.585	.976	1.052	.894	.264
.740	.999	.671	.537	.102
.948	1.000	.202	0.000	.009
1.149	1.000	.080	0.000	.006

Table 1c. Tabulated data for flow case I: 1:6 Hill model (continued).

FOR HILL 1/6   POSITION 12.70CM FROM CREST   FREE STREAM VELOCIT 9.59M/S

Y/DELTA	U(y)/U F.S.	RMSU(ROE/T)**.5	RMSV(ROE/T)**.5	T(y)/T REF
.010	.680	2.052	.915	.080
.018	.711	2.002	1.163	.443
.031	.741	2.040	1.342	.853
.047	.779	2.008	1.343	.972
.063	.788	1.950	1.359	.961
.082	.806	1.885	1.394	1.008
.111	.842	1.765	1.371	.939
.147	.867	1.728	1.378	.976
.176	.875	1.638	1.376	.943
.233	.900	1.530	1.313	.857
.318	.923	1.444	1.279	.828
.405	.962	1.235	1.097	.570
.566	.996	.980	.852	.283
.709	1.000	.650	.583	.068
.872	1.000	.253	0.000	-.134
1.022	1.000	.140	0.000	-.136
1.159	1.000	.081	0.000	-.143

Table 1c. Tabulated data for flow case I: 1:6 Hill model (continued).

FOR HILL 1/6   POSITION 22.86CM FROM CREST   FREE STREAM VELOCIT 9.58M/S

Y/DELTA	U(y)/U F.S.	RMSU(ROE/T)**.5	RMSV(ROE/T)**.5	T(y)/T REF
.005	.589	1.975	1.263	-.186
.013	.602	2.075	1.440	.377
.020	.637	2.146	1.454	.664
.031	.670	2.085	1.441	.749
.045	.681	2.018	1.369	.803
.059	.702	1.948	1.348	.857
.097	.752	1.902	1.347	1.042
.133	.789	1.738	1.268	.973
.164	.825	1.726	1.260	1.024
.259	.876	1.619	1.217	1.022
.342	.909	1.442	1.085	.829
.421	.933	1.254	.974	.651
.527	.966	1.146	.887	.541
.675	.991	.756	.541	.169
.845	.999	.358	0.000	-.053
.991	.997	.144	0.000	-.106
1.144	1.000	.080	0.000	-.115

Table Ic. Tabulated data for flow case I: 1:6 Hill model (continued).

FOR HILL 1/6   POSITION   0.00CM FROM CREST   FREE STREAM VELOCIT 9.68M/S

Y/DELTA	U(y)/U F.S.	RMSU(ROE/T)**.5	RMSV(ROE/T)**.5	T(y)/T REF
.006	1.021	2.590	.916	.558
.014	.943	2.318	1.018	.514
.023	.986	2.076	1.262	.712
.033	.964	1.901	1.349	.747
.046	.949	2.063	1.507	1.190
.058	.949	2.021	1.479	1.168
.067	.927	1.903	1.453	1.054
.095	.934	1.826	1.458	1.033
.114	.942	1.787	1.453	1.035
.134	.919	1.715	1.392	1.051
.173	.912	1.611	1.398	.959
.236	.919	1.524	1.351	.891
.337	.934	1.396	1.253	.747
.440	.964	1.144	1.002	.449
.645	.964	.880	.782	.254
.772	.986	.626	.521	.027
.938	.996	.345	0.000	-.105
1.153	1.000	.198	0.000	-.113
1.405	1.000	.144	0.000	-.110

Table Ic. Tabulated data for flow case I: 1:6 Hill model (continued).

FOR HILL 1/6   POSITION   5.08CM FROM CREST   FREE STREAM VELOCIT 9.66M/S

Y/DELTA	U(y)/U F.S.	RMSU(ROE/T)**.5	RMSV(ROE/T)**.5	T(y)/T REF
.009	.801	2.030	.981	.232
.017	.827	2.027	1.218	.651
.023	.844	2.020	1.320	.824
.039	.861	2.024	1.399	1.082
.057	.885	2.029	1.476	1.312
.073	.893	1.969	1.467	1.293
.105	.901	1.876	1.437	1.232
.145	.909	1.717	1.504	1.121
.179	.917	1.637	1.375	1.026
.206	.924	1.633	1.376	1.099
.298	.947	1.501	1.257	.869
.380	.967	1.388	1.173	.742
.458	.977	1.254	1.059	.594
.538	.990	1.106	.929	.422
.708	1.000	.741	.571	.101
.883	1.000	.296	0.000	-.136
1.006	1.000	.136	0.000	-.162
1.154	1.000	.101	0.000	-1.276

Table IIa. Tabulated data for flow case II
          1:2 Hill model.

FOR HILL 1/2   POSITION 50.80CM FROM CREST   FREE STREAM VELOCIT 9.48M/S

Y/DELTA	U(y)/U F.S.	RMSU(ROE/T)**.5	T(y)/T REF
.001	.351	2.435	.956
.003	.438	2.334	.956
.006	.485	2.365	.956
.008	.512	2.390	.956
.012	.540	2.447	.956
.016	.566	2.511	.955
.028	.614	2.607	.954
.062	.671	2.460	.948
.128	.718	2.376	.918
.192	.748	2.203	.871
.257	.776	2.200	.808
.354	.822	2.118	.691
.453	.877	1.968	.552
.582	.934	1.597	.361
.776	.989	.761	.117
.983	1.000	.269	.000

FOR HILL 1/2   POSITION 30.48CM FROM CREST   FREE STREAM VELOCIT 9.74M/S

Y/DELTA	U(y)/U F.S.	RMSU(ROE/T)**.5	T(y)/T REF
.001	.294	2.297	.850
.003	.390	2.518	.850
.005	.429	2.497	.850
.008	.432	2.409	.850
.019	.490	2.578	.849
.036	.540	2.641	.847
.064	.612	2.664	.842
.093	.645	2.555	.832
.124	.655	2.413	.818
.188	.707	2.327	.777
.250	.737	2.234	.722
.345	.778	2.120	.616
.457	.837	2.004	.469
.563	.885	1.787	.320
.752	.957	.963	.085
.953	1.000	.340	0.000

Table IIa. Tabulated data for flow case II
            1:2 Hill model (continued).

FOR HILL 1/2   POSITION 15.24CM FROM CREST   FREE STREAM VELOCIT 9.69M/S

Y/DELTA	U(y)/U F.S.	RMSU(ROE/T)**.5	T(y)/T REF
.001	.193	2.044	.702
.003	.277	2.561	.702
.005	.296	2.622	.702
.007	.313	2.590	.702
.012	.340	2.646	.702
.028	.418	2.862	.701
.059	.497	2.730	.698
.089	.538	2.602	.692
.119	.597	2.419	.683
.181	.657	2.332	.656
.270	.739	2.250	.597
.364	.799	2.131	.515
.486	.872	1.948	.388
.646	.939	1.485	.214
.777	.934	.671	.091
.927	1.000	.268	.009

FOR HILL 1/2   POSITION 10.16CM FROM CREST   FREE STREAM VELOCIT 9.71M/S

Y/DELTA	U(y)/U F.S.	RMSU(ROE/T)**.5	T(y)/T REF
.001	.050	.548	.607
.003	.105	1.343	.607
.005	.136	1.673	.607
.007	.168	1.953	.607
.012	.213	2.254	.607
.022	.284	2.500	.606
.055	.466	2.814	.604
.085	.532	2.022	.600
.117	.592	2.293	.593
.187	.677	2.124	.569
.266	.730	1.382	.526
.358	.820	.546	.459
.480	.878	1.720	.352
.625	.947	1.395	.216
.761	.985	.788	.102
.918	1.000	.286	.023

Table IIa. Tabulated data for flow case II
1:2 Hill model (continued).

FOR HILL 1/2   POSITION   7.62CM FROM CREST   FREE STREAM VELOCIT 9.70M/S

Y/DELTA	U(Y)/U F.S.	RMSU(ROE/T)**.5
.001	.824	3.607
.003	.277	1.709
.005	.298	1.772
.007	.308	1.918
.014	.360	2.124
.034	.428	2.462
.064	.520	2.552
.094	.589	2.386
.155	.671	2.212
.218	.734	2.118
.307	.790	2.063
.398	.844	2.000
.520	.905	1.759
.703	.976	.976
.897	1.000	.295

FOR HILL 1/2   POSITION   2.54CM FROM CREST   FREE STREAM VELOCIT 9.70M/S

Y/DELTA	U(Y)/U F.S.	RMSU(ROE/T)**.5
.001	.440	2.032
.003	.482	1.809
.005	.492	1.724
.012	.507	1.760
.020	.542	1.915
.033	.576	2.117
.060	.650	2.204
.092	.690	2.211
.154	.734	2.158
.217	.780	2.077
.314	.831	2.052
.415	.873	1.994
.504	.913	1.783
.695	.963	1.096
.900	.999	.036

Table IIa. Tabulated data for flow case II
           1:2 Hill model (continued).

FOR HILL 1/2   POSITION   0.00CM FROM CREST   FREE STREAM VELOCIT 9.71M/S

Y/DELTA	U(y)/U F.S.	RMSU(ROE/T)**.5
.001	.602	2.011
.003	.635	1.748
.006	.640	1.670
.008	.643	1.750
.021	.681	2.006
.046	.691	2.145
.087	.729	2.161
.130	.753	2.094
.164	.772	2.073
.228	.802	2.047
.294	.836	2.039
.390	.876	1.946
.489	.912	1.792
.653	.966	1.222
.748	.985	.815
.892	1.000	.327

Table IIb.   Tabulated data for flow case II
1:6 Hill model.

FOR HILL 1/6   POSITION 50.80CM FROM CREST   FREE STREAM VELOCIT 9.57M/S

Y/DELTA	U(y)/U F.S.	RMSU(ROE/T)**.5	T(y)/T REF
.001	.340	2.350	1.000
.003	.452	2.367	1.000
.005	.483	2.410	1.000
.008	.501	2.366	1.000
.014	.545	2.449	1.000
.024	.579	2.518	.999
.036	.620	2.521	.997
.061	.648	2.440	.992
.093	.690	2.332	.980
.123	.787	2.404	.964
.185	.763	2.201	.918
.248	.790	2.168	.855
.341	.845	2.080	.737
.434	.889	1.964	.601
.558	.929	1.713	.405
.705	.975	1.168	.191
.821	.987	.452	.059
.946	1.000	.221	0.000

FOR HILL 1/6   POSITION 35.56CM FROM CREST   FREE STREAM VELOCIT 9.40M/S

Y/DELTA	U(y)/U F.S.	RMSU(ROE/T)**.5	T(y)/T REF
.001	.304	2.294	.925
.003	.411	2.443	.925
.005	.450	2.442	.925
.007	.472	2.450	.925
.012	.501	2.472	.925
.028	.591	2.604	.924
.059	.649	2.538	.918
.100	.696	2.403	.905
.140	.728	2.282	.884
.184	.760	2.195	.854
.244	.794	2.143	.803
.304	.832	2.076	.739
.394	.871	2.031	.627
.486	.918	1.841	.501
.608	.960	1.286	.331
.731	.987	.880	.177
.921	1.000	.314	.032

Table IIb. Tabulated data for flow case II
            1:6 Hill model (continued).

FOR HILL 1/6   POSITION 20.32CM FROM CREST   FREE STREAM VELOCIT 10.21M/S

Y/DELTA	U(y)/U F.S.	RMSU(ROE/T)**.5
.001	.356	2.432
.003	.456	2.497
.005	.494	2.341
.008	.503	2.346
.014	.523	2.489
.027	.559	2.626
.052	.608	2.637
.088	.655	2.594
.157	.698	2.464
.220	.761	2.421
.284	.797	2.356
.376	.884	2.308
.473	.927	2.087
.594	.972	1.665
.720	.992	1.110
.919	1.000	.266

FOR HILL 1/6   POSITION 12.70CM FROM CREST   FREE STREAM VELOCIT 10.78M/S

Y/DELTA	U(y)/U F.S.	RMSU(ROE/T)**.5
.001	.407	2.589
.003	.520	2.542
.005	.549	2.307
.008	.570	2.225
.013	.591	2.214
.026	.633	2.394
.052	.677	2.414
.080	.708	2.368
.116	.748	2.327
.181	.811	2.315
.235	.832	2.269
.332	.881	2.202
.460	.923	1.955
.639	.979	1.344
.758	.995	.912
.919	1.000	.350

Table IIb. Tabulated data for flow case II
1:6 Hill model (continued).

FOR HILL 1/6   POSITION   7.62CM FROM CREST   FREE STREAM VELOCIT 9.54M/S

Y/DELTA	U(y)/U F.S.	RMSU(ROE/T)**.5
.001	.500	2.568
.003	.613	2.428
.006	.643	2.196
.008	.650	2.091
.015	.685	2.176
.027	.696	2.270
.063	.741	2.287
.127	.793	2.209
.209	.826	2.138
.289	.859	2.146
.387	.892	2.037
.517	.938	1.791
.645	.994	1.306
.777	1.000	.751
.919	1.000	.320

FOR HILL 1/6   POSITION   0.00CM FROM CREST   FREE STREAM VELOCIT 9.26M/S

Y/DELTA	U(y)/U F.S.	RMSU(ROE/T)**.5
.001	.767	2.462
.003	.860	2.264
.006	.883	2.036
.008	.880	2.040
.014	.872	2.003
.021	.877	2.109
.033	.886	2.195
.067	.874	2.168
.107	.860	2.107
.174	.860	2.062
.275	.870	2.032
.375	.889	1.911
.524	.951	1.572
.654	.980	1.246
.781	.995	.822
.917	1.000	.402

APPENDIX

Turbulence Measurements

Following is a short discussion of the general principles involved in hot-wire anemometry. The specifics used in the data evaluation are also discussed.

The basis of hot-wire anemometry is measuring the instantaneous heat loss from a cylinder due to change in surrounding conditions. The sensing elements used in this study were extremely small metal wires. These wires were heated above the ambient temperature by a commercial anemometer. As the flow conditions in the tunnel varied, the anemometer responded to the change in heat loss by balancing a wheatstone bridge. The response is considered instantaneous up to at least frequencies of 5,000 hertz. The rate of heat loss is indicated by the change in voltage required to maintain the wire at a desired temperature.

There is a variety of conditions which will cause a change in the heat transfer rate, 1) flow velocity, U; 2) change in the ambient air temperature; 3) physical properties of the air; 4) the length of the wire; 5) orientation of the wire with respect to the flow; and 6) solid objects which act as heat sinks.

Heat is lost from the wire in three ways: radiation, conduction, and convection. Generally in hot-wire anemometry the first two are considered negligible and not compensated for. The third, convection, is made up of two parts, free convection and forced convection. Free convection is important only with extremely low velocities. In this experiment the velocities were great enough so that free convection was not a problem. As a result, forced convection governed the measurements.

Stated earlier were six factors which will change the heat transfer
rate from the wire. It was assumed that the physical properties of the
air and the wire did not change. In addition the temperature of the air
was held constant. The only solid body encountered during the testing
was that of the tunnel floor. With no flow a check was made of the heat
loss to the tunnel floor. There was no significant heat loss for the
region of interest of this study, Figure 31. It was concluded that the
heat loss from the hot wire was a result of the instantaneous velocities,
mean velocity, and the geometric positioning of the probe.

Providing that the previous assumptions are valid, then voltage
output from the hot wire would be a function of U_{tot} and ϕ, the angle
of attack.

$$E_{out} = E(U_{tot}, \phi) \ .$$ (A-1)

The angle ϕ is that angle the wire makes with the instantaneous
velocity and the x axis, Figure 32.

Following a discussion presented by Sandborn (9) where he writes
that a perturbation in the velocity results in a perturbation in the
voltage then the response of a hot wire for a two-dimensional flow

$$e = \frac{dE}{dU} u + \frac{dE}{d\phi} \frac{v}{U} \ .$$ (A-2)

This equation is the basis of the valuation of the hot-wire data.
Squaring the equation and taking the mean, gives

$$\overline{e^2} = \left(\frac{dE}{dU}\right)^2 \overline{u^2} + 2 \frac{dE}{dU} \frac{dE}{d\phi} \frac{\overline{uv}}{U} + \left(\frac{dE}{d\phi}\right)^2 \frac{\overline{v^2}}{U^2}$$ (A-3)

and letting

$$S_u = \frac{dE}{dU} \quad \text{and} \quad S_v = \frac{1}{U}\frac{dE}{d\phi}$$

then

$$\overline{e^2} = S_u^2\overline{u^2} + a\, S_u S_v \overline{uv} + S_v^2\overline{v^2} \quad . \tag{A-4}$$

This equation can be used for either the cross-wire probe or the single horizontal wire. The cross-wire probe application is discussed first followed by the horizontal wire probe.

As described earlier the cross-wire probe is made up of two individual wires. One mounted parallel to the y-axis and the other lying in the x-y plane. (This configuration makes the data reduction less complicated than the usual x cross wire.) A wire placed parallel to the y-axis or normal to the flow is insensitive to the velocity component in the y-direction. As shown by Sandborn (9) the sensitivity to angle, S_u, varies as approximately the cosine of the angle. Thus for even slight misalignment up to 5° the value of S_v is essentially zero. This reduces equation for a normal wire to

$$\overline{e_n^2} = S_u^2\overline{u^2} \quad . \tag{A-5}$$

Henceforth S_u for the normal wire will be called S_1.

The second wire of the cross-wire probe was yawed approximately 40° from horizontal. This wire then calls for a calibration with respect to the mean velocity for each angle of incidence. The $\overline{e^2}$ of the yawed wire is the same as equation (A-4) or

$$\overline{e_y^2} = S_2^2\overline{u^2} + 2\, S_2 S_v \overline{uv} + S_v^2\overline{v^2} \tag{A-6}$$

where S_u for the yawed wire is not S_2. At this point the equations governing the A.C. output of the hot wires have three unknowns $\overline{u^2}$, $\overline{v^2}$ and $\overline{uv}$. To evaluate the flow properties a third equation was needed. This equation came from multiplying the A.C. output of the two wires, which yielded

$$\overline{e_n e_y} = S_1 S_2 \overline{u^2} + S_1 S_v \overline{uv} \tag{A-7}$$

where $\overline{e_n e_y}$ will be represented as $\overline{e_1 e_2}$.

The evaluation of the turbulence sensed by the horizontal wire is very similar to that of the normal wire on the cross-wire probe. Because the probe is parallel to the x-axis any rotation about the z-axis causes no change in the voltage due to change in angle or S_v is zero. For the horizontal wire

$$\overline{e^2} = S_u^2 \overline{u^2} . \tag{A-8}$$

To summarize, the turbulent terms evaluated from the cross-wire data were found using the following equations:

$$\sqrt{\overline{u^2}} = \sqrt{\overline{e_1^2}}/S_1 \tag{A-9}$$

$$\overline{uv} = (\overline{e_1 e_2} - S_1 S_2 \overline{u^2})/(S_1 S_v) \tag{A-10}$$

$$\sqrt{\overline{v^2}} = [(\overline{e^2} - S_2^2 \overline{u^2} - 2 S_2 S_v \overline{uv})/S_v^2]^{1/2} . \tag{A-11}$$

For the horizontal probe data

$$\sqrt{\overline{u^2}} = \sqrt{\overline{e^2}}/S_u \tag{A-12}$$

HOT-WIRE CALIBRATION

To calibrate the hot-wire probes the carriage was moved forward of the model and the probes raised to the free stream. When situated in the free stream the probes were outside the boundary layer, which reduces turbulence to a minimum for calibration. The standard used was a pitot-static tube mounted directly on the probe support. The wires were then subjected to a number of flow velocities ranging from 3.5 m/s to 16 m/s. The mean voltage required to maintain the overheat was recorded. This same procedure was repeated several times during the testing. Because the cross-wire probe needed additional calibration for angle change the probe was rotated in the x-y plane. The angles varied from -10° to +30° from the measuring position. At each angle setting chosen a complete velocity calibration, as described above, was made.

Once the hot-wire probes were heated they were not disconnected until the testings were complete. This helps to reproduce the same calibration from one time to the next. During the surveys the mean velocity was measured with a total pressure probe. This gave a check for the calibration during the actual sampling period.

Two methods were used to reduce the calibration data. The first used for the cross-wire data was a graphical method. The second and more adaptable to computers was the application of King's Law.

To find the sensitivity of a hot wire a relation must be known between the mean voltage of the hot wire for a known velocity, $\bar{U}$. A plot of $\bar{E}$ versus $\bar{U}$ from the calibration was made for both wires of the cross-wire probe data, Figure 33. From these plots the mean velocity for the surveys were taken. To find the sensitivity of the hot wire for a given velocity a second curve was constructed. The curve was formed

by graphically evaluating $\frac{dE}{dU}$ for both wires at known velocities,

Figure 34, and then plotting $\overline{U}$ versus S_u.

The method used to evaluate the data digitally employed King's Law. This involves relating the output of the hot wire to the velocity by an equation. The form used was

$$\overline{E^2} = A + B \ U^m \tag{A-13}$$

where A represents the equivalent square of the voltage for U = 0 and B and m are constants. Although m is different for each wire in most instances it is very close to .5. Differentiating gives S_u or

$$\frac{dE}{dU} = \frac{mB}{2EU^{(m-1)}} \ . \tag{A-14}$$

For the data at hand, setting m = .5 to find velocity and sensitivity proved to be very satisfactory, Figure 34.

The sensitivity of the wire to change in angle of incidence was done graphically. As stated earlier a complete voltage-velocity calibration was recorded for each angle setting of the probe. A series of velocity curves worked up. The individual curves represented different probe rotations. From each of the curves a voltage output for a designated velocity was read. A voltage versus angles was plotted. The relation is a linear one so the slope of the line gave $\frac{dE}{d\phi}$ for the designated velocity. The final result is S_v for the given velocity. Again

$$S_v = \frac{dE}{d\phi} \frac{1}{U} \ .$$

This evaluation was continued until the wire had a complete curve of $\overline{U}$ versus S_v. Figure 35 is an example of a sensitivity to angle curve.